

**Synthesis, Characterization and Substitution Reaction Studies of Pyridyl  
*N,N'*-Bidentate Palladium(II) Complexes. A Kinetic and Mechanistic  
Study.**

by  
**Pinky Ncomela Mjwara**

**216045884**

**Thesis**  
**Submitted in fulfilment of the academic requirements**  
**for the degree of Master of Science in Chemistry.**

**College of Agriculture, Engineering and Science,**  
**University of KwaZulu-Natal**

**Pietermaritzburg**

**Supervisor(s): Dr S. Sithebe & Dr T.R Papo**

**February 2023**



**UNIVERSITY OF  
KWAZULU-NATAL**

---

**INYUVESI  
YAKWAZULU-NATALI**

## DECLARATION 1

I, Pinky Ncomela Mjwara, hereby declare that:

1. The research report in this thesis, except where otherwise indicated, is my original research.
2. This thesis has not been submitted for any degree or examination at any other university.
3. This thesis does not contain other persons' data, pictures, graphs or other information, unless specifically acknowledged as being sourced from other persons.
4. This thesis does not contain other persons' writing, unless specifically acknowledged as being sourced from other researchers. Where other written sources have been quoted, then:
  - (a) Their words have been re-written, but the general information attributed to them has been referenced.
  - (b) Where their exact words have been used then their writing has been placed in italics and inside quotation marks and referenced.
5. This thesis does not contain text, graphics or tables copied and pasted from the internet, unless specifically acknowledged and the source being detailed in the thesis and in the References sections.

  
\_\_\_\_\_  
Pinky Ncomela Mjwara (Student)

As the supervisor of the student, I approve the submission of this MSc Thesis for examination.

  
\_\_\_\_\_  
Dr S. Sithebe (Supervisor)

  
\_\_\_\_\_  
Dr T.R Papo (Co-supervisor)

## DECLARATION 2 – CONFERENCE PRESENTATIONS AND PUBLICATIONS

Some parts of this research have been presented in the following conferences:

1. Pinky N. Mjwara, Dr Siphamandla Sithebe & Dr Tshephiso Papo. College of Agriculture, Engineering and Science Online Postgraduate Research and Innovation Symposium (PRIS). December 2022. Flash Presentation. Synthesis and Substitution Kinetics Studies of Pyridyl *N,N'*-Bidentate Palladium(II) Complexes.

2. Pinky N. Mjwara, Dr Siphamandla Sithebe & Dr Tshephiso Papo. 44<sup>th</sup> SACI National Convention, Chemistry for Sustainable Development in Africa. Stellenbosch. January 2023. Flash & Poster Presentation. Synthesis and Substitution Kinetics of Pyridyl *N,N'*-Bidentate Palladium(II) Complexes.

Publication:

1. Pinky N. Mjwara, Tshephiso R. Papo & Siphamandla Sithebe. bis[N-(4-Bromophenyl)pyridine-2-carboxamidato]palladium. Molbank 2022, 2022(4), M1496; <https://doi.org/10.3390/M1496>.

## **DEDICATION**

*This work is dedicated to my mother, Mrs D.C Mjwara, thank you Ma.*

## **ACKNOWLEDGEMENTS**

My utmost gratitude goes to my supervisors, Dr S. Sithebe and Dr T.R Papo, for granting me the opportunity to work on this project; their encouragement, guidance and patience made this all possible. I would also like to thank UKZN and the National Research Foundation for their financial support. Thank you to all my colleagues from Warren Laboratory and Room 22, for the laughter and meaningful talks. Lastly, I am grateful to my family and close friends, for their love and emotional support.

## Table of Content

DECLARATION 1 .....	i
DECLARATION 2 – CONFERENCE PRESENTATIONS AND PUBLICATIONS .....	ii
DEDICATION .....	iii
ACKNOWLEDGEMENTS .....	iv
Table of Content .....	v
List of Abbreviations .....	viii
List of Figures .....	xi
List of Schemes.....	xiii
Abstract.....	xiv
CHAPTER 1 .....	1
1. Introduction .....	1
1.1 The Development of Cancer .....	1
1.2 Causes of Cancer .....	2
1.3 Treatment of Cancer .....	2
1.4 Use of Metals in Cancer Treatment .....	3
1.4.1 Mechanism of Action of Pt-based Drugs .....	3
1.4.2. Drawbacks of <i>Cisplatin</i> .....	5
1.5 Use of Pd(II) Complexes in Cancer Treatment .....	6
1.5.1 Mononuclear Palladium Complexes .....	7
1.5.2 Mononuclear Nitrogen Containing Pd(II) Complexes .....	7
1.5.3 N’N Bidentate Pd(II) Complexes.....	9
1.6 References .....	11
CHAPTER 2 .....	14
2.1 Substitution Reactions of Pd(II) Complexes .....	14
2.1.1 The Influence of Spectator Ligands on the Rate of Substitution in Pd(II) Complexes .....	14
2.1.2 Influence of Ionic Strength on The Rate of Substitution in Pd(II) Complexes.....	19

2.1.3 Influence of Incoming Biomolecules on The Rate of Substitution in Pd(II) Complexes.....	20
2.2 Instrumental Techniques Used in Chemical Kinetics .....	20
2.2.1 UV-Visible Spectrophotometry .....	20
2.2.2 Stopped Flow Spectrophotometry.....	21
2.3 Statement of Problem.....	22
2.4 Justification of Study.....	23
2.5 Aims and Objectives.....	23
2.5.1 Aims .....	23
2.5.2 Objectives.....	23
2.6 References .....	24
CHAPTER 3 .....	27
3.1 General Introduction.....	27
3.2 Chemicals and Reagents .....	28
3.3 Physical Measurements .....	28
3.3.1 <sup>1</sup> H and <sup>13</sup> C NMR Spectroscopy .....	28
3.3.2 FTIR Spectroscopy.....	28
3.3.3 Mass Spectrometry.....	29
3.3.4 DFT-Computational Modelling.....	29
3.3.5 Stopped Flow & UV-Visible Spectrophotometer .....	29
3.3.6 Preparation of Solutions for Kinetic Analysis.....	29
3.4 Synthesis of Ligands.....	30
3.5 Synthesis of Pd(II) Complexes .....	33
3.6 Results and Discussion .....	36
3.6.1 Synthesis of Ligands and Complexes .....	36
3.7 DFT-Computational Modelling and Analysis.....	42
3.8 Substitution Kinetic Analysis.....	47
3.8.1 Kinetic Measurements .....	47
3.8.2 <sup>1</sup> H NMR Spectroscopy .....	47

3.8.3 First Substitution Step.....	49
3.8.3.1 Concentration Dependence.....	49
3.8.3.2 Temperature Dependence.....	52
3.8.4 Second Substitution Step.....	53
3.8.4.1 Concentration Dependence.....	54
3.8.4.2. Temperature Dependence.....	57
3.9 Conclusion.....	58
3.10 References.....	60
CHAPTER 4.....	63
Synthesis of Novel Palladium(II)-Pyridine Carboxamide Complexes.....	63
4.1 Introduction.....	63
4.2 Chemicals and Reagents.....	63
4.3 Physical Measurements.....	64
4.4 Synthesis of the Ligand.....	64
4.5 Synthesis of the Pd(II) Complexes.....	65
4.6 Results and Discussion.....	66
4.6.1 Synthesis of Ligand and Complexes.....	66
4.6.2 X-ray Crystallography.....	68
4.7 Conclusion.....	70
4.8 References.....	71
CHAPTER 5.....	74
5.1 Overall Conclusions and Future Work.....	74
5.1.1 Conclusion.....	74
5.1.2 Recommendations for Future Work.....	74
Appendix.....	76

## List of Abbreviations

B3LYP	Becke-3-Lee-Yang-Parr
BRCA1	Breast cancer gene 1
BRCA2	Breast cancer gene 2
COSY	Correlated spectroscopy
DFT	Density function theory
DMTU	Dimethylthiourea
DNA	Deoxyribonucleic acid
d	Doublet
$\Delta H^\ddagger$	Enthalpy of activation
$\Delta S^\ddagger$	Entropy of activation
eV	Electron volt
FT-IR	Fourier-transform infrared spectroscopy
5-GMP	Guanosine-5-monophosphate
GSH	Glutathione
HOMO	Highest occupied molecular orbital
Hz	Hertz
I	Ionic strength
<i>I</i>	Transmitted radiation
<i>I</i> <sub>0</sub>	Incident radiation
<i>J</i>	Coupling constant
K	Kelvin
<i>K</i> <sub>2</sub>	Second order

$K_{obs}$	Observed pseudo first-order constant
kPa	Kilopascal
$l$	Length
L-Cys	L-Cysteine
L-Met	L-Methionine
LANL2DZ	Los Alamos National Laboratory 2 double $\zeta$
LC-MS	Liquid chromatography – mass spectroscopy
LUMO	Lowest unoccupied molecular orbital
m	Multiplet
M	Molar
MHz	Megahertz
mM	Millimolar
NBO	Natural bond orbital
NMR	Nuclear magnetic resonance
Nu	Nucleophile
$\eta$	Chemical hardness
PDT	Photodynamic therapy
ppm	Parts per million
s	Singlet
T	Temperature
t	Triplet
TMTU	Tetramethylthiourea
TOF-MS	Time-of-flight mass spectrometry
TU	Thiourea

$\mu$	Electronegativity
UV-Vis	Ultraviolet-visible
WHO	World health organisation
$\omega$	Electrophilicity index
s,m,hr (time)	Second, Minute, Hour

## List of Figures

<b>Figure 1. 1:</b> Different DNA-Pt adducts formed from the interaction of cisplatin with DNA. <sup>295</sup>	
<b>Figure 1. 2:</b> Cisplatin and follow-up platinum-based anticancer drugs. <sup>32</sup> .....	6
<b>Figure 1. 3:</b> Mononuclear ethylenediamine-palladium(II) complexes with different substituents on the pyridine. <sup>49</sup> .....	8
<b>Figure 1. 4:</b> trans-Palladium bis(quinonyl-phosphonate) and the quinolmethylphosphonate ester complexes as early examples of Pd(II) anticancer complexes. <sup>50,51</sup> .....	9
<b>Figure 1. 5:</b> Bipyridine and phenanthroline based palladium complexes for binding with phage PMA2 DNA. <sup>54</sup> .....	10
<b>Figure 2. 1:</b> Pyridine- and pyrrole-based complexes designed to study the influence of electronic and steric effects on the reactivity of Pd(II) complexes. <sup>3,6</sup> .....	15
<b>Figure 2. 2:</b> Pd(II) complexes with ligands containing bis(2-pyridylmethyl)amine and bis(8-quinolinyl)amine moieties. <sup>4</sup> .....	16
<b>Figure 2. 3:</b> Palladium(II) complexes with $\pi$ -conjugated carboxamide ligands. <sup>7</sup> .....	17
<b>Figure 2. 4:</b> Tridentate 2,6-bis(benzazole)pyridine Pd(II) complexes designed to study the effects of heteroatoms on the cytotoxicity of palladium(II) complexes. <sup>8</sup> .....	18
<b>Figure 2. 5:</b> Palladium (II) complexes with different pyrazolyl ligands. <sup>9</sup> .....	19
<b>Figure 2. 6:</b> Schematic diagram of a stopped-flow reaction analyser. ....	22
<b>Figure 3. 1:</b> An overlay <sup>1</sup> H NMR spectra of ligand <b>L1</b> and corresponding <b>PdL1</b> complex showing a notable downfield shift of all the aromatic protons and distinct changes in the methylene and amine protons. ....	38
<b>Figure 3. 2:</b> COSY NMR spectrum showing the ABX spin system for the protons of the methylene group of the chelating ring (H <sup>A</sup> and H <sup>B</sup> ) and the aniline proton (H <sup>X</sup> ) in <b>PdL1</b> . ....	39
<b>Figure 3. 3:</b> An overlay <sup>13</sup> C NMR spectra of ligand <b>L5</b> and corresponding <b>PdL5</b> complex showing a notable downfield shift of all the aromatic and amine protons and no changes in the methylene hydrogen atoms. ....	40
<b>Figure 3. 4:</b> An overlay FT-IR spectra of ligand <b>L4</b> and corresponding <b>PdL4</b> complex showing distinctive peaks to characterize the free ligand and its complex. ....	41
<b>Figure 3. 5:</b> <sup>1</sup> H NMR spectra of <b>L1</b> , <b>PdL1</b> and the substituted reaction of <b>PdL1</b> with six equivalents of <b>TU</b> at 30 °C. ....	48

<b>Figure 3. 6:</b> Kinetic trace obtained from the Stopped-Flow spectrophotometer showing a single exponential fit for the reaction between <b>PdL1</b> and <b>TU</b> in ultra-pure water followed at 295 nm, I = 0.1 M at 298 K.....	49
<b>Figure 3. 7:</b> Dependence of $k_{obs}$ on the concentration of the entering nucleophiles for the displacement of chloride on <b>PdL4</b> complex in water, I = 0.1 M (LiCl), T = 298 K. ....	50
<b>Figure 3. 8:</b> Plot of $\ln(k_2/T)$ against $1/T$ for the reaction of <b>PdL4</b> with the three nucleophiles at various temperatures in the temperature range 288 – 308 K. ....	52
<b>Figure 3. 9:</b> UV-Visible spectral changes for the reaction between <b>PdL1</b> and <b>DMTU</b> at 298 K, I = 0.1 M. ....	54
<b>Figure 3. 10:</b> Kinetic trace obtained from the UV-Vis spectrophotometer showing a single exponential fit for the reaction between <b>PdL1</b> and <b>DMTU</b> in ultra-pure water followed at 295 nm, I = 0.1 M at 298 K. ....	55
<b>Figure 3. 11:</b> Plots of $k_{obs}$ against concentration of the <b>PdL1</b> complex with <b>TU</b> , I = 0.1 M (LiCl), T = 298 K.....	56
<b>Figure 3. 12:</b> Plot of $\ln(k_2/T)$ against $1/T$ for the reaction of <b>PdL3</b> with the three nucleophiles at various temperatures in the temperature range 288 – 308 K. ....	58
<b>Figure 4. 1:</b> The ORTEP diagram of <b>Pd1</b> and <b>Pd2</b> with the thermal ellipsoids drawn at the 50% probability level.....	69
<b>Figure 5. 1:</b> Alternative biomolecules for further studies. ....	<b>Error! Bookmark not defined.</b>

## List of Schemes

<b>Scheme 3. 1:</b> Synthesis route of the ligands ( <b>L1 - L5</b> ) and their corresponding Pd(II) complexes ( <b>PdL1 - PdL5</b> ).....	36
<b>Scheme 3. 2:</b> Proposed stepwise substitution reaction with the thiourea nucleophiles.....	47
<b>Scheme 4. 1:</b> Synthesis of N-(4-bromophenyl) pyridine-2-carboxamide and corresponding Pd(II) complexes, <b>Pd1</b> and <b>Pd2</b> .....	67

## Abstract

The influence of structural as well as electronic properties of bidentate N,N chelates with different substituents on the mononuclear Pd(II) complexes were investigated. The complexes were synthesized and characterized by various spectroscopic methods such as  $^1\text{H}$  &  $^{13}\text{C}$  NMR, FT-IR, LC-MS, CHN and single x-ray crystallography. For the first set of complexes (Chapter 3), we studied the unexplored kinetics and mechanistic behaviour of *N,N'*-pyridyl Pd(II) complexes, viz. dichloro-(*N*-((pyridin-2-yl)methyl)aniline)palladium(II) (**PdL1**), dichloro-(4-fluoro-*N*-((pyridin-2-yl)methyl)aniline)-palladium(II) (**PdL2**), dichloro-(4-bromo-*N*-((pyridin-2-yl)methyl)aniline)-palladium(II) (**PdL3**), dichloro-(4-methoxy-*N*-((pyridin-2-yl)methyl)aniline)-palladium(II) (**PdL4**) and dichloro-(4-ethyl-*N*-((pyridin-2-yl)methyl)aniline)-palladium(II) (**PdL5**). The substitution behaviour of coordinated chloride atoms by three bio-relevant thiourea nucleophiles, viz. thiourea (**TU**), *N,N'*-dimethylthiourea (**DMTU**) and *N,N,N',N'*-tetramethylthiourea (**TMTU**), of different steric demands was studied in a 0.1 M solution of ultra-pure water under *pseudo*-first order conditions. The reactions were studied as a function of concentration and temperature using standard Stopped-Flow and UV-Vis spectrophotometric technique. The substitution of the chloride atoms from the Pd metal by thiourea nucleophiles was a two-step reaction where the chloride *trans* to the pyridine ligand was substituted first, since the pyridine has a stronger *trans* effect compared to the amine group. The reactivity of mononuclear Pd(II) complexes containing bidentate N,N'-donor ligands with different substituents depends on the electronic effects of the complexes. The reactivity of the complexes increased with the presence of electron withdrawing substituents and decreased when an electron donating group was attached on the *para* position of the aniline moiety. The electron withdrawing groups influence the pull of electrons from the electron deficient amine that is coordinated to the metal center which results in the loss of electron density from the ligand moiety and increases the electrophilicity of the metal center and thus the substitution reaction. The reactivity of the nucleophiles depends on steric effects, with the bulky **TMTU** being the least reactive. The negative entropies and second order kinetics for all the substitution reactions support an associative mode of substitution mechanism. DFT calculations were performed to account for the observed reactivity of all the complexes studied.

For the second set of novel Pd(II) complexes (Chapter 4), viz. bis[N-(4-bromophenyl)pyridine-2-carboxamidato] Palladium (**Pd1**) and Palladium(II) [N-(4-bromophenyl)-2-pyridinecarboxamide], pyridine chloride (**Pd2**), crystals were obtained and the structures were studied. **Pd1** crystallizes in the monoclinic crystal system and in the P21/c space group, and **Pd2** crystallizes in the orthorhombic system, with the space group Pbcu.

# CHAPTER 1

## 1. Introduction

### 1.1 The Development of Cancer

Cancer remains one of the greatest threats to increased human life expectancy in the 21<sup>st</sup> century.<sup>1</sup> It is ranked the number one cause of death in developed countries and the second leading cause of death in developing countries.<sup>2</sup> According to a 2021 report by the World Health Organization (WHO), cancer claimed the lives of nearly 10 million people in 2020 alone. Of these deaths, the most common were caused by cancer of the lung (1.8 million), colorectum (935 thousand), liver (830 thousand), stomach (768 thousand), breast (684 thousand), esophagus (544 thousand), pancreas (466 thousand) and prostate (375 thousand) cases.<sup>3</sup>

Cancer is a group of *chronic or acute* diseases characterized by an uncontrollable growth in normal cells, leading to the formation of a tissue mass of cells known as a tumor.<sup>4</sup> The primary tumor can be life-threatening by obstructing vessels or organs and disrupting their function. If diagnosed early, this initial tumor can be treated through local surgery, aided by a combination of other methods such as chemotherapy, radiotherapy, or vaccine-related treatments. This type of tumor is usually benign as it remains confined to its location of origin.<sup>4-6</sup>

The most common cause of death is usually metastasis, the spread of the primary tumor throughout the body *via* the circulatory or lymphatic systems to vital body organs, establishing secondary tumors.<sup>5</sup> During the process of metastasis, the tumor cells can penetrate through the walls of lymphatic vessels and distribute to draining lymph nodes or directly invade the thin walls of the blood capillaries and spread to far-reaching sites in the body. Furthermore, tumors can also spread across body cavities *via* organs. This type of tumour cell is known as malignant, and its ability to distribute throughout the body makes local surgery infeasible.<sup>4-6</sup>

The cloning of cancerous cells and their proliferation is a multistep process in which cells undergo a series of changes that gradually become malignant.<sup>5</sup> This process, known as tumorigenesis, commences from tumor initiation, a result of genetic alteration leading to abnormal proliferation of a single cell and clinical derivation of tumor cells. With additional mutations occurring in the cell, the population of tumor cells increases; this stage is typically known as tumor progression.<sup>5, 6</sup> Only a slow rise in the rate of cancer cell proliferation is required to outgrow the average cell population. It is worth noting that tumor progression

depends on the type of tissue or organ; for example, organs such as the bone marrow account for cell loss by a high rate of cell division.<sup>6</sup> In contrast, the adult tissue of the liver typically maintains a steady number of cells and therefore, the gradual growth in population of cancerous cells rapidly exceeds that of normal cells.

## **1.2 Causes of Cancer**

Biomedical research has revealed that proliferation is a common characteristic of all cancers. However, the etiology of these diseases can be explained by various theories attributed to internal, external, or hereditary factors. Mutations cause majority of cancers, and changes in DNA, i.e., addition or loss of DNA, or alternate epigenetics.<sup>5,6</sup>

There are two types of genetic mutations: point mutation and translocation mutations.<sup>5</sup> The former is when only one base of a DNA sequence is altered, resulting in a new codon that encodes for a specific (incorrect) amino acid at a corresponding protein position. Translation mutation involves the movement of an entire gene from one chromosome to another. Cancer genesis may occur if the proteins corresponding to these specific altered DNA sequences are crucial in the control of cell growth.<sup>6</sup>

In humans, mutations often arise from external factors such as virus or bacterial infections, exposure to chemicals (such as tobacco smoke, or asbestos), potent carcinogens (such as exhaust fumes) and harmful radiation (including alpha, beta and gamma rays).<sup>7,8</sup> Additionally, several genes have been identified that, if inherited, can potentially form certain types of cancer. An example would be BRCA1 and BRCA2, genes closely associated with breast cancer, which can be inherited from one generation to the next.<sup>5</sup>

## **1.3 Treatment of Cancer**

Treatment of cancer often involves a combination of methods and approaches, depending on the type and stage of cancer, and most crucially, the location of the cancerous cells.<sup>5</sup> To date, the main treatments are surgery, chemotherapy, and radiotherapy, while other less common treatments such as biochemical therapy, photodynamic therapy (PDT), and antibody-related treatments are being employed.<sup>9-12</sup> Primarily, localized tumors are surgically removed, followed by chemotherapy or radiotherapy to remove the cancerous cells from the affected tissue.

Chemotherapy involves using drugs to destroy tumors or at least prevent proliferation of cancerous cells.<sup>5</sup> This method affords better effects, as the drugs can access multiple sites in the body. However, cancer is complex, and each type is distinct.<sup>5, 6</sup> As such, no single chemical drug with a broad spectrum can actively cure all cancer types. Consequently, cancer treatment remains a monumental task as the commonly used methods are often associated with resistance.<sup>13</sup> Such drawbacks have encouraged efforts towards the design of metal-based drugs as potential antitumor agents.

## 1.4 Use of Metals in Cancer Treatment

The use of inorganic complexes in cancer chemotherapy stems from Barnett Rosenberg's discovery of cis-diamminedichloroplatinum(II), commonly known as *cisplatin*, in 1969 (**Figure 1.2a**).<sup>14</sup> To date, *cisplatin* is the most prestigious anticancer drug used for the treatment of ovarian, testicular, lung and cervical cancers, among others.<sup>15-18</sup>

### 1.4.1 Mechanism of Action of Pt-based Drugs

Anti-cancer drugs have different mechanisms by which they interfere with cancer cell growth. Research focused on *cisplatin's* molecular mechanism of action has assisted researchers in understanding how the drug terminates cancerous cells. It has also been reported that the mode of function of *cis*-Pt based anti-cancer complexes resemble that of *cisplatin*.<sup>19</sup> These drugs are known as DNA interactive agents, they interfere with DNA processing by forming DNA adducts, inter- and intrastrand crosslinks, and DNA-protein crosslinks, which ultimately leads to programmed cell death, apoptosis, through initiation of major signaling pathways.<sup>20</sup>

*Cisplatin* is typically administered through the veins instead of ingestion through the acidic gastrointestinal tract to prevent premature hydrolysis. The blood plasma contains high concentrations of chloride ions, approximately 100 mM, and these conditions aid the neutral *cisplatin* complex to reach its target unaltered.<sup>20</sup> Upon absorption into the cancer cell through passive and active diffusion, *cisplatin* undergoes hydrolysis to form a positively charged aqua species. This is due to low concentration of the chloride ions, ~ 4 mM, which results in the loss of one or both chloride ligands.<sup>21, 22</sup> Inside the cell, the platinum complex encounters numerous biomolecules with a strong affinity for the platinum center, including sulfur donors such as thiols and thioethers. Some of the Pt(II) complex may interact with these molecules to form kinetically stable platinum-sulfur bonded adducts.<sup>23</sup> However, at neutral pH, the positively

charged platinum complex preferably binds with nucleophilic nitrogenous sites of DNA which have less hindrance. The binding of the complex to nitrogen is expected since platinum is a soft metal and therefore have a strong affinity for hard bases such as nitrogen. *Cisplatin* preferably binds to the N7 atoms of guanine and adenine, although the N1 of adenine and the N3 atom of cytosine are also suitable binding sites.<sup>24</sup> The N7 atom of guanine has shown to be the most preferred coordinate site due to accessibility, strong basicity, and the intermolecular hydrogen bond interactions between the N-H proton of *cisplatin* with O6 atom of guanine. This interaction stabilize the binding of Pt(II) complex to the N7 site and consequently, this N7-Pt binding is proposed to be responsible for the antitumor activity of *cisplatin*.<sup>25, 26</sup> The N1 of adenine and the N3 of cytosine are primarily involved in DNA base pairing and therefore, these sites are less likely available for metal binding.<sup>27</sup>

The interaction of *cisplatin* with DNA leads to the formation of DNA-Pt adducts, including interstrand, intrastrand and intramolecular crosslinks (**Figure 1.1**).<sup>24</sup> The most prominent platination is the intrastrand crosslinks between two neighboring deoxyguanosines (GG) which accounts for 65% of all DNA adducts. Intrastrand crosslinks at the AG sequence form about 20% DNA adducts. However, no adducts are observed at the GA sequence. Additionally, a cross-link between two deoxyguanosines separated by a third nucleoside, the GNG sequence, forms about 9% of DNA adducts.<sup>24</sup> Furthermore, DNA interstrand crosslinks have been found to exist between two deoxyguanosines,.However, this rarely occurs as it leads to the twisting of the DNA structure and may only occur when an alternate purine is not in proximity on the same strand and thus only accounts for 1% of the DNA adducts.<sup>24</sup> One other adduct has been observed to form a crosslink between deoxyguanosine and glutathione.<sup>24</sup> Although the mechanism of toxicity of these DNA adducts is still vaguely understood, it is generally accepted that the adducts inhibit DNA replication or suppress DNA transcription by distortion through unwinding, bending, and flattening the minor grooves of the superhelix, and shortening of the double helix, which ultimately induces cell death by apoptosis.<sup>22, 28</sup>

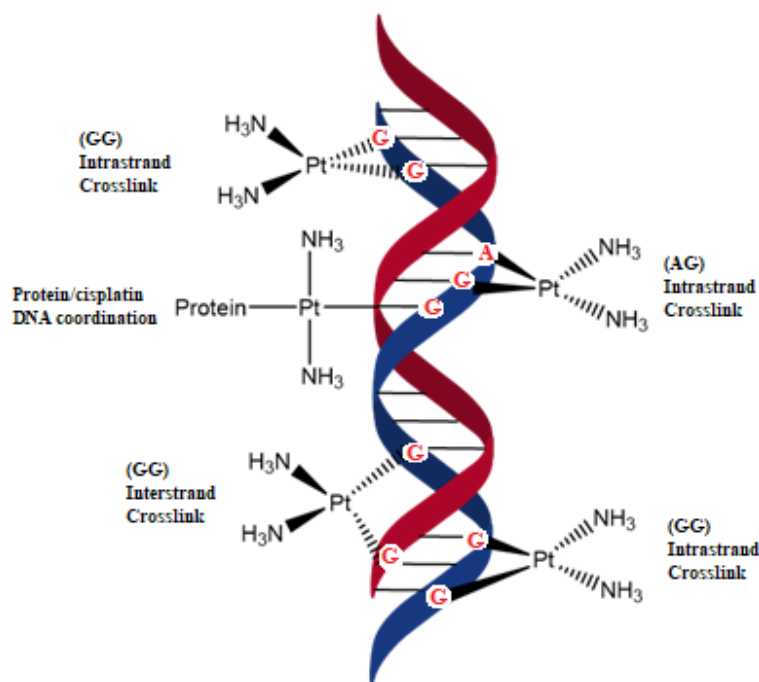


**Figure 1.1:** Different DNA-Pt adducts formed from the interaction of cisplatin with DNA.<sup>29</sup>

#### 1.4.2. Drawbacks of *Cisplatin*

Despite the use of *cisplatin* as the leading anti-cancer drug for over five decades, its efficacy is primarily compromised by inherent and acquired resistance, and severe side effects including neurotoxicity, nephrotoxicity, gastrointestinal toxicity, nausea, and vomiting.<sup>30,31</sup> Many factors contribute to these side effects, including the aquation of the *cisplatin* complex in the blood plasma before diffusion into the cytoplasm, which could lead to an aqua species that is likely to react with non-target cells. This nonspecific attack may lead to toxicity of the drug.<sup>20</sup> However, this can be controlled by high concentrations of chloride ions.

Another factor is the binding of the Pt(II) complex to sulfur containing thiols, forming stable Pt-S bonds, which are inert and considered one of the causes of the development of resistance. In instances where these inert Pt-S compounds are bound to an amino residue of proteins, they are responsible for the acute side effects.<sup>32-34</sup> As a consequence, Pt(II) drugs are usually administered with chemo protecting agents which are S-containing compounds such as thiourea (Tu), cysteine, biotin, glutathione and amifostine. Most of the severe side effects are linked with administration and the lack of selectivity of the drug.<sup>34</sup>

The discovery of *cisplatin* and the side effects associated with the drug has since led to the design of numerous platinum analogues of this drug such as *carboplatin* (*cis*-diammine(cyclobutane-1,1-dicarboxylate-O,O')platinum(II)) (**b**), *oxaliplatin* (*trans*-R,R-

cyclohexane-1,2-diamine](ethanedioato-O,O')platinum(II)) (c) and *satraplatin* (bis-acetato-amine-dichloro-cyclohexylamine-platinum(IV)) (d) (Figure 1.2).<sup>32</sup> *Carboplatin* is a second-generation Pt(II) based anticancer drug effectively used in the treatment of ovarian cancer and has shown fewer side effects than *cisplatin*.<sup>35</sup> *Oxaliplatin* is used to treat colon and rectum cancer and has been observed to be applicable at a broader spectrum than *cisplatin*. The drug *satraplatin* is still in development stages with potential to improve oral administration of anticancer drugs and to treat patients with prostate cancer.<sup>32,35</sup> Despite these efforts, researchers have a challenge in the design and synthesis of metal-based drugs with better efficacy, improved application spectrum, and limited solubility with reduced toxicity.

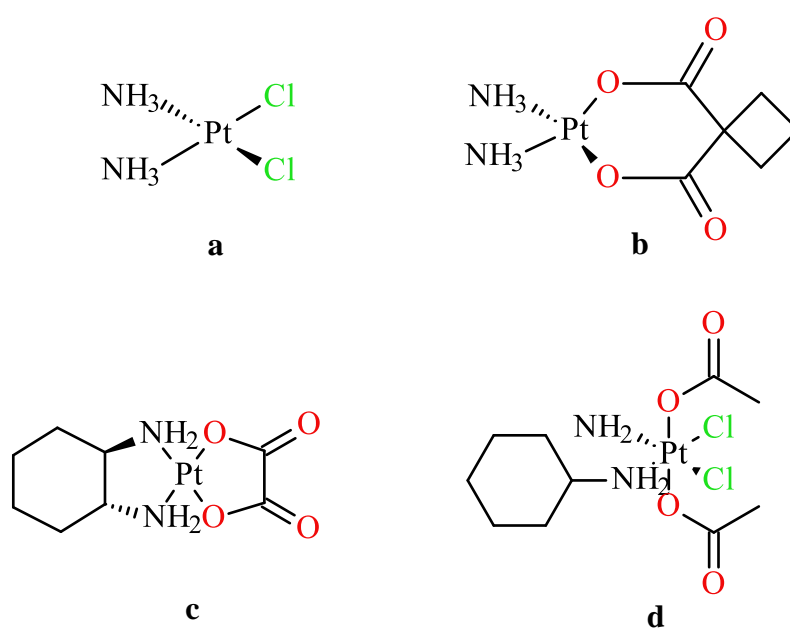


**Figure 1.2:** Cisplatin and follow-up platinum-based anticancer drugs.<sup>32</sup>

Amongst others, complexes of transition metals such as gallium, copper, ruthenium, gold, and palladium have shown the most promising anti-cancer activity.<sup>36-40</sup> Considering the structural similarities between Pt(II) and Pd(II), there has been enormous interest in the study of Pd(II) complexes as potential anticancer drugs.<sup>41</sup> Therefore, the subsequent subsection reviews some of the synthesized palladium complexes and their activity against cancerous cells in comparison to cisplatin and other Pt-based drugs commercially used worldwide.

### 1.5 Use of Pd(II) Complexes in Cancer Treatment

The structural and coordination behavior of Pd(II) complexes closely resemble that of their Pt(II) analogues, on these basis, researchers have pursued the design of Pd(II) compounds as

alternative drugs in cancer treatment.<sup>42</sup> It has been reported that some Pd(II) complexes have significant anticancer activity, with reduced side effects and better solubility when compared to clinically used therapeutic drugs. The challenge, however, has been the rapid aquation and ligand exchange rates in Pd(II) complexes, which is about  $10^5$  faster than their Pt(II) analogues.<sup>43</sup> This drawback has been observed particularly when comparing the activity of *cisplatin* and that of *cispalladium*, *cis*-[Pd(NH<sub>3</sub>)<sub>2</sub>Cl<sub>2</sub>], which does not show any antitumor activity.<sup>44</sup> The Pd(II) analogue undergoes rapid hydrolysis *in vivo*, through interaction with other biomolecules in the cell which prevents it from reaching its target DNA. An effort has been made to develop Pd(II) complexes with slower rates of hydrolysis through the coordination of the metal to different types of ligands and suitable leaving groups.<sup>45</sup> In general, the design of palladium based antitumor drugs follows the same strategies used in the synthesis of platinum drugs, which aids in understanding the mechanism and activity of palladium analogs.<sup>46</sup>

### 1.5.1 Mononuclear Palladium Complexes

Palladium(II) complexes in which a single Pd(II) central atom is coordinated with monodentate or multidentate ligands are generally known as mononuclear palladium(II) complexes. Multidentate (bi- and tridentate) ligands have attracted considerable attention due to their ability to easily influence the stability of the Pd atom through their steric and electronic properties.<sup>47</sup> Furthermore, the structural diversity of these ligands allows them to possess biological properties that influence reaction pathways. A wide variety of neutral multidentate ligands have been employed to stabilize Pd(II) complexes and maintain their structural integrity long enough to reach their targets *in vivo*.<sup>46</sup>

### 1.5.2 Mononuclear Nitrogen Containing Pd(II) Complexes

The rapid hydrolysis of *cis*-palladium complexes, such as *cis*-[Pd(NH<sub>3</sub>)<sub>2</sub>Cl<sub>2</sub>] and the related *cis*-[Pd(dach)Cl<sub>2</sub>], and hence their inactivity against cancerous cells have advocated for the design of Pd(II) complexes with aromatic chelating ligands to impose the *cis*-coordination of the leaving groups.<sup>48</sup> The introduction of aromatic N-containing ligands such as pyridine, imidazole, and 1,10-phenanthroline, and their derivatives to antitumor agents has drawn attention.<sup>19</sup> Nitrogen-containing donor ligands exhibit distinct advantages over other coordinate systems, due to their accessibility and strong chelating properties. As such, a class of mononuclear complexes with the general formula [Pd(en)Cl(L)]NO<sub>3</sub> (**Figure 1.3**), where en

is ethylenediamine; L is the N-chelate ligand (pyridine) which has varying substituents on the *para* position. This class of Pd(II) complexes were reported by Zhao *et. al.* and indicated significant cytotoxicity activity against the human leukemia cell line HL-60.<sup>49</sup> A trend was also observed with the change in the substituent, from H, CH<sub>3</sub>, OH, to NH<sub>2</sub>. The increase in electron donor strength consequently increases the affinity of the nitrogen atom of the pyridine ligands to the palladium center, thereby resulting in a pronounced decrease of the cytotoxic activities of the palladium complexes.<sup>49</sup>

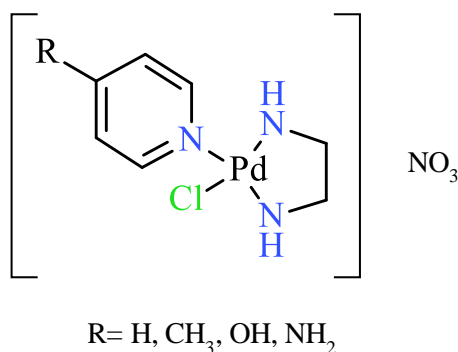


**Figure 1.3:** Mononuclear ethylenediamine-palladium(II) complexes with different substituents on the pyridine.<sup>49</sup>

In attempts to further slowdown the rate of hydrolysis of Pd(II) complexes, bulky monodentate spectator ligands have been utilized to exploit their electronic and steric effects. It has been observed that complexes of this type of ligands tend to adopt a *trans*-geometry, which is different from the *cisplatin* analogue. One of the early examples was put forward by Tusek-Bozic *et. al.* through the synthesis of the Pd complexes, *trans*-[PdCl<sub>2</sub>(2-dqmp)] (**Figure 1.4 e**).<sup>50</sup> Monoethylphosphonate and diethylphosphonate moieties on the quinolmethyl substructure were introduced on these complexes, yielding better solubility of the corresponding complexes. A comparative study revealed that the diethylphosphonate moiety outperformed its monoethylphosphonate analog, the better activity was attributed to the easy dissociation of the chloride ligands from the metal center.<sup>47</sup> This work laid the foundation for designing *trans*-palladium complexes as potential anticancer drugs.

As an extension to the above study, the same group synthesized *trans*-Pd(II) complexes of diethyl and dibutyl esters of ( $\alpha$ -anilino-N-benzyl) phosphonic acid and [ $\alpha$ -(4-benzeneazoanilino)-N-benzyl]phosphonic acid (**Figure 1.4 f, g**). These complexes were studied against KB cell line29 and L1210 cell line and exhibited comparable cytostatic activity to *cisplatin* and the quinolmethylphosphonate ester was found to have better cytotoxicity. The

improvements were due to the presence of N-bonded hydrogen suitable for hydrogen bonding, resulting in potent binding to the nucleic acid fragments.<sup>51</sup>

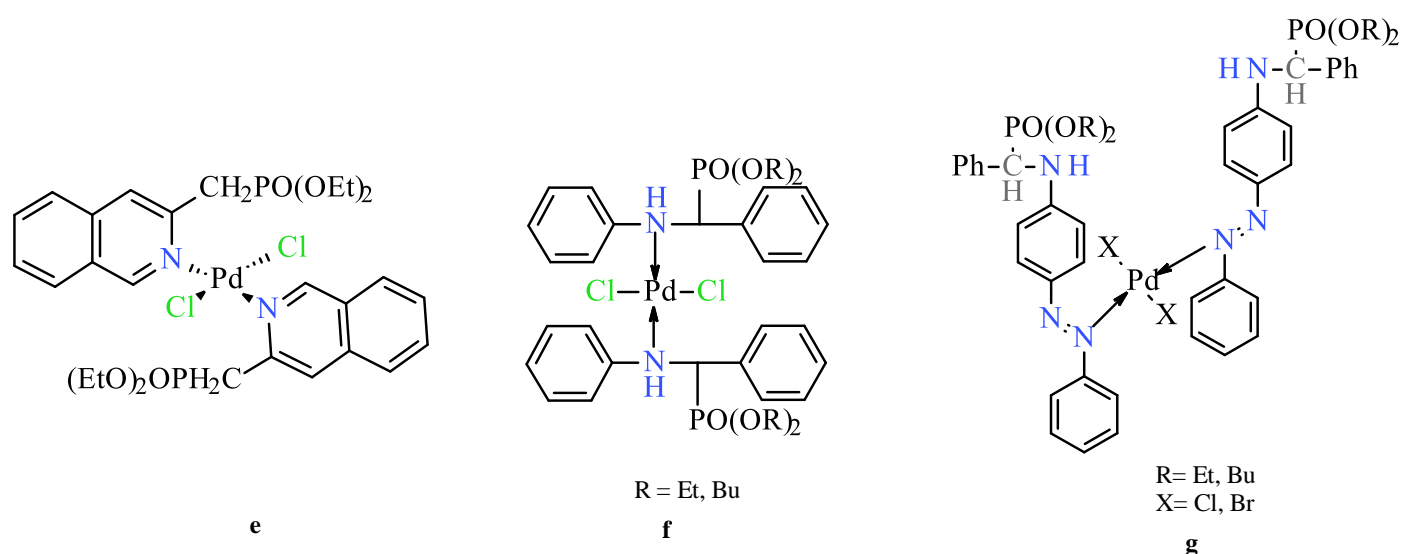


**Figure 1.4:** *trans*-Palladium bis(quinonyl-phosphonate) and the quinolmethylphosphonate ester complexes as early examples of Pd(II) anticancer complexes.<sup>50, 51</sup>

Notable anticancer activity by *trans*-palladium complexes has been observed. However, the structure - activity relationship of Pt(II) anticancer agents stipulates that the *cis*-geometry is a necessary requirement for anticancer activity. As such, attempts have been made to either obtain Pd(II) complexes with a *cis*-geometry or coordinate the metal ion to bidentate ligands to decrease the *cis-trans* isomerism effects.

### 1.5.3 N’N Bidentate Pd(II) Complexes

The coordination of N’N chelate ligands to the Pd(II) metal centre has been shown to decrease the *cis-trans* isomerism. N,N-coordinate bidentate systems typically involves a 2,2'-bipyridyl substructure, substituted ethylene diamine or other nitrogen-containing mixed heterocyclic compounds.<sup>52</sup> Ligands such as 2,2'-bipyridyls have attracted considerable attention due to their natural occurrence in molecules such as caerulomycins or collismycin.<sup>53</sup> Similarly, 1,10-phenanthroline exhibits the same characteristics but also has distinct properties such as rigidity and entropically-favored chelation with different metal ions.<sup>53</sup>

The bidentate properties of substituted-bipyridines and phenanthroline were first exploited by Newkome and co-workers (**Figure 1.5**).<sup>54</sup> The ligands were later modified to change their coordination mode from bidentate to tri- and tetradentate. Studies were performed by binding the complexes to Phage PM2 DNA with aims to understand their interactions based on the

difference in the ligand backbone. A significant difference in the level of DNA binding was observed for tetradentate ligands, even at lower concentration, as compared to other ligands. Although cytotoxicity studies were not conducted on these complexes, these DNA binding results paved a way for developments in this area.<sup>47, 54</sup>

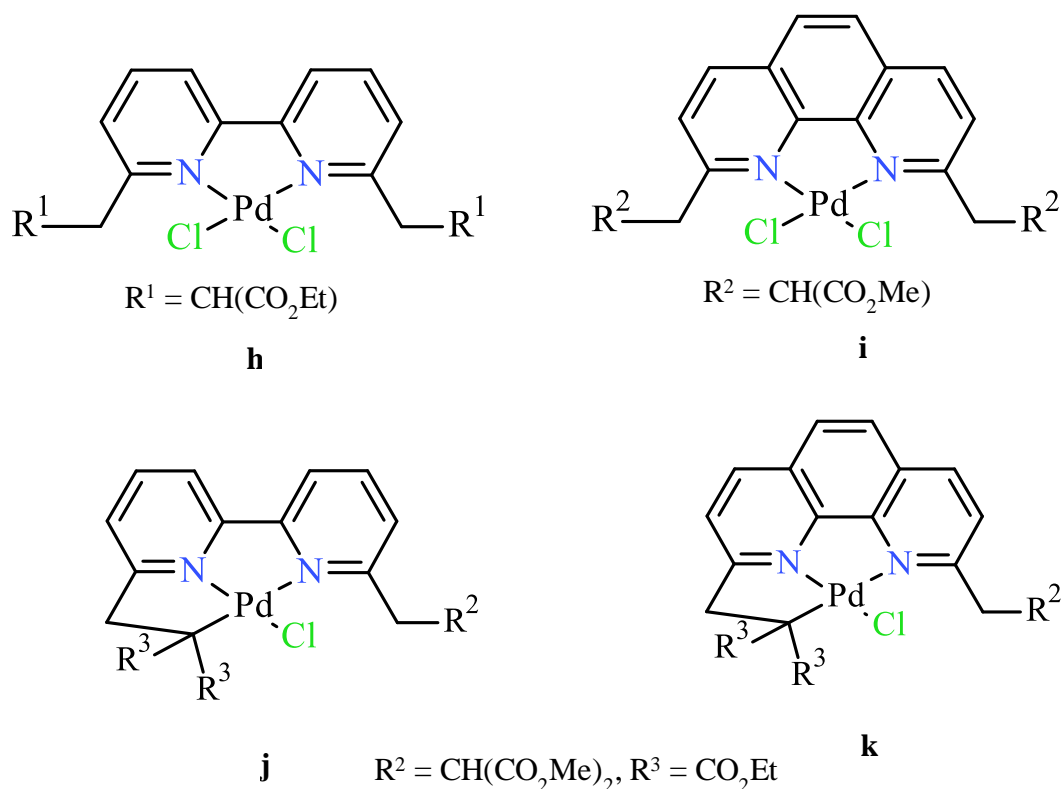


**Figure 1.5:** Bipyridine and phenanthroline based palladium complexes for binding with phage PMA2 DNA.<sup>54</sup>

Many Pd(II) complexes have shown similar or even better anticancer activities than *cisplatin* and other Pt(II) analogues. However, the application of these complexes as pharmaceuticals is still limited. Thus, this area of research is still developing, and further studies are still required, particularly on the mode of action of these complexes against cancer cell lines. A mechanistic understanding of these complexes' targets would aid in the design of more efficient Pd-based drugs. In-depth kinetics and mechanistic studies of palladium complexes would assist in understanding the influence of the spectator ligands on the activity of these complexes. These studies would also aid in understanding the interactions between Pd(II) complexes and sulfur containing biomolecules and DNA, however, the area remains barely explored.

## 1.6 References

1. Hong, Z.; Zan, X.; Yu, T.; Hu, Y.; Gou, H.; Zheng, S.; Gao, X.; Zhou, P., Local delivery of superagonist gene based on polymer nanoparticles for cancer immunotherapy. *Chinese Chemical Letters* **2022**.
2. Organization, W. H., *World health statistics 2008*. World Health Organization: **2008**.
3. Piñeros, M.; Mery, L.; Soerjomataram, I.; Bray, F.; Steliarova-Foucher, E., Scaling up the surveillance of childhood cancer: a global roadmap. *JNCI: Journal of the National Cancer Institute* **2021**, *113* (1), 9-15.
4. Yadav, A. R.; Mohite, S. K., Cancer-A silent killer: An overview. *Asian Journal of Pharmaceutical Research* **2020**, *10* (3), 213-216.
5. Thurston, D. E.; Pysz, I., *Chemistry and pharmacology of anticancer drugs*. CRC press: **2021**.
6. Patrick, G. L., *An introduction to medicinal chemistry*. Oxford university press: **2013**.
7. Parkin, D. M.; Boyd, L.; Walker, L., 16. The fraction of cancer attributable to lifestyle and environmental factors in the UK in 2010. *British journal of cancer* **2011**, *105* (2), S77-S81.
8. Lewandowska, A. M.; Rudzki, M.; Rudzki, S.; Lewandowski, T.; Laskowska, B., Environmental risk factors for cancer-review paper. *Annals of Agricultural and Environmental Medicine* **2018**, *26* (1), 1-7.
9. DeVita Jr, V. T.; Chu, E., A history of cancer chemotherapy. *Cancer research* **2008**, *68* (21), 8643-8653.
10. Baskar, R.; Lee, K. A.; Yeo, R.; Yeoh, K.-W., Cancer and radiation therapy: current advances and future directions. *International journal of medical sciences* **2012**, *9* (3), 193.
11. Gubin, M. M.; Zhang, X.; Schuster, H.; Caron, E.; Ward, J. P.; Noguchi, T.; Ivanova, Y.; Hundal, J.; Arthur, C. D.; Kribber, W.-J., Checkpoint blockade cancer immunotherapy targets tumour-specific mutant antigens. *Nature* **2014**, *515* (7528), 577-581.
12. Vahrmeijer, A. L.; Hutteman, M.; Van Der Vorst, J. R.; Van De Velde, C. J.; Frangioni, J. V., Image-guided cancer surgery using near-infrared fluorescence. *Nature reviews Clinical oncology* **2013**, *10* (9), 507-518.
13. Enriquez-Navas, P. M.; Gatenby, R. A., Evolutionary strategies to overcome cancer cell resistance to treatment. In *Phenotypic Switching*, Elsevier: **2020**; pp 691-703.
14. Rosenberg, B.; Van Camp, L.; Krigas, T., Inhibition of cell division in Escherichia coli by electrolysis products from a platinum electrode. *Nature* **1965**, *205* (4972), 698-699.
15. Ozols, R. F.; Young, R. C. In *High-dose cisplatin therapy in ovarian cancer*, Seminars in oncology, 1985; pp 21-30.
16. de Vries, G.; Rosas-Plaza, X.; van Vugt, M. A.; Gietema, J. A.; de Jong, S., Testicular cancer: Determinants of cisplatin sensitivity and novel therapeutic opportunities. *Cancer Treatment Reviews* **2020**, *88*, 102054.
17. O'Grady, S.; Finn, S. P.; Cuffe, S.; Richard, D. J.; O'Byrne, K. J.; Barr, M. P., The role of DNA repair pathways in cisplatin resistant lung cancer. *Cancer treatment reviews* **2014**, *40* (10), 1161-1170.
18. Lorusso, D.; Petrelli, F.; Coinu, A.; Raspagliesi, F.; Barni, S., A systematic review comparing cisplatin and carboplatin plus paclitaxel-based chemotherapy for recurrent or metastatic cervical cancer. *Gynecologic oncology* **2014**, *133* (1), 117-123.

19. Zhao, G.; Lin, H., Metal complexes with aromatic N-containing ligands as potential agents in cancer treatment. *Current Medicinal Chemistry-Anti-Cancer Agents* **2005**, *5* (2), 137-147.
20. Fuertes, M.; Castilla, J.; Alonso, C.; Prez, J., Cisplatin biochemical mechanism of action: from cytotoxicity to induction of cell death through interconnections between apoptotic and necrotic pathways. *Current medicinal chemistry* **2003**, *10* (3), 257-266.
21. Judson, I.; Kelland, L. R., New developments and approaches in the platinum arena. *Drugs* **2000**, *59* (4), 29-36.
22. Jamieson, E. R.; Lippard, S. J., Structure, recognition, and processing of cisplatin–DNA adducts. *Chemical reviews* **1999**, *99* (9), 2467-2498.
23. Reedijk, J., Why does cisplatin reach guanine-N7 with competing S-donor ligands available in the cell? *Chem Rev* **1999**, *99*, 2499-2510.
24. Lippert, B., Impact of Cisplatin on the recent development of Pt coordination chemistry: a case study. *Coordination chemistry reviews* **1999**, *182* (1), 263-295.
25. Teuben, J.-M.; Reedijk, J., Reaction of DNA oligonucleotides with [Pt (dien) GSMe] 2+(GSMe= S-methylated glutathione) and cis-[Pt (NH<sub>3</sub>)<sub>2</sub> (GSMe)<sub>2</sub>] 2+: evidence of oligonucleotide platinumation via sulfur-coordinated platinum intermediates. *JBIC Journal of Biological Inorganic Chemistry* **2000**, *5* (4), 463-468.
26. Zaki, M.; Arjmand, F.; Tabassum, S., Current and future potential of metallo drugs: Revisiting DNA-binding of metal containing molecules and their diverse mechanism of action. *Inorganica Chimica Acta* **2016**, *444*, 1-22.
27. Eastman, A., The mechanism of action of cisplatin: from adducts to apoptosis. *Cisplatin: chemistry and biochemistry of a leading anticancer drug* **1999**, 111-134.
28. Marques, M., Platinum and palladium polyamine complexes as anticancer agents: the structural factor. *International Scholarly Research Notices* **2013**.
29. Wang, Z.; Zhu, G., DNA Damage Repair Pathways and Repair of Cisplatin-Induced DNA Damage. **2018**.
30. Qi, L.; Luo, Q.; Zhang, Y.; Jia, F.; Zhao, Y.; Wang, F., Advances in toxicological research of the anticancer drug cisplatin. *Chemical research in toxicology* **2019**, *32* (8), 1469-1486.
31. Chu, E.; Sartorelli, A., Cancer chemotherapy. *Lange's Basic and Clinical Pharmacology* **2018**, 948-976.
32. Pinato, O.; Musetti, C.; Sissi, C., Pt-based drugs: the spotlight will be on proteins. *Metallomics* **2014**, *6* (3), 380-395.
33. Bugarčić, Ž. D.; Bogojeski, J.; van Eldik, R., Kinetics, mechanism and equilibrium studies on the substitution reactions of Pd (II) in reference to Pt (II) complexes with bio-molecules. *Coordination Chemistry Reviews* **2015**, *292*, 91-106.
34. Bugarčić, Ž. D.; Bogojeski, J.; Petrović, B.; Hochreuther, S.; van Eldik, R., Mechanistic studies on the reactions of platinum (II) complexes with nitrogen-and sulfur-donor biomolecules. *Dalton Transactions* **2012**, *41* (40), 12329-12345.
35. Bond, G.; Hartley, F., Chemistry of the platinum group metals: recent developments. Elsevier, Amsterdam: **1991**.
36. Chitambar, C. R., Gallium complexes as anticancer drugs. *Met. Ions Life Sci* **2018**, *18*, 281-302.
37. Santini, C.; Pellei, M.; Gandin, V.; Porchia, M.; Tisato, F.; Marzano, C., Advances in copper complexes as anticancer agents. *Chemical reviews* **2014**, *114* (1), 815-862.
38. Lee, S. Y.; Kim, C. Y.; Nam, T.-G., Ruthenium complexes as anticancer agents: A brief history and perspectives. *Drug Design, Development and Therapy* **2020**, *14*, 5375.

39. Lu, Y.; Ma, X.; Chang, X.; Liang, Z.; Lv, L.; Shan, M.; Lu, Q.; Wen, Z.; Gust, R.; Liu, W., Recent development of gold (I) and gold (III) complexes as therapeutic agents for cancer diseases. *Chemical Society Reviews* **2022**.
40. Hussaini, S. Y.; Haque, R. A.; Razali, M. R., Recent progress in silver (I)-, gold (I)/(III)-and palladium (II)-N-heterocyclic carbene complexes: A review towards biological perspectives. *Journal of Organometallic Chemistry* **2019**, 882, 96-111.
41. Onunga, D. O. Controlling the reactivity of mononuclear palladium (II) complexes. Substitution kinetics and mechanisms. **2019**.
42. Montana, A. M.; Batalla, C., The rational design of anticancer platinum complexes: the importance of the structure-activity relationship. *Current medicinal chemistry* **2009**, 16 (18), 2235-2260.
43. Abu-Surrah, A. S.; Kettunen, M., Platinum group antitumor chemistry: design and development of new anticancer drugs complementary to cisplatin. *Current medicinal chemistry* **2006**, 13 (11), 1337-1357.
44. Wimmer, F.; Wimmer, S.; Castan, P.; Cros, S.; Johnson, N.; Colacio-Rodriguez, E., The antitumor activity of some palladium (II) complexes with chelating ligands. *Anticancer research* **1989**, 9 (3), 791-793.
45. Lazarević, T.; Rilak, A.; Bugarčić, Ž. D., Platinum, palladium, gold and ruthenium complexes as anticancer agents: Current clinical uses, cytotoxicity studies and future perspectives. *European journal of medicinal chemistry* **2017**, 142, 8-31.
46. Jahromi, E. Z.; Divsalar, A.; Saboury, A. A.; Khaleghizadeh, S.; Mansouri-Torshizi, H.; Kostova, I., Palladium complexes: new candidates for anti-cancer drugs. *Journal of the Iranian Chemical Society* **2016**, 13 (5), 967-989.
47. Kapdi, A. R.; Fairlamb, I. J., Anti-cancer palladium complexes: a focus on PdX<sub>2</sub>L<sub>2</sub>, palladacycles and related complexes. *Chemical Society Reviews* **2014**, 43 (13), 4751-4777.
48. Abu-Surrah, A. S.; Al-Sa'doni, H. H.; Abdalla, M. Y., Palladium-based chemotherapeutic agents: routes toward complexes with good antitumor activity. *Cancer therapy* **2008**, 6 (6), 1-10.
49. Zhao, G.; Lin, H.; Ping, Y.; Sun, H.; Zhu, S.; Xuncheng, S.; Chen, Y., Ethylenediamine-palladium (II) complexes with pyridine and its derivatives: synthesis, molecular structure and initial antitumor studies. *Journal of inorganic biochemistry* **1999**, 73 (3), 145-149.
50. Tusek-Bozic, L.; Matijasic, I.; Bocelli, G.; Calestani, G.; Furlani, A.; Scarcia, V.; Papaioannou, A., *J. Chem. Soc., Dalton Trans.* **1991**.
51. Coluccia, M.; Nassi, A.; Loseto, F.; Boccarelli, A.; Mariggio, M., D. Giordano, FP Intini, P. Caputo, G. Natile. *J. Med. Chem* **1993**, 36, 510.
52. Mongin, F.; Trécourt, F.; Gervais, B.; Mongin, O.; Quéguiner, G., First synthesis of caerulomycin B. A new synthesis of caerulomycin C. *The Journal of Organic Chemistry* **2002**, 67 (10), 3272-3276.
53. Trécourt, F.; Gervais, B.; Mongin, O.; Le Gal, C.; Mongin, F.; Quéguiner, G., First syntheses of caerulomycin E and collismycins A and C. A new synthesis of caerulomycin A. *The Journal of Organic Chemistry* **1998**, 63 (9), 2892-2897.
54. Newkome, G. R.; Puckett, W. E.; Kiefer, G. E.; Gupta, V. K.; Fronczek, F. R.; Pantaleo, D. C.; McClure, G. L.; Simpson, J. B.; Deutsch, W. A., Chemistry of heterocyclic compounds series. 94. Square-planar cis- and trans-C-palladium (II) complexes of N electron-deficient heteroaromatic ligands. Ligand synthesis, complexation, and spectral analyses and complex interaction with phage PM2 DNA. *Inorganic Chemistry* **1985**, 24 (6), 811-826.

## CHAPTER 2

### 2.1 Substitution Reactions of Pd(II) Complexes

The lability of Pd(II) complexes is  $10^5$ -fold more than their Pt(II) analogues. Such high reactivities suggests that these complexes are ideal models for kinetic and mechanistic studies in the presence of sulfur and nitrogen donor biomolecules. Pd(II) complexes, like Pt(II) complexes, have a remarkably high affinity for sulfur and nitrogen donor ligands. Substitution reactions of these complexes are of fundamental importance for understanding their toxicity and anti-tumor activity, and predicting their possible interaction with the DNA.<sup>1</sup> Palladium complexes have shown that their reactivities depends on the ligand environment surrounding the metal center. The challenge to date is finding ligands that would stabilize specific oxidation states of the central Pd atom. These ligands crucially play an important role in modifying lability and lipophilicity, and imparting ligand exchange behavior.<sup>2</sup>

The study of mechanistic behavior of complexes involves their reaction with relevant S-/N-donor biological nucleophiles and monitoring of the substitution reaction. The rate of ligand substitution by nucleophiles can be influenced by many factors including the electronic properties of spectator, and labile ligands, the nucleophilicity and/or bulkiness of the incoming biomolecules, and the solvent system. The ligands' structural orientation influences the steric and chemical properties of the complex, hence its interaction with the labile ligands in substitution reactions. Studying substitution mechanism of complexes against model biomolecules assists in predicting their mechanistic behavior against DNA and other biomolecules in the human body.

#### 2.1.1 The Influence of Spectator Ligands on the Rate of Substitution in Pd(II) Complexes

The effect of spectator ligands on the rate of substitution was explored by Onunga *et al.*<sup>3-6</sup> by designing a series of Pd(II) complexes with varying electronic and steric properties. The substitution reactions of the Pd(II) complexes were studied with neutral thiourea nucleophiles. The results have shown that the substitution of the chloride ligand is controlled by the electrophilicity of the Pd(II) central atom, which is in turn influenced by the electronic and steric properties of the non-labile bulky ligands. For instance, the reactivity of palladium(II) complexes of pyrazolyl-based terpyridyl type of ligands was investigated.<sup>3</sup> The results showed that pyridine-based complexes had higher rates of substitution due to their compelling  $\pi$ -

acceptor character than the pyrazole-based (**Figure 2.1**). The pyrazole complexes with poor  $\pi$ -acceptor ability and the strong  $\sigma$ -donor effect caused by the pyrazolic N-atom were observed to have lower rates of substitution due to decreased ability of  $\pi$ -back bonding (**Figure 2.1 m, n**). The electron-donating or electron-withdrawing strength of the substituents on the ligand was also investigated.<sup>6</sup> A decrease in reactivity was observed for the Pd(II) complex with methyl groups, which donate electrons to the pyrazolic N-atom. This effect causes the electron rich -N, to accumulate excess electron density around the palladium(II) metal center and thus makes the metal less electrophilic (**Figure 2.1 o**).

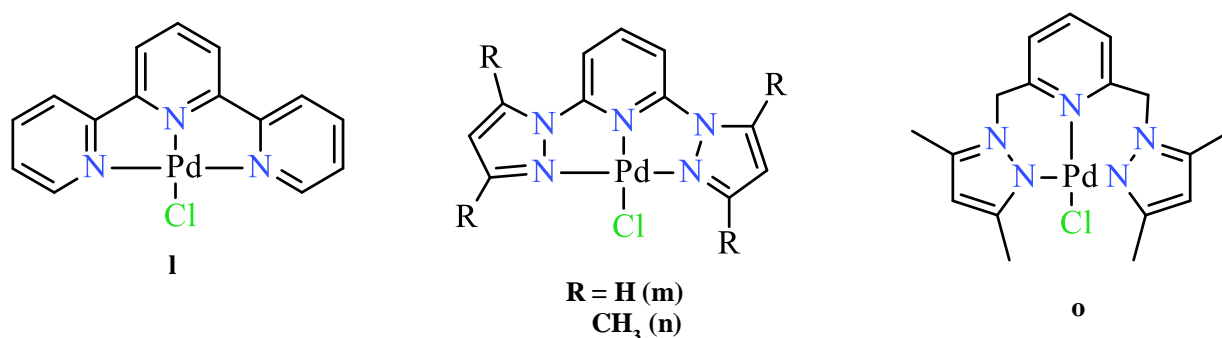


**Figure 2.1:** Pyridine- and pyrrole-based complexes designed to study the influence of electronic and steric effects on the reactivity of Pd(II) complexes.<sup>3,6</sup>

To further demonstrate the influence of electron density around the palladium(II) metal center, the  $\pi$ -acceptor and  $\sigma$ -donor abilities of ligands were investigated. This was achieved by replacing bis(2-pyridylmethyl)amine ligands with bis(8-quinolinyl)amine ligands (**Figure 2.2**), in an attempt to tune the reactivity of palladium(II) complexes.<sup>3,4</sup> It was observed that  $\sigma$ -donation of the 8-quinolinyl moiety weakens the  $\pi$ -back donation effect of the ligand, resulting in a less electrophilic metal center and hence less reactivity. When a strong  $\pi$ -acceptor ligand (bis(2-pyridylmethyl)amine) is replaced by a good  $\sigma$ -donor ligand (bis(8-quinolinyl)amine), the reactivity of the Pd complex with thiourea nucleophiles is reduced by factors of between 25 to 30 fold.

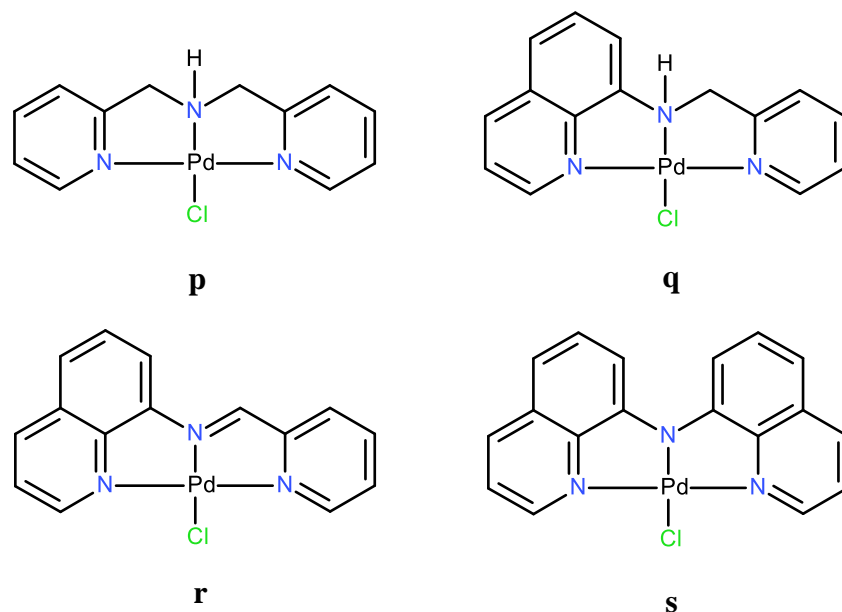


**Figure 2.2:** Pd(II) complexes with ligands containing bis(2-pyridylmethyl)amine and bis(8-quinolinyl)amine moieties.<sup>4</sup>

Omondi and co-workers<sup>7</sup> extended the study by Onunga *et. al.*, by investigating the role of  $\pi$ -conjugation on the substitution reactions of carboxamide palladium(II) complexes (**Figure 2.3**) with thiourea (Tu), L-methionine (L-Met) and guanosine 5'-diphosphate disodium salt. Through substitution reactions they observed that the reactivity of the complexes towards the biological molecules was controlled by the electronic properties of the spectator ligands. For instance, when the strong  $\pi$ -acceptor pyridinyl group was replaced by a good  $\sigma$ -donor quinoline group, the reactivity of the Pd(II) complex was reduced by a factor of 2.81. The decrease in reactivity was due to the reduction of the  $\pi$ -acceptor ability of the ligands through  $\sigma$ -inductive effects, which caused electron build up around the Pd(II) ion of the complex. The presence of a pyrazine unit caused an increase in reactivity when compared to a pyridine unit, due to the higher acidity of the pyrazine group. The replacement of the pyridine moiety with the isoquinolinyl moiety also caused a decrease in reactivities of the complexes. This observation was due to the increased cis- $\sigma$ -inductive effects, which reduced the  $\pi$ -acceptor abilities of the spectator ligand and thus caused the metal centre to be less electrophilic.

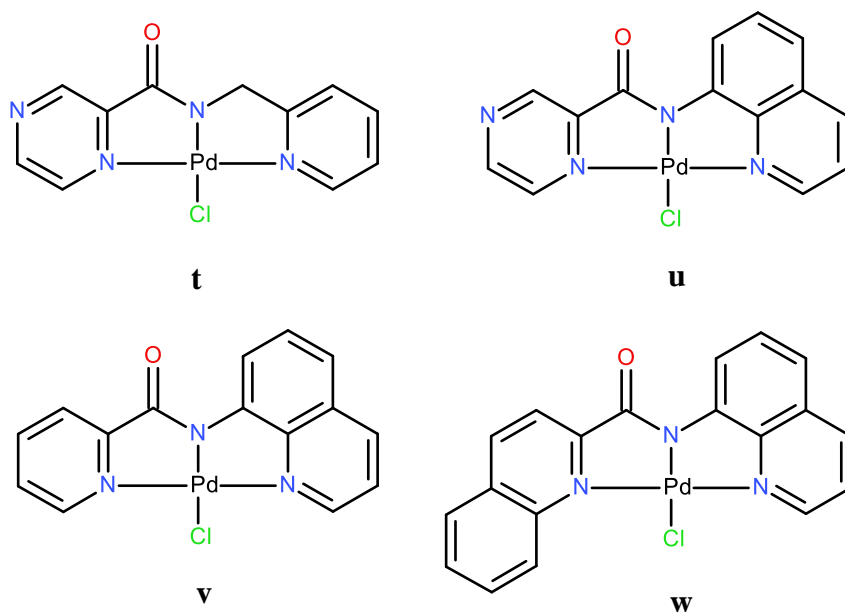


**Figure 2.3:** Palladium(II) complexes with  $\pi$ -conjugated carboxamide ligands.<sup>7</sup>

Another study of the influence of ligands on the reaction rates was conducted by Omondi *et.al*<sup>8</sup> who investigated substitution kinetics, DNA interactions and cytotoxicity of tridentate 2,6-bis(benzazole)pyridine Pd(II) complexes (**Figure 2.4**). They studied the substitution reactions of four complexes with thiourea, L-methionine and guanosine-5'-diphosphate disodium salt. From the results, they concluded that the electronic properties of both the inert ligand and incoming nucleophile controlled the rate of substitution. The  $-NH$  substituted Pd(II) complexes demonstrated the highest kinetic reactivity due to the acidic amine proton, which is more electron deficient compared to the sulfur and oxygen atoms. The  $-NH$  assists with electron withdrawal from the metal center and thus makes the Pd(II) metal center more electrophilic. This complex also displayed cytotoxicity and selectivity comparable to that of *cisplatin*. A comparison of the reactivity between the Pd complex with  $-O-$  and  $-S-$ , showed that the complex with the more electronegative oxygen as a spectator ligand was more reactive. The complex without the additional pyridine moiety on the bis-benzazole ligand demonstrated the least kinetic reactivity.

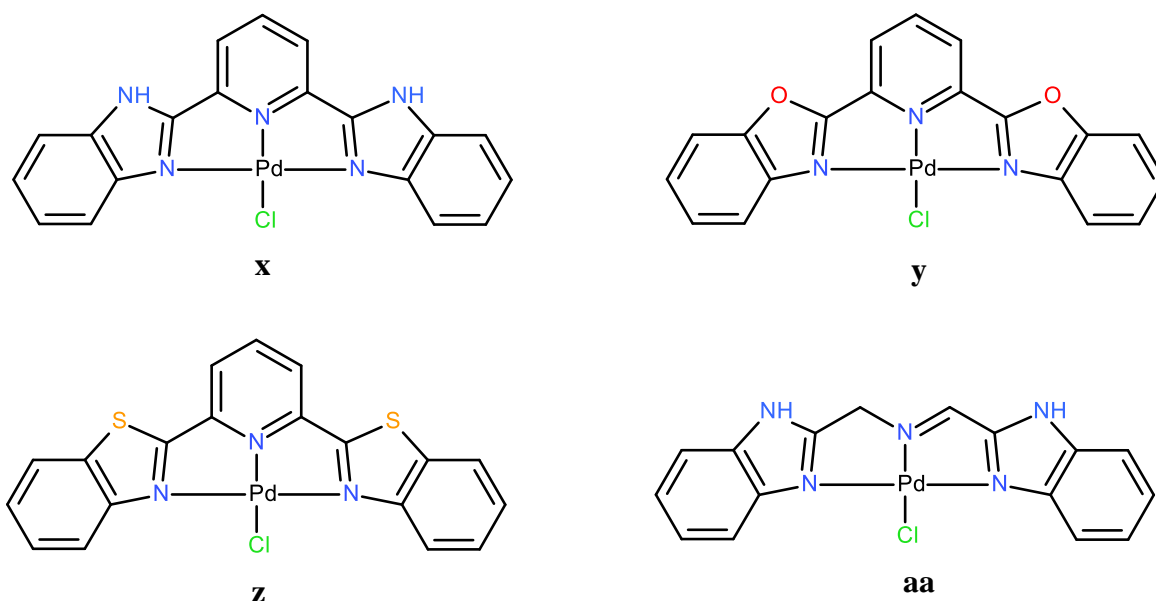


**Figure 2.4:** Tridentate 2,6-bis(benzazole)pyridine Pd(II) complexes designed to study the effects of heteroatoms on the cytotoxicity of palladium(II) complexes.<sup>8</sup>

To further expand the above study, Fadaka *et.al.*<sup>9</sup> studied the competing roles of trans-heteroatoms on carrier ligands on kinetic and biological activities of pyrazolyl Pd(II) complexes. The rates of substitution were studied using biological nucleophiles: thiourea (Tu), L-methionine (L-Met) and guanosine-5-monophosphate (5-GMP). The electron abilities of the auxiliary ligands influenced the kinetic reactivity of the complexes. The complex with sulphur in the *trans* position to the leaving group was found to be the most reactive due to preference of Pd atom (soft acid) to coordinate with the soft donor S atom as opposed to NH and O atom (hard bases), which leads to the electron accumulation in the bonding. This phenomenon leads to a weak and elongated bond *trans* to the Cl atom, which in turn causes a higher reactivity. The presence of a strong  $\pi$ -acceptor pyridine group in the *trans* position increased the reactivity of the complex in comparison to the complexes with NH and O atoms. The pyridine moiety reduces electron cloud on the Pd(II) ion while NH donates electrons to the metal centre.

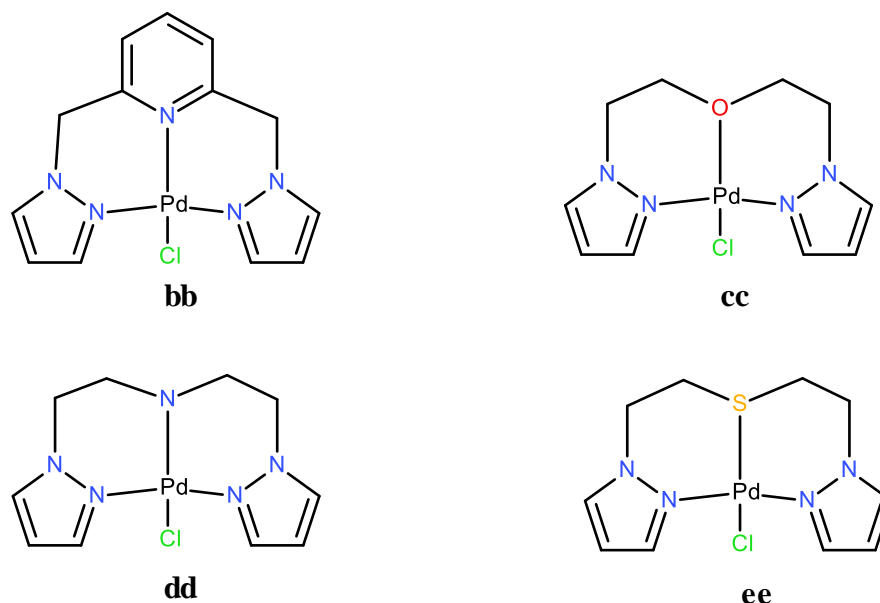


**Figure 2.5:** Palladium (II) complexes with different pyrazolyl ligands.<sup>9</sup>

The above results, amongst others, indicate that the kinetic reactivity of Pd(II) complexes can be controlled by meticulous manipulation of electronic and steric properties of inert ligands.

### 2.1.2 Influence of Ionic Strength on The Rate of Substitution in Pd(II) Complexes.

Supported by our discussion of the mechanism of action of *cisplatin*, it is known that upon injection Pt(II) complexes exist as chlorido species in the blood plasma as it contains high concentrations of chloride ions, approximately 100 mM, conditions that aid in preventing hydrolysis of the neutral complexes. However, due to relatively low concentrations of the chloride ions inside the cell, ~4 mM, the complexes are hydrolyzed and converted into aqua species.<sup>10-12</sup> Therefore, it is crucial to study and understand the kinetic behavior of chlorido and aqua species of Pd(II) complexes in comparison with Pt(II) complexes.

One example of such a study was conducted by Burgarcic *et. al*<sup>1</sup> who investigated the reactivity of both the chlorido and aqua complexes and studied the effects of different chloride concentrations on the rate of substitution with aims to find the optimum chloride concentration that would prevent the rapid hydrolysis of the chlorido Pd(II) complexes. The reaction of [Pd(triimidimidimethane)Cl] with Thiourea nucleophile showed a shift in the equilibrium from the labile aqua complex to the more inert chlorido complex when the chloride concentration was increased to at least 5 mM NaCl. Therefore, an optimum chloride concentration of 10 mM NaCl was maintained to prevent the aquation of the species completely.

### 2.1.3 Influence of Incoming Biomolecules on The Rate of Substitution in Pd(II) Complexes.

Although DNA is the main target of anticancer agents, it is crucial to take into consideration other molecules in the human cells such as enzymes, proteins, amino acids, and other biomolecules that interact with the drug before it reaches its target and understand the influence of such interactions on the reactivity of the drug. These biomolecules include sulfur donors such as thiols and thioethers, hard molecules with a strong affinity for the soft platinum center and hence, the related palladium center. Since the concentration of these biomolecules is remarkably high in the human body, it is essential to study their substitution reactions with Pd(II) complexes.<sup>13</sup>

Burgarcic *et. al.* studied the interaction of sulfur-donor biomolecules with Pd(II) complexes. The group studied reaction of nucleophiles such as L-Methionine (L-Met), L-Cysteine (L-Cys), Glutathione (GSH), and thiourea nucleophiles namely, Thiourea (TU), Dimethylthiourea (DMTU) and Tetramethylthiourea (TMTU).<sup>14</sup> The use of these biomolecules was for different purposes. For instance, L-Met and L-Cys are examples of sulfur-containing amino acids in the human body. GSH is used as a model of peptides, while the thiourea nucleophiles, which resemble urea, are used to study the biological role played by sulfur-containing molecules in the human blood.<sup>15</sup> The results showed that the rate of substitution is influenced by the electrophilicity of the metal center, the nucleophilicity of the biomolecule and the steric effects of both the inert and the incoming biomolecule.<sup>1</sup> The leaving group and the incoming nucleophile have relative effect on the rate of substitution. Thus, the effect of the leaving group is not discussed in this chapter.

## 2.2 Instrumental Techniques Used in Chemical Kinetics

The rate of substitution of complexes can be practically measured by physical methods such as spectroscopic techniques. Two spectroscopic techniques *viz.* UV-Visible spectrophotometry and stopped-flow spectrophotometry used in this project are discussed in detail below.

### 2.2.1 UV-Visible Spectrophotometry

UV/visible spectrophotometry is a technique used to monitor the transmittance or absorbance of reactions at different concentrations ranging from  $10^{-4}$  to  $10^{-6}$  M, absorbance is measured at a specified wavelength range of electromagnetic radiation. The UV-Vis spectrophotometer

generally comprises of two light sources, the deuterium arc lamp (visible region 160-375 nm) and the tungsten-halogen lamp (350-2500 nm), however, most recently a single xenon flash lamp has been used to cover the entire ultraviolet-visible region with good intensity.<sup>16</sup> The light sources produce a broad-spectrum white light; thus, the instrument is also equipped with a monochromator which narrows down the light to a specific wavelength band. In a double beam spectrophotometer, the light from the monochromator is split into two beams: a reference and a sample beam, using a rotating wheel with mirror segments. Each beam enters the sample chamber through separate optical paths, allowing for the blank and sample to be measured simultaneously.<sup>17</sup> The stray light of selected wavelength that passes through the monochromator with an intensity  $I_0$ , enters the sample compartment where it passes through glass, plastic, or quartz cuvettes with length  $l$ , containing the sample of interest. The amount of light absorbed by the sample is the difference between the incident radiation ( $I_0$ ) and the transmitted radiation ( $I$ ).<sup>16</sup> A detector then converts the light from the sample into an electrical signal. UV-Vis typically consists of a photomultiplier tube detector or silicon diode detector. The signal from the detector is thereafter displayed on a readout device.<sup>16</sup>

### 2.2.2 Stopped Flow Spectrophotometry

This technique is typically used to monitor rapid reactions which would be untraceable by standard absorption spectroscopy. It is a great instrument to use for substitution reactions of Pd(II) complexes since these reactions are fast. For instance, the Pd(II) complexes investigated in this study had reactions that completed in less than 6 seconds. Stopped flow allows for the reaction rate to be determined within milliseconds and requires a small volume of reactants. This involves rapid mixing of two reactants which are held in two separate reservoirs (syringe pumps) in equal amounts, at a desired temperature.<sup>18, 19</sup> The reaction is initiated by a gas-piston driven mechanism (800 kPa) compressing the reactant syringes, forcing the reactant solutions into the “mixing chamber” where they are mixed. The reaction solution then proceeds into the stop syringe, which fills up until it strikes the stop block, thereby stopping the flow of solution but leaving the reaction mixture in the observation cell.<sup>18, 19</sup>

With the mixed solution stationary in the observation cells, detection (usually by UV-Vis spectrophotometry) commences in the reaction analyzer. The monochromatic light that passes through the sample mixture in the observation chamber at a specific wavelength is measured as the reaction progresses into completion. Using a photomultiplier, the transmitted light is

converted into an electrical signal, which is then interpreted as absorbance and recorded as a function of time.<sup>18, 19</sup> A representation of the stopped flow analyzer is indicated in **Figure 2.6**.

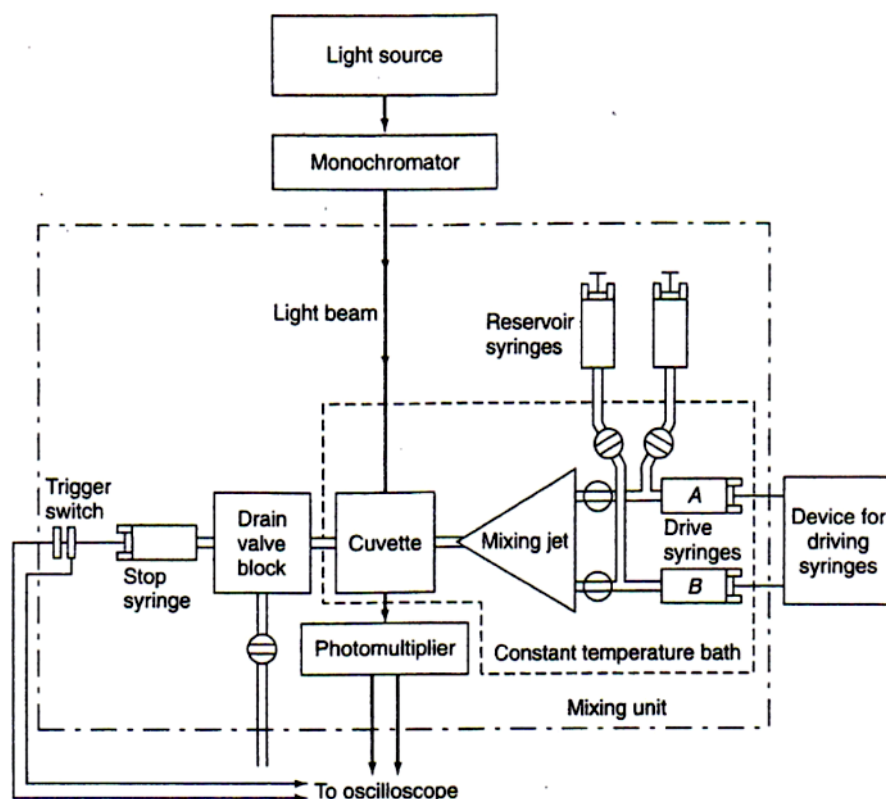


**Figure 2.6:** Schematic diagram of a stopped-flow reaction analyzer.

### 2.3 Statement of Problem

In spite of the accomplishments of current platinum drugs, these compounds are still predominantly associated with acute toxicity, limited anticancer applications and resistance.<sup>20, 21</sup> The resistance occurs due to drug accumulation in cancer cells, inactivation of thiol containing molecules, and enhanced DNA repair.<sup>21</sup> Thus, there is a critical need to design and identify novel alternative metal complexes with reduced toxicity as they are expected to have different chemical behavior, hydrolytic rates, and improved application spectrum.<sup>22-25</sup> The kinetic behavior of metal complexes largely depends on the steric and electronic properties of the ligands coordinated to the metal center. While the substitution rates of these metal complexes have been explored and reported in literature, there is still a wide range of ligands that have not been coordinated to palladium with intentions of fine tuning the kinetic reactivity of these complexes, especially those coordinated to bidentate ligands.

## 2.4 Justification of Study

The shortcomings of platinum-based drugs have advocated for the development of alternative metal-based therapeutics that possess reduced toxicity, improved selectivity and a broader spectrum of application.<sup>24</sup> Amongst the promising transition metallodrugs are palladium(II) complexes which closely resemble the platinum-based complexes in structure and thermodynamics.<sup>20, 26</sup> Despite the similarities, some palladium(II) drugs have shown good cytotoxicity against numerous cell lines, fewer side effects, and better aqueous solubility than their platinum-based counterparts. However, with the use of palladium(II) anticancer drugs, researchers have encountered great challenges since these drugs exchange ligands  $10^4$  -  $10^5$  times faster than their platinum (II) analogues.<sup>27</sup> This then results in poor antitumor activity due to their rapid hydrolysis of the leaving groups that are prone to dissociate in solution which in turn prevents the complexes from reaching their DNA targets for effective therapeutic function.<sup>28</sup> To counteract these limitations, previous reports have shown that the proper choice of ligands coordinated to palladium(II) is crucial, as they play an important role in modifying reactivity by stabilizing specific oxidation states while maintaining their non-labile state.<sup>1</sup> Additionally, the biological activity of platinum(II) drugs involves binding with DNA and other thiol containing biomolecules.<sup>29, 30</sup> Therefore, it is crucial to study the kinetic and substitution behavior of the palladium(II) drugs using appropriate sulfur containing nucleophiles to monitor their mechanistic interactions in comparison to the intensely investigated platinum(II) drugs. In the current project we focus on designing Pd(II) complexes with bidentate ligands and investigating their kinetic and mechanistic reactions in aqueous media. We want to understand the mode of substitution with complexes bearing bidentate N,N donor ligands.

## 2.5 Aims and Objectives

### 2.5.1 Aims

The aim of this work was to synthesize, characterize, and study the substitution kinetics of chloride ligands from pyridyl N,N'-bidentate mononuclear Pd(II) complexes with different substituents.

### 2.5.2 Objectives

1. To synthesize bidentate mononuclear palladium(II) complexes of N-(pyridin-2-ylmethyl) aniline chelate ligands with different substituents and N-(4-bromophenyl)-pyridine-2-carboxamide.
2. To characterize the Pd(II) complexes with  $^1\text{H}$ ,  $^{13}\text{C}$  NMR, FT-IR, LC-MS, CHN elemental analysis, and single X-Ray crystallography.
3. To conduct kinetics of ligand substitution reactions of the synthesized palladium(II) complexes with bio-relevant thiourea nucleophiles; thiourea (**Tu**), N,N'-dimethylthiourea (**Dmtu**) and N,N,N',N'-tetramethylthiourea (**Tmtu**).
4. To elucidate the experimental results by utilizing density function theory (DFT) calculations.

## 2.6 References

1. Bugarčić, Ž. D.; Bogojeski, J.; van Eldik, R., Kinetics, mechanism and equilibrium studies on the substitution reactions of Pd (II) in reference to Pt (II) complexes with bio-molecules. *Coordination Chemistry Reviews* **2015**, *292*, 91-106.
2. Jahromi, E. Z.; Divsalar, A.; Saboury, A. A.; Khaleghizadeh, S.; Mansouri-Torshizi, H.; Kostova, I., Palladium complexes: new candidates for anti-cancer drugs. *Journal of the Iranian Chemical Society* **2016**, *13* (5), 967-989.
3. Onunga, D. O. Controlling the reactivity of mononuclear palladium (II) complexes. Substitution kinetics and mechanisms. **2019**.
4. Onunga, D. O.; Jaganyi, D.; Mambanda, A., The role of 8-quinolinyl moieties in tuning the reactivity of palladium (II) complexes: a kinetic and mechanistic study. *Journal of Coordination Chemistry* **2019**, *72* (3), 499-515.
5. Onunga, D. O.; Bellam, R.; Mutua, G. K.; Sitati, M.; BalaKumaran, M. D.; Jaganyi, D.; Mambanda, A., Controlling the reactivity of [Pd-(II)(N boolean AND N boolean AND N) Cl] plus complexes using 2, 6-bis (pyrazol-2-yl) pyridine ligands for biological application: Substitution reactivity, CT-DNA interactions and in vitro cytotoxicity study. **2020**.
6. Onunga, D. O.; Bellam, R.; Mutua, G. K.; Sitati, M.; BalaKumaran, M. D.; Jaganyi, D.; Mambanda, A., Controlling the reactivity of [Pd (II)(N^ N^ N) Cl]+ complexes using 2, 6-bis (pyrazol-2-yl) pyridine ligands for biological application: Substitution reactivity, CT-DNA interactions and in vitro cytotoxicity study. *Journal of Inorganic Biochemistry* **2020**, *213*, 111261.
7. Omondi, R. O.; Sibuyi, N. R.; Fadaka, A. O.; Meyer, M.; Jaganyi, D.; Ojwach, S. O., Role of  $\pi$ -conjugation on the coordination behaviour, substitution kinetics, DNA/BSA interactions, and in vitro cytotoxicity of carboxamide palladium (ii) complexes. *Dalton Transactions* **2021**, *50* (23), 8127-8143.
8. Omondi, R. O. Tuning the steric and electronic parameters of mixed-donor palladium (II) complexes: coordination chemistry, substitution kinetics and biological activities. **2021**.
9. Fadaka, A. O.; Omondi, R. O.; Fatokun, A. A., Synthesis, substitution kinetics, DNA/BSA binding and cytotoxicity of tridentate N^ E^ N (E= NH, O, S) pyrazolyl palladium (II) complexes. **2022**.

10. Fuertes, M.; Castilla, J.; Alonso, C.; Prez, J., Cisplatin biochemical mechanism of action: from cytotoxicity to induction of cell death through interconnections between apoptotic and necrotic pathways. *Current medicinal chemistry* **2003**, *10* (3), 257-266.
11. Jamieson, E. R.; Lippard, S. J., Structure, recognition, and processing of cisplatin–DNA adducts. *Chemical reviews* **1999**, *99* (9), 2467-2498.
12. Judson, I.; Kelland, L. R., New developments and approaches in the platinum arena. *Drugs* **2000**, *59* (4), 29-36.
13. Reedijk, J., Why does cisplatin reach guanine-N7 with competing S-donor ligands available in the cell? *Chem Rev* **1999**, *99*, 2499-2510.
14. Bugarčić, Ž. D.; Bogojeski, J.; Petrović, B.; Hochreuther, S.; van Eldik, R., Mechanistic studies on the reactions of platinum (II) complexes with nitrogen-and sulfur-donor biomolecules. *Dalton Transactions* **2012**, *41* (40), 12329-12345.
15. Alessio, E., *Bioinorganic medicinal chemistry*. John Wiley & Sons: **2011**.
16. Penner, M. H., Ultraviolet, visible, and fluorescence spectroscopy. In *Food analysis*, Springer: **2017**, 89-106.
17. Østergaard, J., UV/VIS spectrophotometry and UV imaging. In *Analytical Techniques in the Pharmaceutical Sciences*, Springer: **2016**, 3-27.
18. Skoog, D. A.; West, D. M.; Holler, F. J.; Crouch, S. R., *Fundamentals of analytical chemistry*. Cengage learning: **2013**.
19. Wilkins, R. G., *Kinetics and mechanism of reactions of transition metal complexes*. VCH Weinheim: **1991**; Vol. 4.
20. Chen, X.; Xie, M.; Liu, W.; Ye, Q.; Yu, Y.; Hou, S.; Gao, W.; Liu, Y., Synthesis and structure of platinum (II) complexes containing an asymmetric chelating diamine 2-morpholinoethylamine as the carrier. *Inorganica chimica acta* **2007**, *360* (8), 2851-2856.
21. Raguz, S.; Yagüe, E., Resistance to chemotherapy: new treatments and novel insights into an old problem. *British journal of cancer* **2008**, *99* (3), 387-391.
22. Warad, I.; Eftaiha, A. a. F.; Al-Nuri, M. A.; Husein, A. I.; Assal, M.; Abu-Obaid, A.; Al-Zaqri, N.; Hadda, T. B.; Hammouti, B., Metal ions as antitumor complexes-Review. *J. Mater. Environ. Sci* **2013**, *4* (4), 542-557.
23. Storr, T.; Thompson, K. H.; Orvig, C., Design of targeting ligands in medicinal inorganic chemistry. *Chemical Society Reviews* **2006**, *35* (6), 534-544.
24. Farrell, N., Multi-platinum anti-cancer agents. Substitution-inert compounds for tumor selectivity and new targets. *Chemical Society Reviews* **2015**, *44* (24), 8773-8785.
25. Lazarević, T.; Rilak, A.; Bugarčić, Ž. D., Platinum, palladium, gold and ruthenium complexes as anticancer agents: Current clinical uses, cytotoxicity studies and future perspectives. *European journal of medicinal chemistry* **2017**, *142*, 8-31.
26. Hadizadeh, S.; Najafzadeh, N.; Mazani, M.; Amani, M.; Mansouri-Torshizi, H.; Niapour, A., Cytotoxic effects of newly synthesized palladium (II) complexes of diethyldithiocarbamate on gastrointestinal cancer cell lines. *Biochemistry Research International* **2014**.
27. Coskun, M. D.; Ari, F.; Oral, A. Y.; Sarimahmut, M.; Kutlu, H. M.; Yilmaz, V. T.; Ulukaya, E., Promising anti-growth effects of palladium (II) saccharinate complex of terpyridine by inducing apoptosis on transformed fibroblasts in vitro. *Bioorganic & medicinal chemistry* **2013**, *21* (15), 4698-4705.
28. Heydari, M.; Moghadam, M. E.; Tarlani, A.; Farhangian, H., DNA as a target for anticancer phen-imidazole Pd (II) complexes. *Applied Biochemistry and Biotechnology* **2017**, *182* (1), 110-127.

29. Divsalar, A.; Saboury, A. A.; Ahadi, L.; Zemanatiyar, E.; Mansouri-Torshizi, H., Investigation of effects of newly synthesized Pt (II) complex against human serum albumin and leukemia cell line of K562. *BMB reports* **2010**, *43* (11), 766-771.
30. Barry, N. P.; Sadler, P. J., Exploration of the medical periodic table: towards new targets. *Chemical Communications* **2013**, *49* (45), 5106-5131.

## CHAPTER 3

### 3.1 General Introduction

The study of alternative transition metal complexes, other than Pt-based complexes, as potential anticancer drugs has gained momentum over the last few decades due to the side effects associated with *cisplatin* and its derivatives.<sup>1, 2</sup> Amongst these metals, palladium(II) complexes have emerged as potential candidates, owing the interest to their structural and thermodynamic resemblance to Pt(II) complexes. Essentially, Pd(II) complexes have demonstrated better solubility, reduced toxicity and improved activity against cisplatin-resistant cells.<sup>3-5</sup>

Nonetheless, the main challenge with the development of Pd(II) antitumor agents is their fast hydrolysis ( $10^5$  more than Pt) and strong affinity for nitrogen and sulphur containing biomolecules.<sup>6, 7</sup> The interactions of palladium complexes with sulphur-coordinating biomolecules result in the formation of side products that hinder the complexes from reaching their DNA targets and performing their anticancer function. Consequently, the careful design of suitable ligands to fine-tune the stability and reactivity of Pd(II) complexes is crucial.<sup>8, 9</sup>

In efforts to control the kinetic reactivity of Pd(II) complexes, inert N-donor chelate ligands have been studied due to their affinity for palladium. The strong coordination of the nitrogen atom to the metal centre ensures stability of the Pd(II) complex while the ligands maintain their non-labile state.<sup>10, 11</sup> For instance, the kinetic reactivity of palladium complexes coordinated to pyrazolyl, pyridyl, quinolinyl and benzoazole containing ligands has been intensely studied by Onunga *et. al.*<sup>12-14</sup> In essence, the results have shown that the thermodynamic stability and kinetic reactivity of Pd(II) complexes can be fine-tuned through careful manipulation of electronic and steric properties of the chelating ligands.<sup>15</sup>

Pyridylmethyl-amines are common bidentate ligands that have been coordinated to several transition metals. The structural versatility of these ligands has allowed for various modifications through the introduction of substituents on the amine and pyridyl units.<sup>16, 17</sup> However, there remains limited information on the thermodynamic and kinetic reactivity of Pd(II) complexes coordinated to N,N-bidentate pyridyl-methylamine ligands.

In this study, five ligands **L1**, **L2**, **L3**, **L4** and **L5** and their corresponding Pd(II) complexes **PdL1**, **PdL2**, **PdL3**, **PdL4** and **PdL5** were synthesized using literature methods.<sup>16-18</sup> The compounds have similar pyridyl units but differ in substituents on the aniline moiety. We herein report the substitution behaviour of these complexes with thiourea nucleophiles namely, thiourea (**TU**), dimethylthiourea (**DMTU**) and tetramethylthiourea (**TMTU**).

### 3.2 Chemicals and Reagents

All syntheses of ligands and Pd(II) complexes were performed under inert nitrogen atmosphere. The solvents hexane and dichloromethane (DCM) were purchased from Sigma-Aldrich and dried following relevant methods: hexane was dried through standard distillation methods, while dichloromethane was stored in activated 3 Å molecular sieves. Other solvents such as ethyl acetate, acetonitrile, ethanol, deuterated chloroform, deuterated DMSO and deuterated DMF were purchased from Sigma-Aldrich and were used without further purification. Furthermore, the chemicals 2-pyridinecarboxaldehyde, aniline, 4-fluoroaniline, 4-bromoaniline, 4-methoxyaniline, 4-ethylaniline, sodium triacetoxyborohydride, sodium hydrogen carbonate, magnesium sulfate, silica gel, and palladium (II) chloride were also purchased from Sigma-Aldrich and used without any further purification.

### 3.3 Physical Measurements

Physical properties such as colour, percentage yield and melting points of each synthesized compound were determined and summarized under each compound.

#### 3.3.1 <sup>1</sup>H and <sup>13</sup>C NMR Spectroscopy

<sup>1</sup>H and <sup>13</sup>C NMR spectra were acquired on Bruker Avance III 500 MHz or 400 MHz and 100 MHz spectrometers with a 5 mm TBIZ probe at 30°C. Chemical shifts were recorded in ppm relative to the solvent residual peak, CDCl<sub>3</sub> and DMSO-d<sub>6</sub> for ligands and complexes, respectively. NMR abbreviations s, d, t and m were used to denote singlet, doublet, triplet and multiplet. All coupling constants (*J*) were calculated and reported in Hertz (Hz). Exemplary <sup>1</sup>H and <sup>13</sup>C NMR spectra of the ligands and the complexes are shown in the appendix section.

#### 3.3.2 FTIR Spectroscopy

Spectral data was acquired using a Bruker Alpha II FT-IR spectrometer and the data was recorded as percentage transmittance at the respective wavenumber (cm<sup>-1</sup>) within the range 500 - 4000 cm<sup>-1</sup>. Exemplary IR spectra of the ligands and the complexes are shown in the appendix section.

### 3.3.3 Mass Spectrometry

Low-resolution spectral data was collected on a Waters TOF Micro-mass LCT Premier spectrometer for the synthesized complexes. Elemental compositions of the complexes were determined using CHNS Thermo Scientific Flash 2000 analyser. Exemplary LC-MS spectra of the ligands and the complexes are shown in the appendix section.

### 3.3.4 DFT-Computational Modelling

Using Gaussian 09 program suite<sup>19</sup>, the theoretical ground-state structures of **PdL1 - PdL5** were optimized at gas phase using B3LYP (Becke 3-Lee-Yang-Parr) functional mode in combination with 6-31G (C and H), 6-311+G (N, S and Cl), and (Los Alamos National Laboratory 2 double  $\zeta$ ) LANL2DZ (Pd) basis sets.<sup>20-22</sup>

### 3.3.5 Stopped Flow & UV-Visible Spectrophotometer

An Applied Photophysics SX 20 stopped-flow spectrophotometer and a Cary 3500 UV-Vis spectrometer coupled with an online acquisition system were used to follow the substitution reactions.

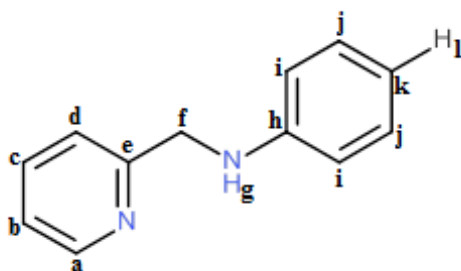
### 3.3.6 Preparation of Solutions for Kinetic Analysis

Stock solutions of Pd(II) complexes and freshly prepared solutions of nucleophiles were prepared by dissolving known amounts of each in ultra-pure water with an ionic strength of 0.1 M (LiCl). Lithium chloride was added to prevent spontaneous solvolysis of the chloro Pd(II) complexes. The complex concentrations were maintained at 0.05 mM, while the solutions of **TU** and **DMTU** were prepared at concentration of 50-fold in excess. **TMTU** solutions were prepared to afford concentrations 100-fold more than that of the metal complex. This was due to an observed slow reactivity of the nucleophile, in comparison to **TU** and **DMTU**. Consecutive dilutions of the stock solutions of nucleophiles (**TU** and **DMTU**) afforded solutions 10, 20, 30 and 40-fold more than the concentration of the complexes. The subsequent **TMTU** solutions were 20, 40, 60, and 80-fold more concentrated than the metal complexes. The subsequent dilutions of nucleophile solutions ensured *pseudo* first-order conditions. Equal volumes of complexes and nucleophiles were administered for mixing on the Stopped-Flow spectrophotometer. All concentration dependence reactions were carried out at a constant temperature of 298 K, while temperature dependence reactions were investigated over a range of 288 – 308 K, at 5 K intervals to determine the activation parameters;  $\Delta H^\ddagger$  and  $\Delta S^\ddagger$ .

### 3.4 Synthesis of Ligands

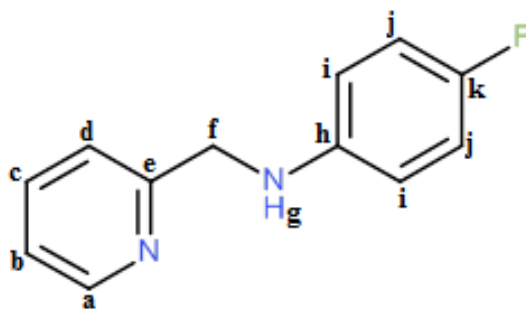
To prepare **L1** – **L5**, the *para* substituted anilines (1 mmol) and 2-pyridinecarboxaldehyde (0.0951 ml, 1 mmol) were dissolved in dry dichloromethane (10 mL) and then solid sodium triacetoxyborohydride (0.3179 g, 1.5 mmol) was added. The reaction mixture was stirred at room temperature under nitrogen gas for 6 hours and the progress of the reaction was monitored by TLC using Hexane/Ethyl acetate 7:3. The resulting reaction mixture was quenched with saturated sodium hydrogen carbonate solution which was then extracted three times with dichloromethane. The combined organic phase layer was dried over magnesium sulfate and the solvent was removed under reduced pressure to obtain an oily yellow liquid. The crude product was purified using column chromatography (Hexane/Ethyl acetate 7:3). The desired ligands isolated are described hereafter.

#### 3.4.1. *N*-(pyridin-2-ylmethyl) aniline (**L1**):



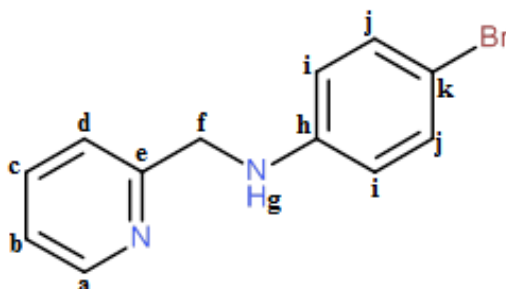
**L1** was obtained as a yellow oil (95.6 mg, 51.89%). <sup>1</sup>H NMR (400 MHz, CDCl<sub>3</sub>, ppm): 8.60 (d, 1H, -**H<sub>a</sub>**-, *J* = 4.81 Hz), 7.65 (t, 1H, *J* = 7.65 Hz, -**H<sub>c</sub>**-), 7.36 (d, 1H, *J* = 7.92 Hz, -**H<sub>d</sub>**-), 7.24 (m, 3H, -**H<sub>b</sub>**-, -**H<sub>j</sub>**-), 6.78-6.67 (m, 3H, -**H<sub>i</sub>**-, -**H<sub>l</sub>**-), 4.35 (s, 2H, -**H<sub>f</sub>**-), 4.27 (s, 1H, -**H<sub>g</sub>**-). <sup>13</sup>C NMR (CDCl<sub>3</sub>, 400 MHz): 158.58, 149.09, 147.93, 136.76, 129.27, 122.14, 121.66, 117.61, 113.09, 49.26. FT-IR (liquid neat; cm<sup>-1</sup>) 3386.90 (-NH), 1597.51 (C=C), 1264.76 (C-N aromatic).

3.4.2. 4-Fluoro-N-(pyridin-2-ylmethyl) aniline (**L2**):



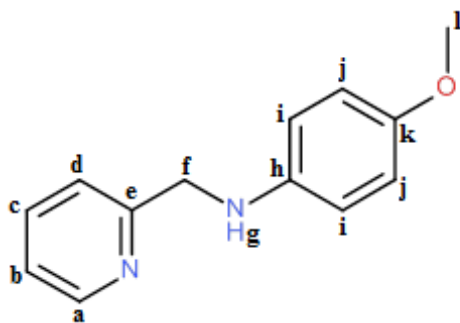
**L2** was obtained as an orange oil (127.9 mg, 63.24%).  $^1\text{H}$  NMR (400 MHz,  $\text{CDCl}_3$ , ppm): 8.57 (d, 1H,  $J = 4.90$  Hz,  $-\text{H}_a$ -), 7.62 (t, 1H,  $J = 7.75$  Hz,  $-\text{H}_c$ -), 7.30 (d, 1H,  $J = 7.95$  Hz,  $-\text{H}_d$ -), 7.16 (t, 1H,  $J = 5.63$  Hz,  $-\text{H}_b$ -), 6.68 (t, 2H,  $J = 8.84$  Hz,  $-\text{H}_j$ -), 6.59 (m, 2H,  $-\text{H}_i$ -), 4.41 (s, 1H,  $-\text{H}_g$ ), 4.40 (s, 2H,  $-\text{H}_f$ -).  $^{13}\text{C}$  NMR ( $\text{CDCl}_3$ , 100 MHz): 158.32, 149.16, 144.36, 144.35, 136.69, 122.18, 121.66, 115.74, 115.52, 113.86, 113.79, 49.81. FT-IR (liquid neat;  $\text{cm}^{-1}$ ) 3264.34 (NH), 1501.16 (C=C), 1301.22 (C-N aromatic), 1203.19 (C-F).

3.4.3. 4-Bromo-N-(pyridin-2-ylmethyl) aniline (**L3**):



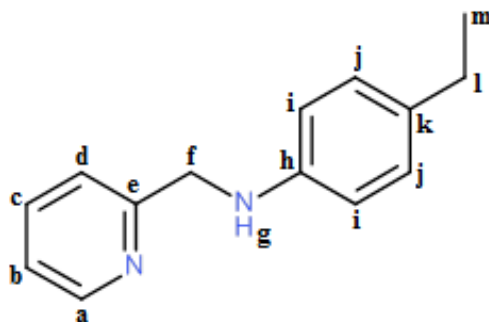
**L3** was obtained as a dark orange oil (135.7 mg, 51.57%).  $^1\text{H}$  NMR (500 MHz,  $\text{CDCl}_3$ , ppm): 8.52 (d, 1H,  $J = 4.58$  Hz,  $-\text{H}_a$ -), 7.68 (t, 1H,  $J = 7.69$  Hz,  $-\text{H}_c$ -), 7.32 (d, 1H,  $J = 8.21$  Hz,  $-\text{H}_d$ ), 7.22 (m, 3H,  $-\text{H}_b$ -,  $-\text{H}_j$ -), 6.47 (d, 2H,  $J = 8.77$  Hz,  $-\text{H}_i$ -), 4.41 (s, 2H,  $-\text{H}_f$ -), 3.85 (s, 1H,  $\text{H}_g$ ).  $^{13}\text{C}$  NMR ( $\text{CDCl}_3$ , 500 MHz): 157.57, 148.01, 146.56, 138.04, 131.98, 122.70, 122.29, 114.68, 109.46, 48.50. FT-IR (liquid neat;  $\text{cm}^{-1}$ ) 3283.65 (-NH), 1589.74 (C=C), 1312.06 (C-N aromatic), 605.60 (C-Br).

#### 3.4.4. 4-Methoxy-N-(pyridin-2-ylmethyl) aniline (**L4**):



**L4** was obtained as a dark orange oil (96.6 mg, 45.08%).  $^1\text{H}$  NMR (400 MHz,  $\text{CDCl}_3$ , ppm): 8.59 (d, 1H,  $J = 5.16$  Hz,  $-\text{H}_{\text{a-}}$ ), 7.66 (t, 1H,  $J = 1.83$  Hz,  $-\text{H}_{\text{c-}}$ ), 7.37 (d, 1H,  $J = 7.73$  Hz,  $-\text{H}_{\text{d}}$ ), 7.20 (t, 1H,  $J = 6.19$  Hz,  $-\text{H}_{\text{b-}}$ ), 7.81-6.79 (m, 2H,  $-\text{H}_{\text{j-}}$ ), 6.78 - 6.63 (m, 2H,  $-\text{H}_{\text{i-}}$ ), 4.44 (s, 2H,  $-\text{H}_{\text{f-}}$ ), 4.09 (s, 1H,  $-\text{H}_{\text{g-}}$ ), 3.74 (s, 3H,  $-\text{H}_{\text{l-}}$ ).  $^{13}\text{C}$  NMR ( $\text{CDCl}_3$ , 100 MHz): 158.77, 152.36, 148.95, 141.98, 136.90, 122.17, 121.83, 114.93, 114.45, 55.78, 50.20. FT-IR (liquid neat;  $\text{cm}^{-1}$ ) 3277.26 ( $-\text{NH}$ ), 1502.66 (C=C), 1290.3 (C-N aromatic), 1225.65 (C-O).

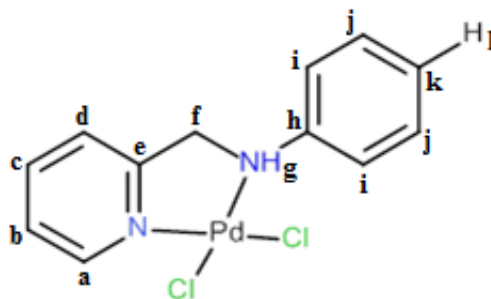
#### 3.4.5. 4-Ethyl-N-(pyridin-2-ylmethyl) aniline (**L5**):



**L5** was obtained as a dark orange oil (102 mg, 48.04%).  $^1\text{H}$  NMR (400 MHz,  $\text{CDCl}_3$ , ppm): 8.62 (d, 1H,  $J = 5.11$  Hz,  $-\text{H}_{\text{a-}}$ ), 7.63 (t, 1H,  $J = 7.60$  Hz,  $-\text{H}_{\text{c-}}$ ), 7.36 (d, 1H,  $J = 7.94$  Hz,  $-\text{H}_{\text{d}}$ ), 7.18 (t, 1H,  $J = 6.25$  Hz,  $-\text{H}_{\text{b-}}$ ), 7.07 (d, 2H,  $J = 8.53$  Hz,  $-\text{H}_{\text{j-}}$ ), 6.66 (d, 2H,  $J = 8.53$  Hz,  $-\text{H}_{\text{i-}}$ ), 4.48 (s, 2H,  $-\text{H}_{\text{f-}}$ ), 4.39 (s, 1H,  $-\text{H}_{\text{g-}}$ ), 2.60 (m, 2H,  $-\text{H}_{\text{l-}}$ ), 1.25 (t, 3H,  $-\text{H}_{\text{m-}}$ ),  $^{13}\text{C}$  NMR ( $\text{CDCl}_3$ , 100 MHz): 158.98, 149.16, 145.98, 136.69, 133.40, 128.62, 122.07, 121.64, 113.24, 49.69, 27.99, 15.99. FT-IR (liquid neat;  $\text{cm}^{-1}$ ) 3385.35 ( $-\text{NH}$ ), 2947.94 (C-H alkane), 1512.12 (C=C), 1261.96 (C-N aromatic).

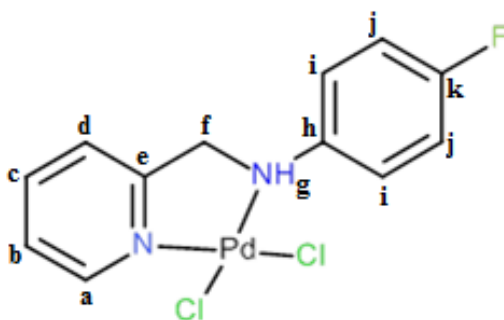
### 3.5 Synthesis of Pd(II) Complexes

#### 3.5.1 dichloro-(*N*-((pyridin-2-yl)methyl)aniline)-palladium(II) (**PdL1**)



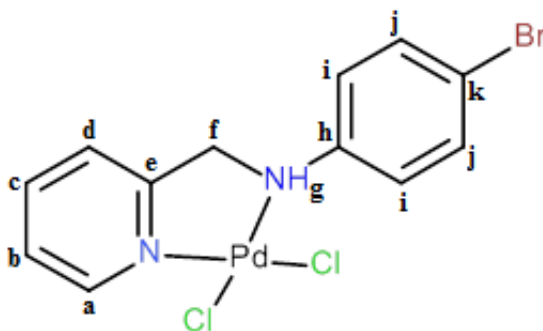
A solution of **L1** (40 mg, 0.22 mmol) in dry DCM (10 ml) was added to a solution of  $[\text{Pd}(\text{CH}_3\text{CN})_2\text{Cl}_2]$  (57.07 mg, 0.22 mmol) in 5 ml of dry DCM.  $[\text{Pd}(\text{CH}_3\text{CN})_2\text{Cl}_2]$  was synthesized from the reflux reaction of  $\text{PdCl}_2$  and acetonitrile. The reaction mixture was stirred overnight at room temperature, under nitrogen gas. The solvent was reduced by rotary evaporator, the resulting solid residue was filtered and washed with cold ethanol (10 ml  $\times$  3), to obtain a yellow solid (64.85 mg, 81.53%). Mp: 246.3 - 249.6 °C.  $^1\text{H}$  NMR (500 MHz  $\text{DMSO-d}_6$ , ppm): 8.76 (m, 2H,  $-\text{H}_{\text{g-}}$ ,  $-\text{H}_{\text{a-}}$ ), 8.18 (t, 1H,  $J = 7.90$  Hz,  $-\text{H}_{\text{c-}}$ ), 7.78 (d, 1H,  $J = 8.00$  Hz,  $-\text{H}_{\text{d-}}$ ), 7.61 (t, 1H,  $J = 6.60$  Hz,  $-\text{H}_{\text{b-}}$ ), 7.32 (t, 2H,  $J = 7.43$  Hz,  $-\text{H}_{\text{j-}}$ ), 7.23 (t, 1H,  $J = 7.33$  Hz,  $-\text{H}_{\text{l-}}$ ), 7.11 (d, 2H,  $J = 7.77$  Hz,  $-\text{H}_{\text{i-}}$ ), 4.98 (m, 1H,  $-\text{H}_{\text{f-}}$ ), 4.40 (d, 1H,  $J = 16.66$  Hz,  $-\text{H}_{\text{f-}}$ ).  $^{13}\text{C}$  NMR (100 MHz,  $\text{DMSO-d}_6$ , ppm): 164.33, 149.40, 146.85, 141.00, 129.81, 126.40, 124.79, 122.53, 121.46, 61.29. FT-IR (liquid neat;  $\text{cm}^{-1}$ ) 3372.10 ( $-\text{NH}$ ), 1649.06 ( $\text{C}=\text{N}$ ). TOF-MS  $\text{ES}^+$ :  $m/z = 384.94$  (calculated  $m/z$  361.56),  $[(\text{M} + \text{Na})^+]$ .

#### 3.5.2 dichloro-(4-fluoro-*N*-((pyridin-2-yl)methyl)aniline)-palladium(II) (**PdL2**)



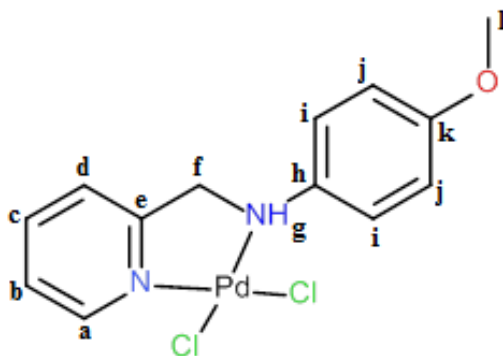
The complex **PdL2** was prepared according to a similar procedure as **PdL1** except for the use of **L2** (47 mg, 0.2 mmol). **PdL2** was obtained as a yellow solid (68.7 mg, 90.50 %). Mp: 244.5 - 247.2 °C. <sup>1</sup>H NMR (500 MHz, DMSO-d<sub>6</sub>, ppm): 8.83 (s, broad, 1H, -**H<sub>g</sub>**-) 8.77 (d, 1H, *J* = 5.81 Hz, -**H<sub>a</sub>**-), 8.17 (t, 1H, *J* = 7.74 Hz, -**H<sub>c</sub>**-), 7.76 (d, 1H, *J* = 8.18 Hz, -**H<sub>d</sub>**-), 7.60 (t, 1H, *J* = 6.65 Hz, -**H<sub>b</sub>**-), 7.18 (t, 4H, -**H<sub>i</sub>**- -**H<sub>j</sub>**-), 4.92 (dd, 1H, -**H<sub>f</sub>**-), 4.44 (d, 1H, *J* = 17.04 Hz, -**CH<sub>2</sub>**NC<sub>5</sub>H<sub>4</sub>-). <sup>13</sup>C NMR (100 MHz, DMSO-d<sub>6</sub>, ppm): 163.89, 149.43, 143.18, 140.99, 124.83, 123.60, 123.53, 122.60, 116.36, 61.56. FT-IR (liquid neat; cm<sup>-1</sup>) 3374.34 (-NH), 1652.33 (C=N), 992.91 (C-F). TOF-MS ES<sup>+</sup>, *m/z* = 422.98 (calculated *m/z* 379.55), [M<sup>+</sup> - Cl + DMSO]. Anal. % Calculated for C<sub>12</sub>H<sub>11</sub>FCl<sub>2</sub>N<sub>2</sub>Pd: C, 37.97; H, 2.92; N, 7.38. Found (%): C, 37.69; H, 2.97; N, 7.22.

### 3.5.3 dichloro-(4-bromo-*N*-((pyridin-2-yl)methyl)aniline)-palladium(II) (**PdL3**)



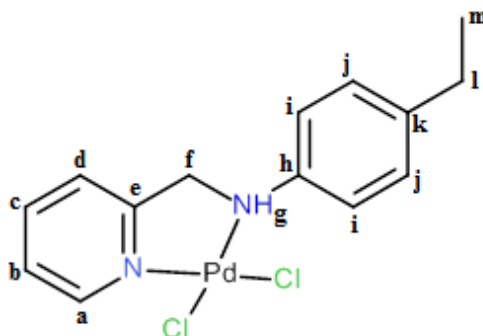
The complex **PdL3** was prepared according to a similar procedure as **PdL1** except for the use of **L3** (52.40 mg, 0.2 mmol). **PdL3** was obtained as a yellow solid (71.4 mg, 81.05 %). Mp: 266.2 - 268.8 °C. <sup>1</sup>H NMR (400 MHz DMSO-d<sub>6</sub>, ppm): 8.89 (s, broad, 1H, -**H<sub>g</sub>**-) 8.77 (d, 1H, *J* = 5.98 Hz, -**H<sub>a</sub>**-), 8.18 (t, 1H, *J* = 7.82 Hz, -**H<sub>c</sub>**-), 7.77 (d, 1H, *J* = 7.82 Hz, -**H<sub>d</sub>**-), 7.61 (t, 1H, *J* = 6.62 Hz, -**H<sub>b</sub>**-), 7.53 (d, 2H, *J* = 8.43 Hz, -**H<sub>j</sub>**-), 7.10 (d, 2H, *J* = 9.03 Hz, -**H<sub>i</sub>**-) 4.93 (m, 1H, -**H<sub>f</sub>**-), 4.49 (d, 1H, *J* = 16.54 Hz, -**H<sub>f</sub>**-). <sup>13</sup>C NMR (100 MHz, DMSO-d<sub>6</sub>, ppm): 163.91, 149.44, 146.18, 141.03, 132.58, 124.85, 123.79, 122.60, 118.90, 61.09. FT-IR (liquid neat; cm<sup>-1</sup>) 3447.85 (-NH), 1651.75 (C=N), 616.98 (C-Br). TOF-MS ES<sup>+</sup>, *m/z* = 482.92 (calculated *m/z* 440.46), [M - Cl + DMSO].

### 3.5.4 dichloro-(4-methoxy-N-((pyridin-2-yl)methyl)aniline)-palladium(II) (**PdL4**)



The complex **PdL4** was prepared according to a similar procedure as **PdL1** except for the use of **L4** (26.7 mg, 0.12 mmol). **PdL4** was obtained as a yellow solid (37.3 mg, 79.38 %). Mp: 214.2 - 216.8 °C. <sup>1</sup>H NMR (400 MHz DMSO-d<sub>6</sub>, ppm): 8.77 (s, 1H, -**H<sub>a-</sub>**) 8.65 (s, 1H, -**H<sub>g-</sub>**), 8.17 (t, 1H, *J* = 7.71 Hz, -**H<sub>c-</sub>**), 7.76 (d, 1H, *J* = 7.81 Hz, -**H<sub>d-</sub>**), 7.60 (t, 1H, *J* = 6.61 Hz, -**H<sub>b-</sub>**), 7.07 (d, 2H, *J* = 8.89 Hz, -**H<sub>j-</sub>**), 6.88 (d, 2H, *J* = 8.89 Hz, -**H<sub>i-</sub>**) 4.94 (m, 1H, -**H<sub>f-</sub>**), 4.34 (d, 1H, *J* = 16.87 Hz, -**H<sub>f-</sub>**), 3.73 (s, 3H, -**H<sub>l-</sub>**). FT-IR (liquid neat; cm<sup>-1</sup>) 3376.48 (-NH), 1652.38 (C=N), 993.18 (C-O).

### 3.5.5 dichloro-(4-ethyl-N-((pyridin-2-yl)methyl)aniline)-palladium(II) (**PdL5**)



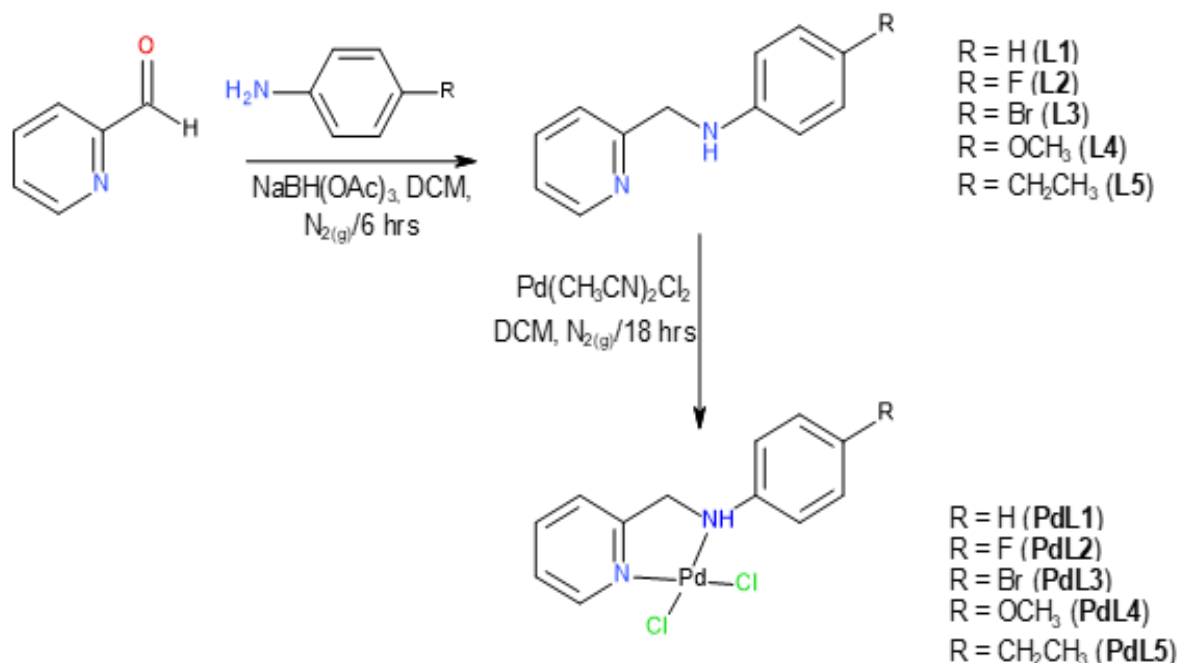
The complex **PdL5** was prepared according to a similar procedure as **PdL1** except for the use of **L5** (25.46 mg, 0.12 mmol). **PdL5** was obtained as a yellow solid (27.2 mg, 58.18 %). Mp: 187.3 - 190.2 °C. <sup>1</sup>H NMR (500 MHz DMSO-d<sub>6</sub>, ppm): 8.76 (d, 1H, *J* = 5.96 Hz, -**H<sub>a-</sub>**), 8.69 (s, 1H, -**H<sub>g-</sub>**), 8.17 (t, 1H, *J* = 7.86 Hz, -**H<sub>c-</sub>**), 7.77 (d, 1H, *J* = 7.56 Hz, -**H<sub>d-</sub>**), 7.60 (t, 1H, *J* = 6.65 Hz, -**H<sub>b-</sub>**), 7.15 (d, 2H, *J* = 8.61 Hz, -**H<sub>j-</sub>**), 7.02 (d, 2H, *J* = 8.48 Hz, -**H<sub>i-</sub>**), 4.97 (m, 2H, -**H<sub>f-</sub>**), 4.34 (d, 1H, *J* = 16.83 Hz, -**H<sub>f-</sub>**), 2.5 (m, 2H, -**H<sub>l-</sub>**), 1.25 (t, 3H, *J* = 7.50 Hz, -**H<sub>m-</sub>**). <sup>13</sup>C NMR (100 MHz, DMSO-d<sub>6</sub>, ppm): 164.38, 149.39, 144.59, 142.04, 140.95, 128.63, 124.74,

122.54, 113.09, 61.50, 28.05, 16.47. FT-IR (liquid neat;  $\text{cm}^{-1}$ ) 3372.91 (-NH), 1651.42 (C=N). TOF-MS  $\text{ES}^+$ ,  $m/z = 433.04$  (calculated  $m/z$  389.62),  $[\text{M}^+ - \text{Cl} + \text{DMSO}]$ .

### 3.6 Results and Discussion

#### 3.6.1 Synthesis of Ligands and Complexes

The ligands (**L1 - L5**) were synthesized according to a modified method by Munding, *et. al.*<sup>18</sup> via a condensation reaction of 2-pyridinecarboxaldehyde and the corresponding para substituted aniline: aniline (**L1**), 4-fluoroaniline (**L2**), 4-bromoaniline (**L3**), 4-methoxyaniline (**L4**) and 4-ethylaniline (**L5**), in the presence of sodium triacetoxyborohydride. The sodium triacetoxyborohydride is used as a reducing agent in the reaction. The ligands were obtained as orange-yellow oils in moderate yields (45 - 63%). The corresponding Pd(II) complexes (**PdL1 - PdL5**) were synthesized according to a procedure reported by Kim, *et. al.*<sup>17</sup>, by treating the ligands with  $[\text{Pd}(\text{CH}_3\text{CN})_2\text{Cl}_2]$  (**Scheme 3.1**) to obtain products in good to excellent yields (58 - 90%). The ligands were characterised by  $^1\text{H}$  NMR,  $^{13}\text{C}$  NMR and FTIR spectroscopy. Whilst the purity of the Pd(II) complexes were confirmed by  $^1\text{H}$  NMR,  $^{13}\text{C}$  NMR, COSY NMR, FT-IR spectroscopy, melting point, TOF-Mass Spectrometry and elemental analysis.



**Scheme 3.1:** Synthesis route of the ligands (**L1 - L5**) and their corresponding Pd(II) complexes (**PdL1 - PdL5**).

The  $^1\text{H}$  NMR spectra of ligands **L1** - **L5** were obtained in chloroform ( $\text{CDCl}_3$ ) to confirm their purity. In general, a signature peak at 4.41 - 4.51 ppm was observed for all synthesized ligands (**Figure A1, A4, A7, A10, A13**, in the appendix section). This singlet signal was assigned to the protons of the diastereotopic methylene group of the ligand, this validates the reduction of the aldehyde carbonyl ( $\text{C}=\text{O}$ ) by the sodium triacetoxyborohydride reagent and hence the coupling of the pyridyl moiety to the aniline. The chemical shifts recorded for this signature peak correspond to those reported for ligand **L1**<sup>16</sup> and for ligand **L2**.<sup>17</sup> Further confirming occurrence of the condensation reaction and hence formation of the ligands is the presence of a broad (-NH) peak observed as a singlet adjacent to the region of the methylene group protons. This amine hydrogen atom resonates at 3.95 – 4.55 ppm for all synthesized ligands. Similar observations were reported by Gomez *et. al.*<sup>16</sup> (**L1**) and Kim *et. al.*<sup>17</sup> (**L2**).

$^1\text{H}$  NMR spectra of the Pd(II) complexes (**PdL1** - **PdL5**) were obtained in  $\text{DMSO-d}_6$ , (**Figure A16, A20, A24, A28, A30**, in the appendix section). When comparing of the  $^1\text{H}$  NMR spectra of the ligands to the corresponding spectra of the Pd(II) complexes (**Figure 3.1**) an overall downfield shift was observed for all the aromatic protons of the complexes. For instance, while **H<sub>a</sub>** proton resonated at 8.61 ppm in **L1**, a downfield shift to 8.76 ppm was observed for the same proton on the corresponding complex **PdL1**. Additionally, while the diastereotopic methylene group protons were observed as a singlet on the free ligand  $^1\text{H}$  NMR spectra, a well-resolved ABX spin system for the protons of the methylene group of the chelating ring ( $\text{H}^{\text{A/b}}$  and  $\text{H}^{\text{B/A}}$ ) and the amine proton ( $\text{H}^{\text{X}}$ ) was observed for all complexes. Furthermore, a diagnostic change was observed for the amine proton through a significant shift from the 4.0 - 4.5 ppm region to about 8.8 ppm for all complexes. This shift indicates a successful coordination of the ligand with the palladium atom.

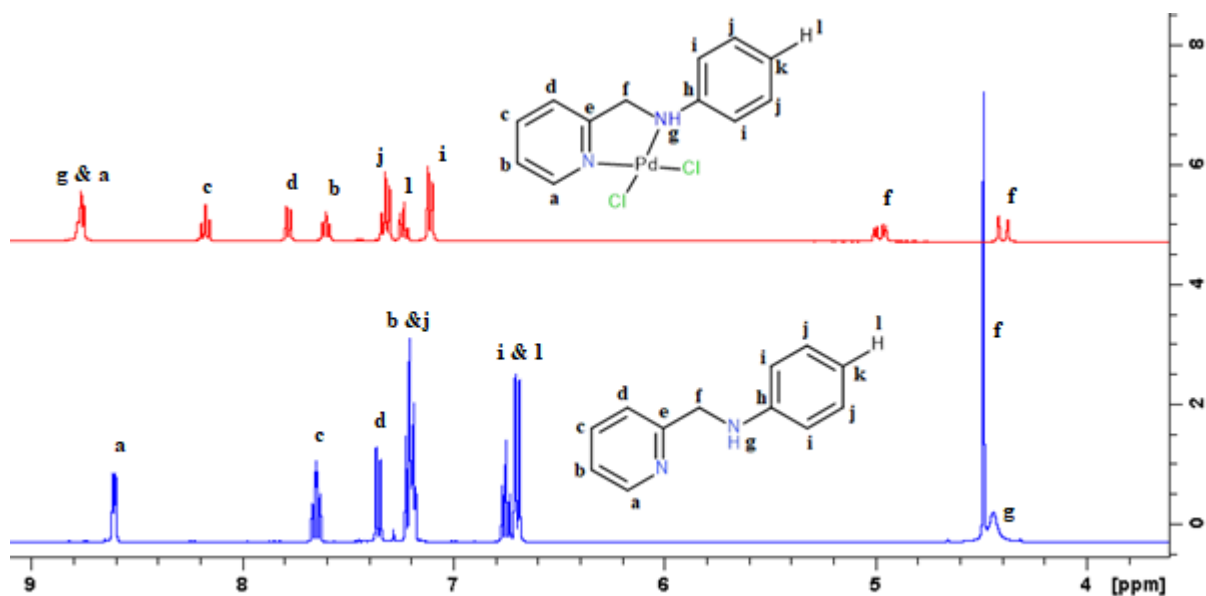


**Figure 3.1:** An overlay  $^1\text{H}$  NMR spectra of ligand **L1** and corresponding **PdL1** complex showing a notable downfield shift of all the aromatic protons and distinct changes in the methylene and amine protons.

To further elucidate the coupling between the diastereotopic methylene group protons and the amine proton, COSY spectra for the complexes was obtained. In all the complexes (**PdL1-PdL5**), the protons of the methylene group of the chelating ring ( $\text{H}^{\text{A/B}}$  and  $\text{H}^{\text{B/A}}$ ) coupled to the amine proton ( $\text{H}^{\text{X}}$ ), as shown in **Figure 3.2**. This coupling, combined with the downfield shift of the aniline hydrogen atom indicates a successful coordination of the ligand with the palladium atom.

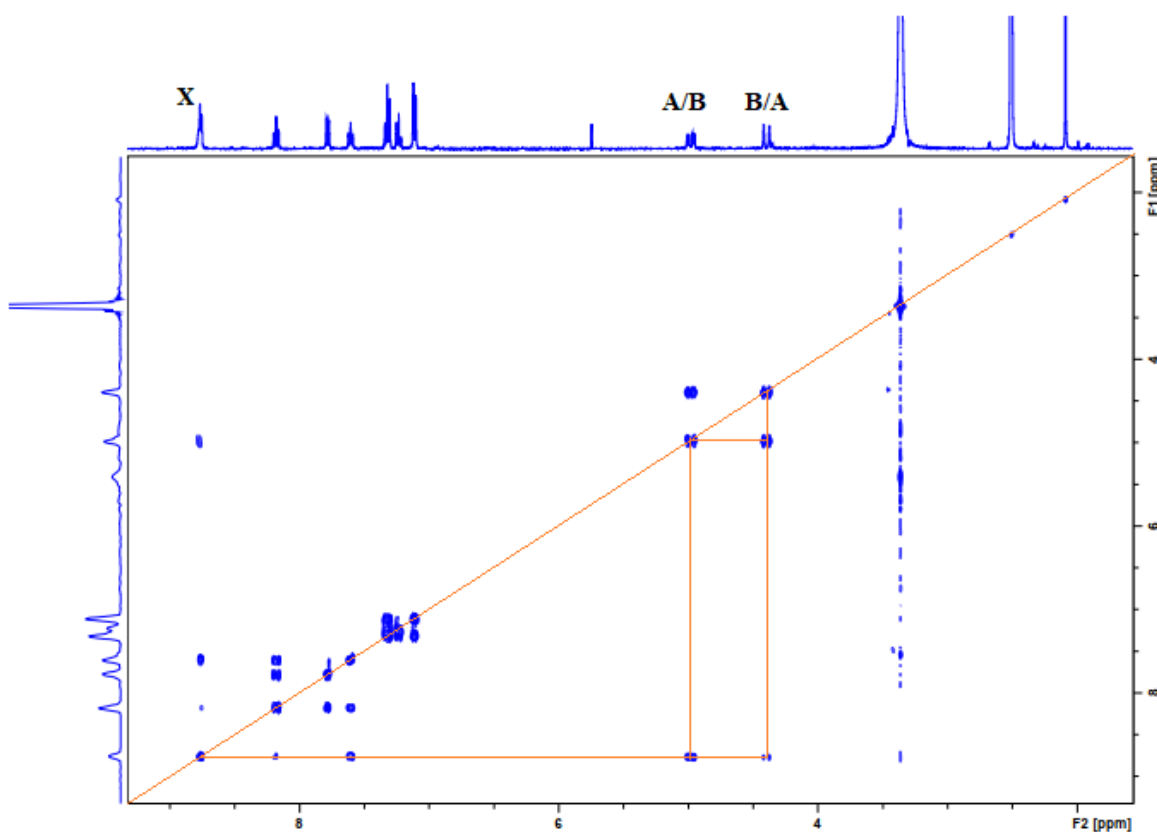


**Figure 3.2:** COSY NMR spectrum showing the ABX spin system for the protons of the methylene group of the chelating ring ( $H^A$  and  $H^B$ ) and the aniline proton ( $H^X$ ) in **PdL1**.

$^{13}\text{C}$  NMR was also used to structurally characterize the synthesized ligands (**L1-L6**) and their corresponding complexes (**PdL1 – PdL5**) (Appendix section, **Figure A2, A5, A8, A11, A14, A17, A21, A25, A31**). The data obtained from  $^{13}\text{C}$  NMR were consistent with the  $^1\text{H}$  NMR data and the number of carbons observed in the spectra correspond to that calculated in the molecular formula of the ligands and their respective complexes. For the ligand **L5** and the corresponding complex **PdL5** (**Figure 3.3**), two distinctive peaks were observed at 16.0 ppm ( $\text{CH}_3$ ) and 28.0 ppm ( $\text{CH}_2$ ) for both the ligand and the complex. A notable downfield shift was observed for all other protons upon complexation, including a shift from 49.8 ppm to 55.2 ppm for the carbon corresponding to the methylene group. Distinctively, the carbon corresponding to **Ce**, the additional carbon of the chelating ring, also showed a significant downfield shift upon complexation, these observations further validate the coordination of the ligands with the palladium metal atom.

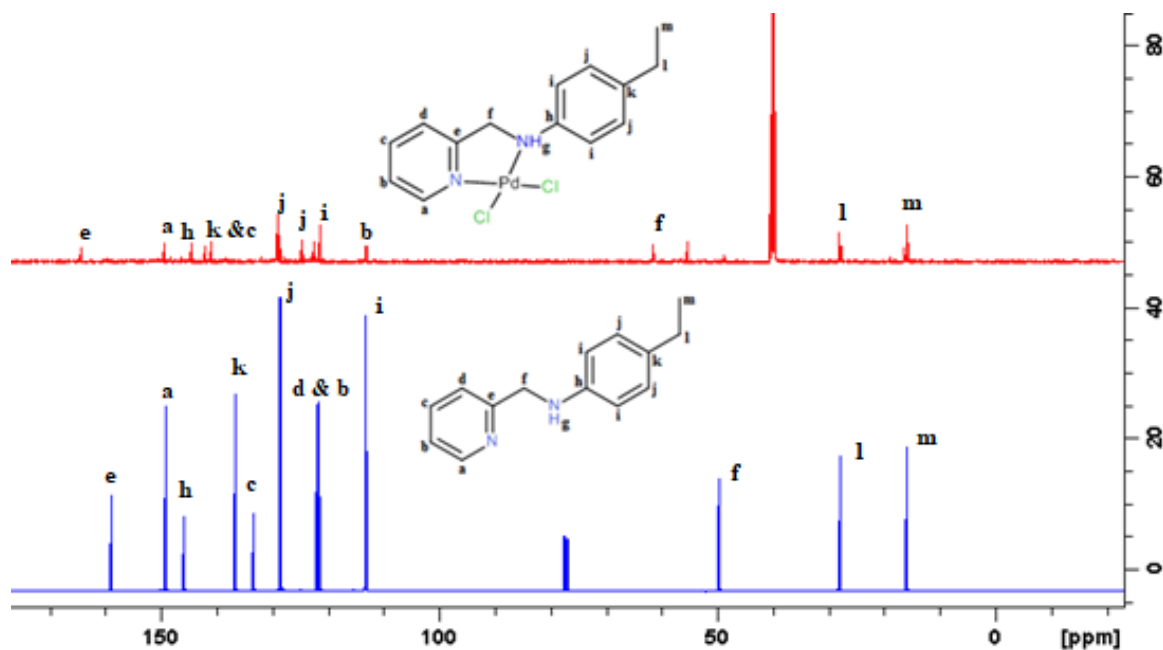


**Figure 3.3:** An overlay  $^{13}\text{C}$  NMR spectra of ligand **L5** and corresponding **PdL5** complex showing a notable downfield shift of all the aromatic and amine protons and no changes in the methylene hydrogen atoms.

FT-IR was also employed for the spectroscopic elucidation of the ligands and the complexes (Appendix section, **Figure A3, A6, A9, A12, A15, A18, A22, A26, A29, A32**). For instance, the -NH stretch of ligand **L4** and the corresponding complex, **PdL4** were observed at  $3277.26\text{ cm}^{-1}$  and  $3376.48\text{ cm}^{-1}$ , respectively. Distinctively, the amine stretch is broader and more pronounced on the complex spectrum, which indicates a change in the chemical properties of the -NH group and suggest coordination of the ligand to the palladium metal atom. **Table 3.1** indicates the summarised FTIR and LC-MS spectroscopic data.

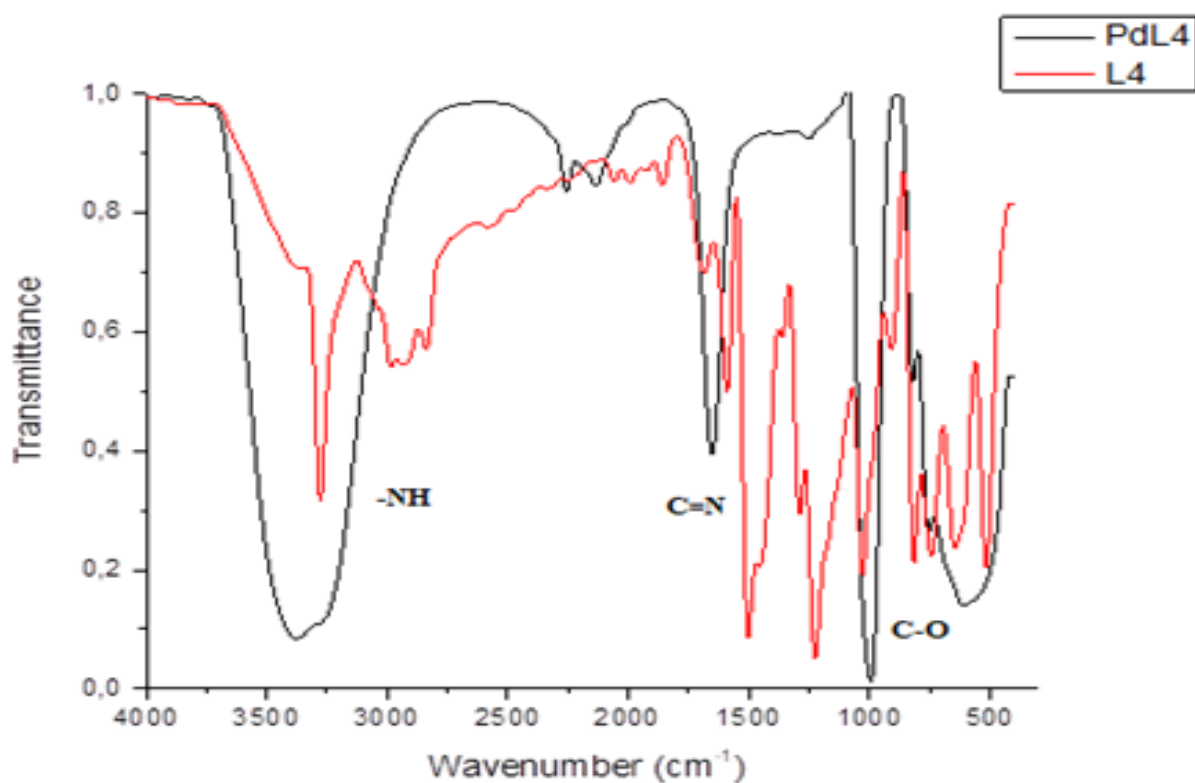


**Figure 3.4:** An overlay FT-IR spectra of ligand **L4** and corresponding **PdL4** complex showing distinctive peaks to characterize the free ligand and its complex.

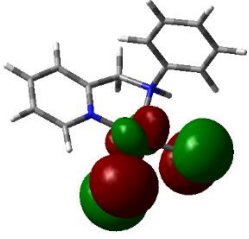
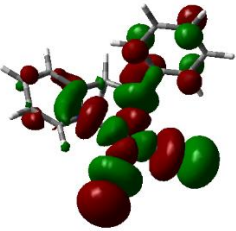
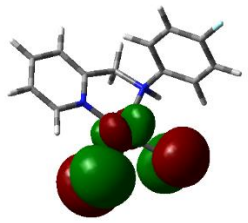
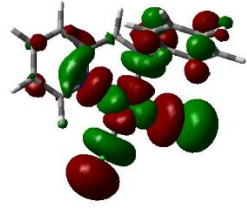
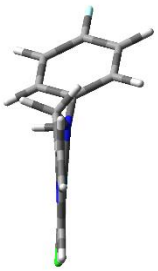
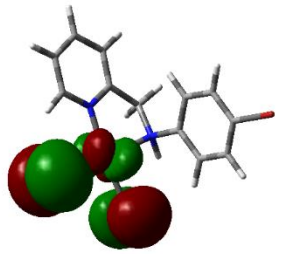
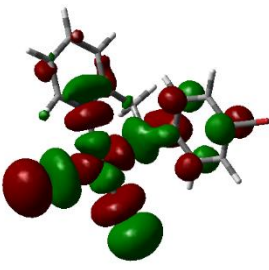
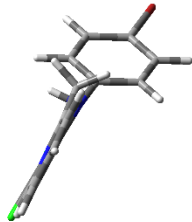
**Table 3.1:** Selected infrared spectroscopic and mass spectral data for free ligands and their corresponding complexes.

Compound	U (cm <sup>-1</sup> )			m/z	
	-NH	C-N	C-R*	Theoretical	Experimental [M <sup>+</sup> - Cl + DMSO]
<b>L1</b>	3386.90	1264.76	-		
<b>L2</b>	3264.34	1301.22	1203.19		
<b>L3</b>	3283.65	1312.06	605.60		
<b>L4</b>	3277.26	1290.30	1225.60		
<b>L5</b>	3385.35	1261.96	2947.94		
<b>PdL1</b>	3372.10	1649.06	-	359.94	404.99
<b>PdL2</b>	3374.34	1652.33	992.91	377.93	422.98
<b>PdL3</b>	3447.85	1651.75	616.98	437.85	482.92
<b>PdL4</b>	3376.48	1652.38	993.18	389.95	-
<b>PdL5</b>	3372.91	1651.42	-	387.97	433.04

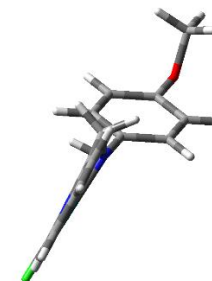
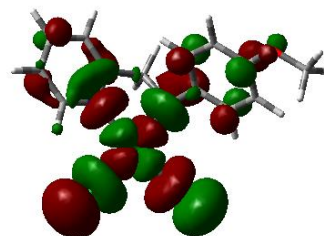
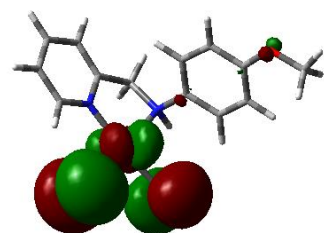
### 3.7 DFT-Computational Modelling and Analysis

In efforts to gain insight on the electronic and structural properties of the synthesized Pd(II) complexes, computational simulations and optimized DFT calculations were performed. The data obtained was used to elucidate the reactivity of the synthesized complexes. The optimized geometry of frontier molecular orbitals (HOMO and LUMO) and planarity of the complexes are presented in **Table 3.2**, while the calculated DFT data is summarized in **Table 3.3**.

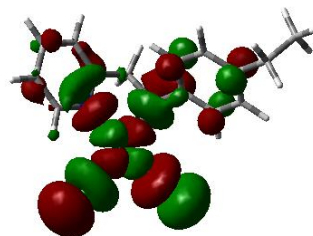
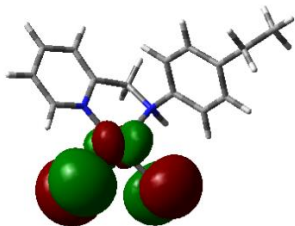
**Table 3.2:** Geometry optimized structures and DFT calculated HOMO and LUMO maps.

Complex	HOMO	LUMO	Orientation
PdL1	 The HOMO orbital map for PdL1 shows a complex structure with a central Pd atom coordinated to two ligands. The HOMO is represented by large red and green lobes, indicating high electron density in the coordination region.	 The LUMO orbital map for PdL1 shows a complex structure with a central Pd atom coordinated to two ligands. The LUMO is represented by large red and green lobes, indicating high electron density in the coordination region.	 The orientation diagram for PdL1 shows a complex structure with a central Pd atom coordinated to two ligands. The orientation is represented by a stick model with a blue line indicating the direction of the complex.
PdL2	 The HOMO orbital map for PdL2 shows a complex structure with a central Pd atom coordinated to two ligands. The HOMO is represented by large red and green lobes, indicating high electron density in the coordination region.	 The LUMO orbital map for PdL2 shows a complex structure with a central Pd atom coordinated to two ligands. The LUMO is represented by large red and green lobes, indicating high electron density in the coordination region.	 The orientation diagram for PdL2 shows a complex structure with a central Pd atom coordinated to two ligands. The orientation is represented by a stick model with a blue line indicating the direction of the complex.
PdL3	 The HOMO orbital map for PdL3 shows a complex structure with a central Pd atom coordinated to two ligands. The HOMO is represented by large red and green lobes, indicating high electron density in the coordination region.	 The LUMO orbital map for PdL3 shows a complex structure with a central Pd atom coordinated to two ligands. The LUMO is represented by large red and green lobes, indicating high electron density in the coordination region.	 The orientation diagram for PdL3 shows a complex structure with a central Pd atom coordinated to two ligands. The orientation is represented by a stick model with a blue line indicating the direction of the complex.

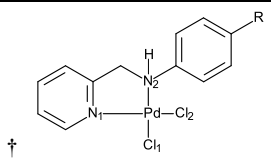
PdL4



PdL5



**Table 3.3:** Summary of DFT calculated parameters for the Pd(II) complexes.

	H	F	Br	OCH <sub>3</sub>	CH <sub>2</sub> CH <sub>3</sub>
<b>Property</b>					
<b>Bond lengths (Å)</b>					
Pd—Cl <sub>1</sub>	2.372	2.370	2.370	2.374	2.374
Pd—Cl <sub>2</sub>	2.382	2.383	2.383	2.385	2.384
Pd—N <sub>1</sub>	2.068	2.067	2.068	2.067	2.068
Pd—N <sub>2</sub>	2.139	2.140	2.142	2.134	2.137
<b>Bond angles (°)</b>					
N <sub>1</sub> -Pd-N <sub>2</sub>	81.51	81.49	81.49	81.55	81.46
N <sub>1</sub> -Pd-Cl <sub>1</sub>	93.75	93.79	93.82	93.75	93.74
N <sub>2</sub> -Pd-Cl <sub>2</sub>	89.09	88.90	88.84	88.75	89.04
Cl <sub>1</sub> -Pd-Cl <sub>2</sub>	95.64	95.82	95.85	95.99	95.77
<b>Natural charges</b>					
Pd	0.094	0.093	0.094	0.093	0.091
Cl1	-0.272	-0.267	-0.266	-0.277	-0.275
Cl2	-0.301	-0.299	-0.299	-0.307	-0.303
N1	-0.258	-0.259	-0.259	-0.258	-0.258
N2	-0.535	-0.534	-0.534	-0.532	-0.532
<b>Point group symmetry</b>					
Dipole moment (Debye)	13.7083	13.3631	13.3631	12.6360	13.9099
$\mu$	-4.3449	-4.4939	-4.9468	-4.2752	-4.2911
$\eta$	1.8089	1.8042	1.7973	1.8225	1.8156
$\omega$	5.3180	5.5967	6.8076	5.0144	5.0711
HOMO (eV)	-6.154	-6.298	-6.292	-6.098	-6.107
LUMO (eV)	-2.536	-2.690	-2.697	-2.453	-2.475
$\Delta E$ (eV)	3.618	3.608	3.595	3.645	3.631

† All complexes studied follow the same numbering.

The frontier orbitals of all complexes have similar features due to the similar basic structures. The DFT optimized structures in **Table 3.2** reveal that the highest occupied molecular orbital (HOMO) electron densities of all the Pd complexes are predominantly localized on the 4*d*-orbitals of the Pd(II) metals and the 3*p*-orbitals of the chloride ligands. **PdL4** shows a minimal electron contribution on the methoxy substituent of the inert ligand. The HOMO of the Pd(II) metal center demonstrate a transfer of electrons from the metal to the LUMO of the inert ligand. On the other hand, the LUMOs are distributed in all the complexes along the chloride, palladium, and N-(pyridin-2-ylmethyl) aniline ligand. The presence of LUMO electrons on the inert ligands further indicate their potential  $\pi$ -acceptor abilities, which may be attributed to the presence of the  $\pi$ -acceptor pyridyl ring.

Also presented in **Table 3.2**, are DFT optimized planarity structures showing a similar planarity of all the complexes, with the pyridyl moiety and chloride ligands in-plane with the metal center, while the *para* substituted aniline moiety is noticeably out-of-plane for all the complexes. This is due to the flexibility brought by the methylene group within the inert ligand. The computational data is comparable with that reported in literature for **PdL1**, **PdL2** and **PdL4**.<sup>17, 23-26</sup>

Even though the structure modification and different substitutions almost have no impact on the composition of the frontier orbitals, the trend in the computed energy gap,  $\Delta E_{\text{LUMO-HOMO}}$  noticeably increases in the order **PdL3** < **PdL2** < **PdL1** < **PdL5** < **PdL4** (**Table 3.3**). This trend indicates an increase of electron donation density around the Pd(II) metal center. The increase in the HOMO energy level followed a similar trend. Similarly, this trend was observed in the increase in the LUMO energy level, signifying a decrease in the  $\pi$ -acceptor abilities of the chelating ligands.

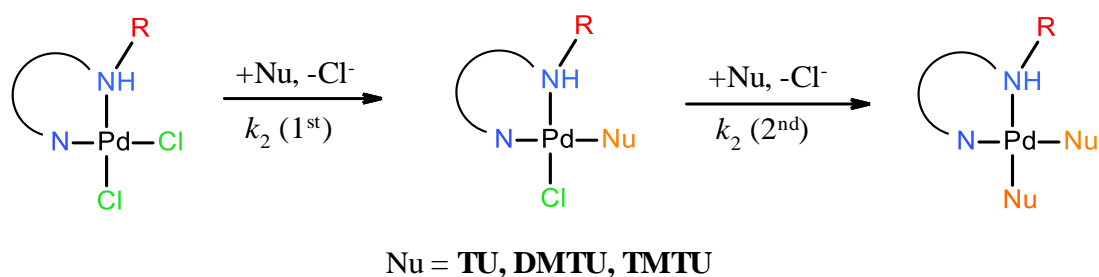
Based on the computational data presented in **Table 3.3**, the introduction of alternate electron withdrawing and electron donating substituents on the inert ligand have little to no significant effect on the Pd – Cl bond length, bond angle or NBO charges of the palladium metal. However, a notable impact is observed in the overall electrophilicity of the complexes; with an increase in electrophilicity in the presence of electron withdrawing substituents, i.e., Br (6.8076) and F (5.5968), and reduced electrophilicity for electron donating groups, CH<sub>2</sub>CH<sub>3</sub> (5.0711) when using **PdL1** as a reference. The dipole moment of complexes with electron withdrawing groups **PdL2** and **PdL3** is lower than that of **PdL1**, the unsubstituted aniline complex, while the **PdL5**, with electron donating group (CH<sub>2</sub>CH<sub>3</sub>) has the highest dipole moment (13.9099).

## 3.8 Substitution Kinetic Analysis

### 3.8.1 Kinetic Measurements

Substitution of labile chloride ligands from the Pd(II) complexes by three thiourea nucleophiles, *viz.* thiourea (TU), N,N'-dimethylthiourea (DMTU) and N,N,N',N'-tetramethylthiourea (TMTU) was studied under *pseudo* first-order conditions, as a function of concentration and temperature using the UV-Visible and Stopped-Flow spectrophotometer. The UV-Visible spectrophotometer allowed for the determination of the best suitable wavelength to use for the kinetic analysis by following the change in absorbance spectrophotometrically. Wavelengths selected for kinetic analysis are presented in **Table A.1**, Appendix section.

Since the Pd(II) complexes used in the study contain two types of nitrogen bonded to the Pd metal, i.e. the aromatic pyridine and the sp<sup>3</sup>-hybridized primary amine, it is therefore important to understand which chloride ligand will be substituted first. The chloride *trans* to the pyridine ligand will be substituted first, since the pyridine has a stronger *trans* effect compared to the amine group. This difference in *trans* effect is strongly supported by the trends in the DFT data in **Table 3.3**. The natural bond orbital (NBO) charges of N<sub>1(py)</sub> and N<sub>2(amine)</sub> or the bond lengths Pd—N<sub>1(py)</sub> and Pd—N<sub>2(amine)</sub> are significantly different. A similar trend was observed for Pt(II) complexes with similar ligands.<sup>27-32</sup> **Scheme 3.2** shows the stepwise substitution reaction of the chloride from the Pd metal by thiourea nucleophiles.



**Scheme 3.2:** Proposed stepwise substitution reaction with the thiourea nucleophiles.

### 3.8.2 <sup>1</sup>H NMR Spectroscopy

To confirm that the first substitution step is due to the displacement of one chloride ligand by the thiourea nucleophile (**TU**, **DMTU**, **TMTU**) while the second substitution step is assigned to second chloride ligand as shown in **Scheme 3.2**, the product of the substitution reaction of **PdL1** by six equivalents of **TU** was monitored using <sup>1</sup>H NMR spectroscopy (**Figure 3.5**). Due

to the fast rate of reaction for the Pd(II) complexes, we could not follow the substitution reaction, but instead we analyzed the product that formed after the reaction was complete.

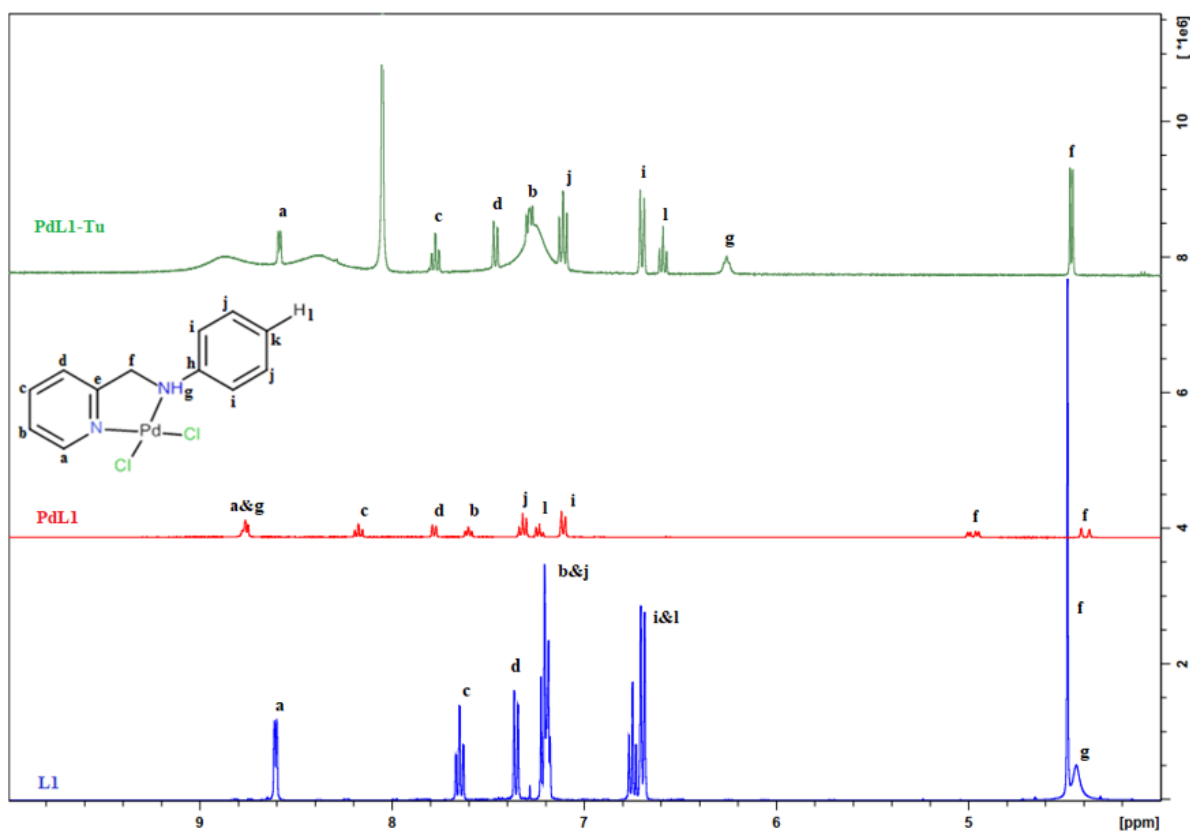


**Figure 3.5:**  $^1\text{H}$  NMR spectra of **L1**, **PdL1** and the substituted reaction of **PdL1** with six equivalents of **TU** at 30 °C.

**Figure 3.5**, shows the  $^1\text{H}$  NMR overlay spectra of the ligand (**L1**), **PdL1** and the product of the reaction between **PdL1** and **TU**. The complex with coordinated **TU**, shows the methylene protons at 4.46 ppm and is now showing as a doublet with a coupling constant of 6.32 Hz. In **PdL1** these protons gave two different signals, 4.98 and 4.40 ppm. The NH appears at as a broad singlet at 6.26 ppm, which when compared to the ligand (4.27 ppm) it is further downfield and indicates that the Pd is still coordinated to it. The proton next to the pyridine ring ( $\text{H}_a$ ) for the ligand is at 8.60 ppm, for **PdL1** is at 8.76 ppm and for the substituted Pd complex is at 8.58 ppm. All the other proton signals in the substituted product shifted downfield when compared with the unsubstituted complex, this is mainly due to the solvent used to run the NMR. Therefore, in this case the pyridine ring is still coordinated to the Pd metal. Also, the broad signals in the region, 9.04 – 8.66; 8.54 – 8.20; 7.39 - 7.15 ppm are due to the coordinated sulfur from the thiourea nucleophile.

### 3.8.3 First Substitution Step

#### 3.8.3.1 Concentration Dependence

All kinetic traces obtained from concentration and temperature dependence analysis gave excellent fits to the single-exponential decay function. Using an online Pro-Data SX programme, the kinetic traces were fitted into a non-linear least square fit to generate the observed *pseudo* first-order rate constant,  $k_{obs}$  (equation 3.1). All the reported rate constants represent an average of at least five to eight independent kinetic runs for each experimental condition. A typical kinetic trace generated from the stopped-flow technique is shown in **Figure 3.6** for the reaction between **PdL1** and **TU** nucleophile.

$$A_t = A_o + (A_o - A_\infty)exp(-k_{obs}t) \quad (3.1)$$

Where,  $A_t$  = absorbance at time  $t$ ,  $A_o$  = absorbance of reaction mixture initially and  $A_\infty$  = absorbance at the end of the reaction.

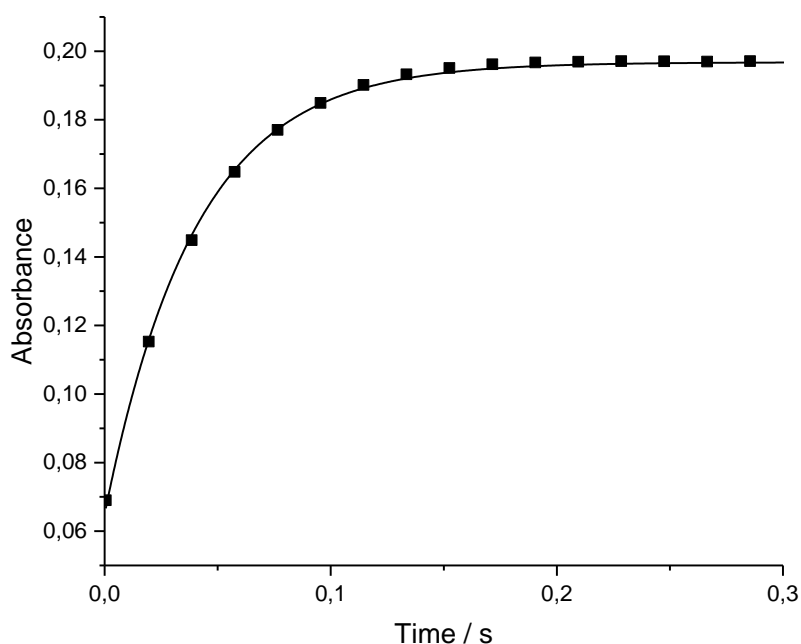


**Figure 3.6:** Kinetic trace obtained from the Stopped-Flow spectrophotometer showing a single exponential fit for the reaction between **PdL1** and **TU** in ultra-pure water followed at 295 nm,  $I = 0.1$  M at 298 K.

Plots of average  $k_{obs}$  against nucleophile concentrations,  $[Nu]$ , afforded a linear regression with zero intercepts for all complexes, from which the second-order rate constants,  $k_2(1^{st})$ , were obtained from the slope of these graphs according to equation 3.2. A representative plot of  $k_{obs}$

versus concentration of all three nucleophiles for **PdL4** is shown in **Figure 3.7**; similar plots are presented in **Figure A34 - 38** of the appendix. The zero-intercept indicates that the substitution was irreversible. The second-order rate constants,  $k_2$ , of the complexes are summarized in **Table 3.4**.

$$k_{obs} = k_2[\text{Nu}] \quad \text{where Nu} = \text{TU, DMTU, TMTU} \quad (3.2)$$

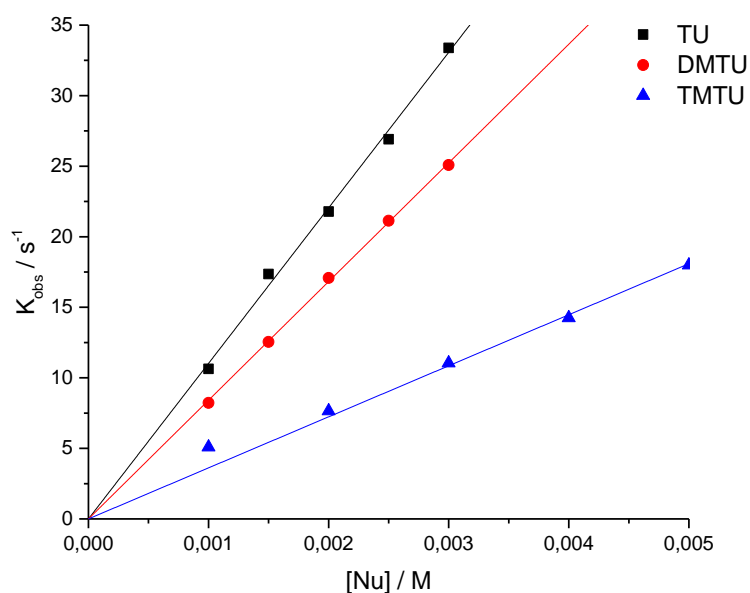


**Figure 3.7:** Dependence of  $k_{obs}$  on the concentration of the entering nucleophiles for the displacement of chloride on **PdL4** complex in water,  $I = 0.1 \text{ M}$  (LiCl),  $T = 298 \text{ K}$ .

The second-order rate constants,  $k_2$ , for the substitution of chloride ligands by thiourea nucleophiles increases in the order **PdL4 < PdL5 < PdL1 < PdL2 < PdL3** for **TU** and **DMTU** nucleophiles. The trend in reactivity is attributed to the difference in electronic effects within the complexes, which is supported by the electrophilicity index, chemical potential, chemical hardness and the  $\Delta E_{\text{LUMO-HOMO}}$ , **Table 3.3**.

The second-order rate constants,  $k_2$ , in **Table 3.4** show that the reactivity of the complexes increases with the presence of electron withdrawing substituents and decreases when an electron donating group is attached on the *para* position of the phenyl group attached the amine. The amine proton in the  $-\text{NH}$  substituted atom is acidic, and therefore more electron deficient, this assists with electron withdrawal from the Pd metal center. The presence of an electron withdrawing group in **PdL2** and **PdL3** leads to increased reactivity when compared to the

unsubstituted **PdL1** complex. Using the rate constants for **TU** to compare the reactivity of the complexes, **PdL1** ( $k_2 = 1.45 \times 10^4 \text{ M}^{-1}\text{s}^{-1}$ ), **PdL2** ( $k_2 = 1.58 \times 10^4 \text{ M}^{-1}\text{s}^{-1}$ ) and **PdL3** ( $k_2 = 1.75 \times 10^4 \text{ M}^{-1}\text{s}^{-1}$ ) and we can clearly see that the reactivity increases with the electron withdrawing strength of the atom on the aniline moiety. The fluorine and bromine groups in **PdL2** and **PdL3** withdraw electrons from aniline moiety of the ligand which in turn pulls electrons from the electron deficient amine that is coordinated to the metal center. This phenomenon results in the loss of electron density from the ligand moiety and increases the electrophilicity of the metal center, which is supported by the DFT calculated electrophilicity index ( $\omega$ ). Complexes with a high value for  $\omega$  characterise strong electrophiles.<sup>33, 34</sup> **PdL3**, with a bromo substituent has the highest electrophilicity index, 6.8076, which further supports the high reactivity when compared for all the other complexes. The reactivity of **PdL3** is further supported by the more negative chemical potential (-4.9468), lower strength of electron acceptor (-4.9468) and lower dipole moment (13.3631), when compared with all the Pd complexes.

Even though fluorine is more electronegative than bromine, the reactivity of **PdL3** is greater than the reactivity of **PdL2** by a factor of 1.11. The slight increase in reactivity of **PdL3**, can be accounted for by looking at the DFT calculated electronic parameters (**Table 3.3**). The presence of either a -F or -Br as an ancillary substituent on the aniline group does not result in a significant change in electronic effects (bond lengths, bond angles or natural charges). However, the electrophilicity index and chemical potential is higher for **PdL3**, whilst the chemical hardness is lower.

In the case of **PdL4** and **PdL5**, with electron donating groups, -CH<sub>2</sub>CH<sub>3</sub> and -OCH<sub>3</sub> on the *para* position of the aniline moiety, the reactivity is lower than that of **PdL1** and complexes with electron withdrawing substituents, **PdL2** and **PdL3**. The positive  $\sigma$ -inductive effect of the ethyl or methoxy substituents increases electron density of the phenyl ring and hence the acidic amine coordinated to the metal. This reduces the electrophilicity of the metal centers, as supported by the lower electrophilicity index of **PdL4** (5.0143) and **PdL5** (5.0711) compared to those for **PdL1** (5.3180), **PdL2** (5.5967) and **PdL3** (6.8076).

The general trend for the substitution of chloride ligands by thiourea nucleophiles follows the order **TMTU** < **DMTU** < **TU**. This order is compatible with the steric demands of the different nucleophiles with the bulkier **TMTU** reacting slower than the less sterically hindered **TU**. However, an exception was observed in the reaction of **PdL3** with **DMTU**, where the  $k_2$  value and hence, the substitution was faster than that of **PdL3** with **TU**. This phenomenon has been

reported in literature, where the inductive effect of **DMTU** overcompensates for the steric effect of this nucleophile.<sup>35</sup>

### 3.8.3.2 Temperature Dependence

Temperature dependence reactions of the second-order rate constants were observed over the temperature range of 288 – 308 K, at 5 K intervals. Typical Eyring plots for **PdL4** with the three nucleophiles are shown in **Figure 3.8**; similar plots are presented in **Figure A39 - 43**, of the appendix. Using the Eyring equation (3.3), the enthalpy of activation ( $\Delta H^\ddagger$ ) and entropy of activation ( $\Delta S^\ddagger$ ) were extrapolated from the slope and the y-intercept, respectively. The enthalpy of activation ( $\Delta H^\ddagger$ ) and entropy of activation ( $\Delta S^\ddagger$ ) are summarized in **Table 3.4**.

$$\ln\left(\frac{k_2}{T}\right) = -\left(\frac{\Delta H^\ddagger}{RT}\right) + \left(\ln\frac{k_B}{h} + \frac{\Delta S^\ddagger}{R}\right) \quad (3.3)$$

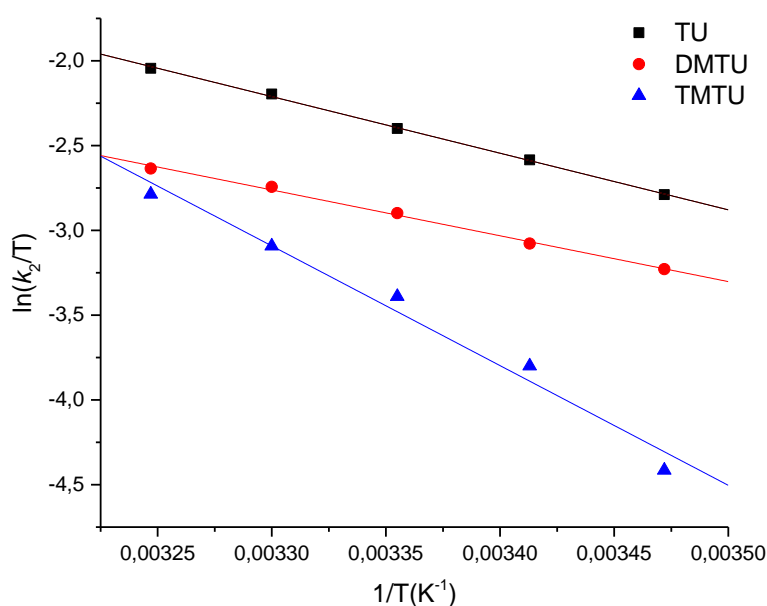


**Figure 3.8:** Plot of  $\ln(k_2/T)$  against  $1/T$  for the reaction of **PdL4** with the three nucleophiles at various temperatures in the temperature range 288 – 308 K.

Based on the results tabulated in **Table 3.4**, the values of enthalpy of activation are positive, while the entropy of activation values are largely negative. This trend in thermodynamic parameters supports an associative mode of activation for the substitution step, which is in line with the square-planar  $d^8$  metal complexes.<sup>36</sup>

**Table 3.4:** Rate constants and activation parameters for the first substitution reactions.

Complex	Nucleophile	$K_2$ (1 <sup>st</sup> ) / M <sup>-1</sup> s <sup>-1</sup> (10 <sup>4</sup> )	$\Delta H^\ddagger$ (1 <sup>st</sup> ) / kJmol <sup>-1</sup>	$\Delta S^\ddagger$ (1 <sup>st</sup> ) / JK <sup>-1</sup> mol <sup>-1</sup>
<b>PdL1</b>	<b>TU</b>	1.45 ± 0.026	28.06 ± 1.30	-122.44 ± 5.35
	<b>DMTU</b>	1.35 ± 0.019	25.10 ± 1.51	-135.85 ± 5.09
	<b>TMTU</b>	0.62 ± 0.014	22.09 ± 2.11	-146.91 ± 7.07
<b>PdL2</b>	<b>TU</b>	1.58 ± 0.032	10.67 ± 0.67	-182.02 ± 2.26
	<b>DMTU</b>	1.45 ± 0.023	26.68 ± 1.38	-130.07 ± 4.63
	<b>TMTU</b>	0.32 ± 0.002	30.39 ± 1.82	-125.13 ± 6.12
<b>PdL3</b>	<b>TU</b>	1.75 ± 0.040	21.15 ± 0.17	-147.37 ± 0.57
	<b>DMTU</b>	1.87 ± 0.039	18.71 ± 1.15	-154.66 ± 3.86
	<b>TMTU</b>	0.71 ± 0.013	32.67 ± 2.62	-114.33 ± 8.79
<b>PdL4</b>	<b>TU</b>	1.10 ± 0.012	27.77 ± 0.53	-124.63 ± 1.77
	<b>DMTU</b>	0.84 ± 0.004	22.47 ± 0.81	-146.70 ± 2.70
	<b>TMTU</b>	0.36 ± 0.004	58.70 ± 4.86	-29.90 ± 16.32
<b>PdL5</b>	<b>TU</b>	1.12 ± 0.010	42.52 ± 2.63	-79.20 ± 8.83
	<b>DMTU</b>	1.10 ± 0.015	32.07 ± 2.24	-113.65 ± 7.52
	<b>TMTU</b>	0.82 ± 0.013	27.20 ± 0.89	-127.15 ± 2.97

### 3.8.4 Second Substitution Step

The second substitution step is the displacement of the chloride that is *trans* to the N<sub>amine</sub> ligand by **TU**, **DMTU** and **TMTU**. The reaction was followed under the same conditions as the first substitution step. **Figure 3.9** shows the spectral changes for the second substitution step, where a steady increase in absorbance was observed until the end of the reaction was reached. The wavelengths selected for kinetic analysis are presented in **Table A.1**, appendix section, and are similar to those used for the first substitution step.

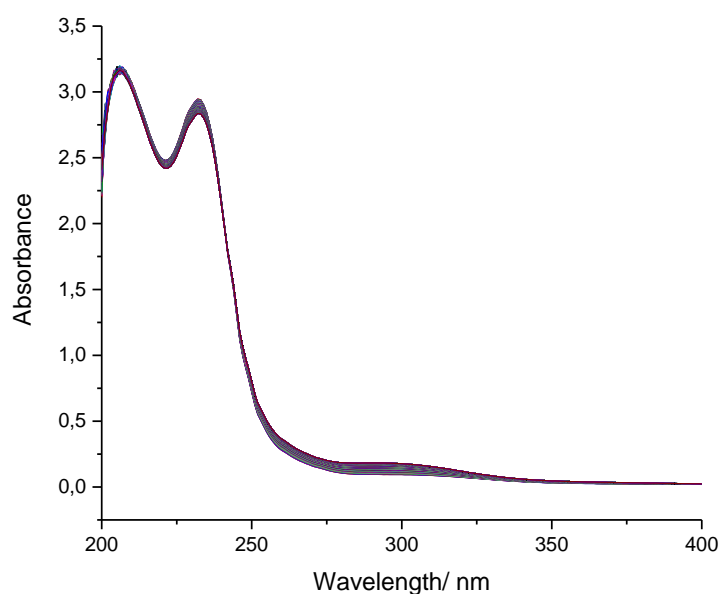


**Figure 3.9:** UV-Visible spectral changes for the reaction between **PdL1** and **DMTU** at 298 K,  $I = 0.1$  M.

#### 3.8.4.1 Concentration Dependence

All the kinetic traces obtained from concentration dependence analysis gave excellent fits to the single-exponential decay function, and we used to generate the observed *pseudo* first-order rate constant,  $k_{\text{obs}}$ . The reported rate constants represent an average of at least five independent kinetic runs for each experimental condition. A typical kinetic trace generated by the UV-Visible is shown in **Figure 3.10** for the reaction between **PdL1** and **DMTU** nucleophile.

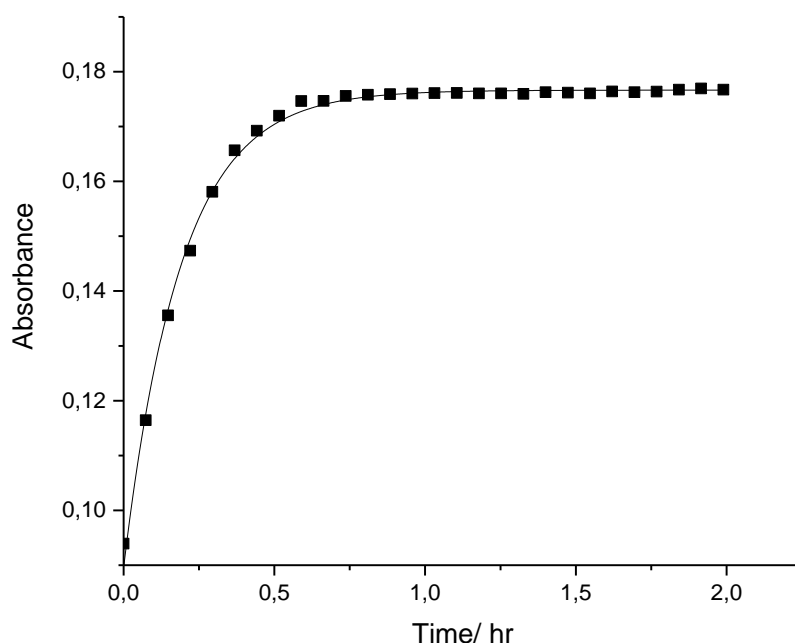


**Figure 3.10:** Kinetic trace obtained from the UV-Vis spectrophotometer showing a single exponential fit for the reaction between **PdL1** and **DMTU** in ultra-pure water followed at 295 nm,  $I = 0.1$  M at 298 K.

The second substitution step is slower due to the coordinated thiourea nucleophile, and the steric effects caused by the first coordinated nucleophile and electron donation towards the Pd(II) metal center, which makes it less electrophilic. The second substitution step for all complexes is independent of concentration, i.e., as concentration increases, the observed rate constant does not change significantly. **Figure 3.11** indicates the effect of concentration change on the first and second substitution steps for **PdL1** and **TU**.

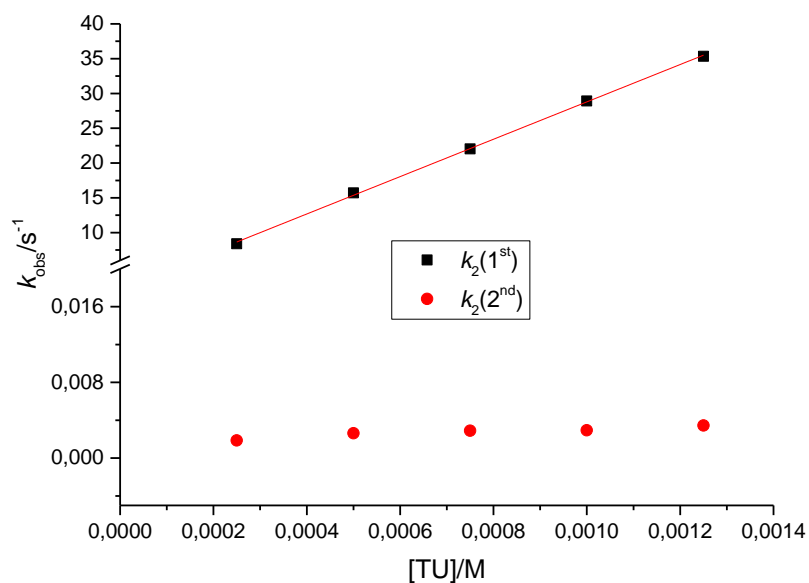


**Figure 3.11:** Plots of  $k_{obs}$  against concentration of the **PdL1** complex with **TU**,  $I = 0.1$  M (LiCl),  $T = 298$  K.

Since the observed rate constant,  $k_{obs}$  for the second substitution step does not depend on the change in concentration of the nucleophiles, it implies that second order rate constant, ( $k_2(2^{nd})$ ), for the second substitution can be expressed by equation 3.4.<sup>27, 30, 37</sup>

$$k_{obs} = k_2 \quad (3.4)$$

The rate of substitution follows the same increasing order as the first substitution step, **PdL4** < **PdL5** < **PdL1** < **PdL2** < **PdL3** for all the nucleophiles (**Table 3.5**).

**Table 3.5:** Rate constants and activation parameters for the second substitution reactions.

Complex	Nucleophile	$k_2(2^{\text{nd}}) / \text{M}^{-1}\text{s}^{-1} (10^{-3})$	$\Delta H^\ddagger(2^{\text{nd}}) / \text{kJmol}^{-1}$	$\Delta S^\ddagger(2^{\text{nd}}) / \text{JK}^{-1}\text{mol}^{-1}$
<b>PdL1</b>	<b>TU</b>	$2.60 \pm 0.025$	$40.32 \pm 1.44$	$-276.46 \pm 4.36$
	<b>DMTU</b>	$1.73 \pm 0.045$	$50.26 \pm 3.93$	$-130.17 \pm 12.01$
	<b>TMTU</b>	$0.94 \pm 0.020$	$64.11 \pm 3.83$	$-88.50 \pm 11.52$
<b>PdL2</b>	<b>TU</b>	$4.44 \pm 0.008$	$18.14 \pm 0.49$	$-229.47 \pm 1.48$
	<b>DMTU</b>	$2.15 \pm 0.023$	$48.33 \pm 3.60$	$-136.03 \pm 11.01$
	<b>TMTU</b>	$0.97 \pm 0.024$	$79.66 \pm 3.66$	$-119.14 \pm 10.99$
<b>PdL3</b>	<b>TU</b>	$8.94 \pm 0.012$	$34.02 \pm 2.60$	$-169.61 \pm 8.02$
	<b>DMTU</b>	$4.61 \pm 0.009$	$43.03 \pm 2.06$	$-146.10 \pm 6.22$
	<b>TMTU</b>	$1.01 \pm 0.021$	$34.46 \pm 0.82$	$-188.36 \pm 2.61$
<b>PdL4</b>	<b>TU</b>	$2.22 \pm 0.008$	$38.29 \pm 0.45$	$-168.31 \pm 1.52$
	<b>DMTU</b>	$0.88 \pm 0.018$	$59.48 \pm 1.06$	$-103.24 \pm 3.57$
	<b>TMTU</b>	$0.23 \pm 0.019$	$109.46 \pm 4.07$	$-153.09 \pm 13.66$
<b>PdL5</b>	<b>TU</b>	$2.37 \pm 0.018$	$50.47 \pm 4.24$	$-127.72 \pm 12.25$
	<b>DMTU</b>	$1.09 \pm 0.015$	$65.50 \pm 2.99$	$-81.83 \pm 9.98$
	<b>TMTU</b>	$0.48 \pm 0.016$	$62.44 \pm 2.74$	$-104.30 \pm 9.35$

### 3.8.4.2. Temperature Dependence

Temperature dependence reactions of the observed rate constants were monitored over the temperature range of 288 – 308 K, at 5 K intervals. Typical Eyring plots for **PdL3** with the three nucleophiles are shown in **Figure 3.12**; similar plots are presented in **Figure A44 - 48**, in the appendix. The enthalpy of activation ( $\Delta H^\ddagger$ ) and entropy of activation ( $\Delta S^\ddagger$ ) for this step are summarized in **Table 3.5**. The thermodynamic parameters support an associative mode of activation for the second substitution step.

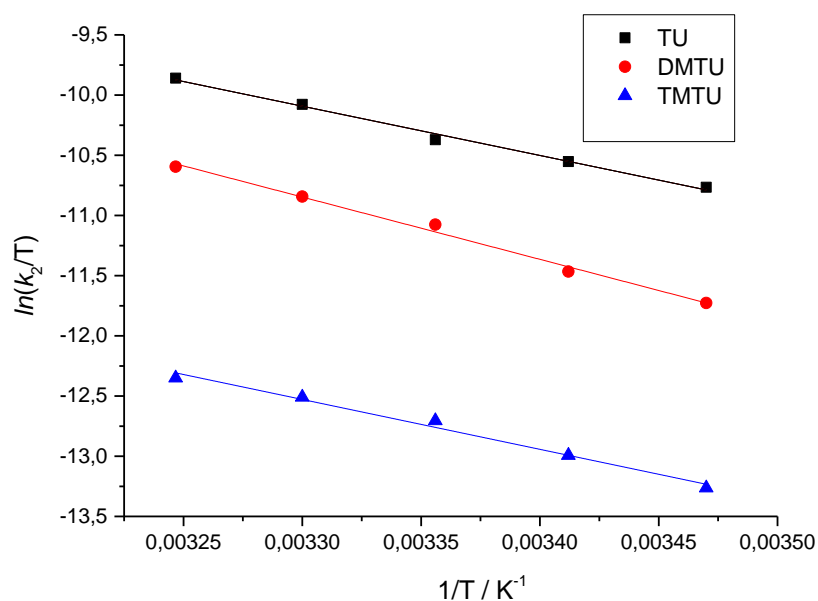


**Figure 3.12:** Plot of  $\ln(k_2/T)$  against  $1/T$  for the reaction of **PdL3** with the three nucleophiles at various temperatures in the temperature range 288 – 308 K.

### 3.9 Conclusion

Five bidentate Pd(II) complexes containing different *para* substituted N-((pyridin-2-yl)methyl)aniline chelating spectator ligands of different electronic properties were synthesized. The purity of the synthesized ligands and complexes were confirmed using <sup>1</sup>H NMR, <sup>13</sup>C NMR, FTIR, LC-MS and elemental analysis. The kinetics and mechanism of their substitution reactions with sulfur-donor nucleophiles were studied under *pseudo* first-order conditions. The substitution of two chloride ligands by the nucleophiles from the Pd(II) complexes was consecutive. The chloride *trans* to the pyridine ligand was substituted first, since the pyridine has a stronger *trans* effect compared to the amine group. The rate of consecutive chloride substitution from the complexes by the nucleophiles followed the order **PdL4** < **PdL5** < **PdL1** < **PdL2** < **PdL3**. The higher reactivity of **PdL3** and **PdL2** is due to the withdrawal of electron density from the aniline moiety of the ligand by the –F and –Br substituents which in turn pulls electrons from the electron deficient amine that is coordinated to the metal center. This results in the loss of electron density from the ligand moiety and increases the electrophilicity of the metal center and thus the substitution reaction. The addition of an electron-donating groups as substituents (**PdL4** and **PdL5**), leads to a decrease in reactivity compared to the electron withdrawing groups (**PdL2** and **PdL3**) and the unsubstituted complex (**PdL1**). The reactivity of the nucleophiles depends on steric effects, with the bulky **TMTU** being the least reactive. The first and second substitution steps are

associatively activated given that the enthalpy of activation are positive while the entropy of activation are negative, which suggest an associative mode of activation for the substitution process.

### 3.10 References

1. Qi, L.; Luo, Q.; Zhang, Y.; Jia, F.; Zhao, Y.; Wang, F., Advances in toxicological research of the anticancer drug cisplatin. *Chemical research in toxicology* **2019**, *32* (8), 1469-1486.
2. Chu, E.; Sartorelli, A., Cancer chemotherapy. *Lange's Basic and Clinical Pharmacology* **2018**, 948-976.
3. Abu-Surrah, A. S.; Kettunen, M., Platinum group antitumor chemistry: design and development of new anticancer drugs complementary to cisplatin. *Current medicinal chemistry* **2006**, *13* (11), 1337-1357.
4. Abu-Surrah, A. S.; Al-Sa'doni, H. H.; Abdalla, M. Y., Palladium-based chemotherapeutic agents: routes toward complexes with good antitumor activity. *Cancer therapy* **2008**, *6* (6), 1-10.
5. Kapdi, A. R.; Fairlamb, I. J., Anti-cancer palladium complexes: a focus on PdX<sub>2</sub>L<sub>2</sub>, palladacycles and related complexes. *Chemical Society Reviews* **2014**, *43* (13), 4751-4777.
6. Coskun, M. D.; Ari, F.; Oral, A. Y.; Sarimahmut, M.; Kutlu, H. M.; Yilmaz, V. T.; Ulukaya, E., Promising anti-growth effects of palladium (II) saccharinate complex of terpyridine by inducing apoptosis on transformed fibroblasts in vitro. *Bioorganic & medicinal chemistry* **2013**, *21* (15), 4698-4705.
7. Bugarčić, Ž. D.; Bogojeski, J.; van Eldik, R., Kinetics, mechanism and equilibrium studies on the substitution reactions of Pd (II) in reference to Pt (II) complexes with bio-molecules. *Coordination Chemistry Reviews* **2015**, *292*, 91-106.
8. Lazarević, T.; Rilak, A.; Bugarčić, Ž. D., Platinum, palladium, gold and ruthenium complexes as anticancer agents: Current clinical uses, cytotoxicity studies and future perspectives. *European journal of medicinal chemistry* **2017**, *142*, 8-31.
9. Jahromi, E. Z.; Divsalar, A.; Saboury, A. A.; Khaleghizadeh, S.; Mansouri-Torshizi, H.; Kostova, I., Palladium complexes: new candidates for anti-cancer drugs. *Journal of the Iranian Chemical Society* **2016**, *13* (5), 967-989.
10. Zhao, G.; Lin, H., Metal complexes with aromatic N-containing ligands as potential agents in cancer treatment. *Current Medicinal Chemistry-Anti-Cancer Agents* **2005**, *5* (2), 137-147.
11. Zhao, G.; Lin, H.; Ping, Y.; Sun, H.; Zhu, S.; Xuncheng, S.; Chen, Y., Ethylenediamine-palladium (II) complexes with pyridine and its derivatives: synthesis, molecular structure and initial antitumor studies. *Journal of inorganic biochemistry* **1999**, *73* (3), 145-149.
12. Onunga, D. O. Controlling the reactivity of mononuclear palladium (II) complexes. Substitution kinetics and mechanisms. **2019**.
13. Onunga, D. O.; Bellam, R.; Mutua, G. K.; Sitati, M.; BalaKumaran, M. D.; Jaganyi, D.; Mambanda, A., Controlling the reactivity of [Pd (II)(N<sup>^</sup> N<sup>^</sup> N) Cl]<sup>+</sup> complexes using 2, 6-bis (pyrazol-2-yl) pyridine ligands for biological application: Substitution reactivity, CT-DNA interactions and in vitro cytotoxicity study. *Journal of Inorganic Biochemistry* **2020**, *213*, 111261.
14. Onunga, D. O.; Jaganyi, D.; Mambanda, A., The role of 8-quinolinyl moieties in tuning the reactivity of palladium (II) complexes: a kinetic and mechanistic study. *Journal of Coordination Chemistry* **2019**, *72* (3), 499-515.

15. Omondi, R. O. Tuning the steric and electronic parameters of mixed-donor palladium (II) complexes: coordination chemistry, substitution kinetics and biological activities. **2021**.
16. Gómez, J.; García-Herbosa, G.; Cuevas, J. V.; Arnáiz, A.; Carbayo, A.; Munoz, A.; Falvello, L.; Fanwick, P. E., Diastereospecific and Diastereoselective Syntheses of Ruthenium (II) Complexes Using N, N 'Bidentate Ligands Aryl-pyridin-2-ylmethylamine ArNH-CH<sub>2</sub>-2-C<sub>5</sub>H<sub>4</sub>N and Their Oxidation to Imine Ligands. *Inorganic chemistry* **2006**, *45* (6), 2483-2493.
17. Kim, S.; Kim, D.; Lee, H.-J.; Lee, H., Palladium (II) complexes containing N, N'-bidentate N-(pyridin-2-ylmethyl) aniline and its derivatives: Synthesis, structural characterisation, and methyl methacrylate polymerisation. *Polyhedron* **2014**, *77*, 66-74.
18. Munding, S.; Jakob, U.; Bichovski, P.; Bannwarth, W., Modification and optimization of the bis-picolyamide-based relay protection for carboxylic acids to be cleaved by unusual complexation with Cu<sup>2+</sup> salts. *The Journal of Organic Chemistry* **2012**, *77* (20), 8968-8979.
19. G.W. Trucks, M.J. Frisch, H.B. Schlegel, G.E. Scuseria, J.R. Cheeseman, M.A. Robb, G. Scalmani, V. Barone, G.A. Petersson, B. Mennucci, H. Nakatsuji, M. Caricato, X. Li, A.F. Izmaylov, H.P. Hratchian, J. Bloino, G. Zheng, M. Hada, J.L. Sonnenberg, M. Ehara, K. Toyota, R. Fukuda, M. Ishida, J. Hasegawa, T. Nakajima, Y. Honda, O. Kitao, T. Vreven, H. Nakai, J.A. Montgomery Jr., J.E. Peralta, M. Bearpark, F. Ogliaro, J.J. Heyd, E. Brothers, K.N. Kudin, R. Kobayashi, V.N. Staroverov, J. Normand, K. Raghavachari, J.C. B.A. Rendell, S.S. Iyengar, J. Tomasi, M. Cossi, J.M.M.N. Rega, M. Klene, J.E. Knox, J.B. Cross, C. Adamo, V. Bakken, J. Jaramillo, R. Gomperts, R.E. Stratmann, O. Yazyev, A.J. Austin, R. Cammi, C. Pomelli, R.L. Martin, J.W. Ochterski, K. Morokuma, V.G. Zakrzewski, G.A. Voth, P. Salvador, J.J. Dannenberg, S. Dapprich, O. Farkas, A.D. Daniels, J.B. Foresman, J.V. Ortiz, J. Cioslowski, D.J. Fox, Gaussian 09 (Revision A. 1), Inc., Wallingford, CT, **2009**.
20. Gaussian09, R. A., 1, mj frisch, gw trucks, hb schlegel, ge scuseria, ma robb, jr cheeseman, g. Scalmani, v. Barone, b. Mennucci, ga petersson et al., gaussian. *Inc., Wallingford CT* **2009**, *121*, 150-166.
21. Hay, P. J.; Wadt, W. R., Ab initio effective core potentials for molecular calculations. Potentials for K to Au including the outermost core orbitals. *The Journal of chemical physics* **1985**, *82* (1), 299-310.
22. Becke, A. D., Density functional calculations of molecular bond energies. *The Journal of Chemical Physics* **1986**, *84* (8), 4524-4529.
23. Park, S.; Lee, J. K.; Lee, H.; Nayab, S.; Shin, J. W., Zinc (II), palladium (II) and cadmium (II) complexes containing 4-methoxy-N-(pyridin-2-ylmethylene) aniline derivatives: Synthesis, characterization and methyl methacrylate polymerization. *Applied Organometallic Chemistry* **2019**, *33* (4), e4797.
24. Lin, Y.-C.; Yu, K.-H.; Huang, S.-L.; Liu, Y.-H.; Wang, Y.; Liu, S.-T.; Chen, J.-T., Alternating ethylene-norbornene copolymerization catalyzed by cationic organopalladium complexes bearing hemilabile bidentate ligands of  $\alpha$ -amino-pyridines. *Dalton Transactions* **2009**, (41), 9058-9067.
25. Diez, V.; Cuevas, J. V.; García-Herbosa, G.; Aullón, G.; Charmant, J. P.; Carbayo, A.; Munoz, A., <sup>1</sup>H NMR Direct Observation of Enantiomeric Exchange in Palladium (II) and Platinum (II) Complexes Containing N, N 'Bidentate Aryl-pyridin-2-ylmethylamine Ligands. *Inorganic chemistry* **2007**, *46* (2), 568-577.
26. Al-Allaf, T.; Castan, P.; Turpin, R.; Wimmer, S.; Bernardinelli, G., Solvolysis of palladium (II) and platinum (II) complexes of asymmetric ligands: Synthesis and

- structural characterization of [Pd (AMP)(dmsO) Cl] BF<sub>4</sub> and [Pt (AMP)(dmsO) Cl] ClO<sub>4</sub>. *Transition Metal Chemistry* **1992**, *17*, 579-582.
27. Ghosh, G. K.; Misra, K.; Linert, W.; Moi, S. C., Interaction of glutathione with cis-(2-aminomethylpyridine) diaqua platinum (II) perchlorate in aqueous medium: their kinetics and mechanism. *Synthesis and Reactivity in Inorganic, Metal-Organic, and Nano-Metal Chemistry* **2013**, *43* (6), 714-721.
  28. Hochreuther, S.; Nandibewoor, S. T.; Puchta, R.; van Eldik, R., Thermodynamic and kinetic behaviour of [Pt (2-methylthiomethylpyridine)(OH<sub>2</sub>)<sub>2</sub>]<sup>2+</sup>. *Dalton Transactions* **2012**, *41* (2), 512-522.
  29. Papo, T. R.; Jaganyi, D.; Mambanda, A., Substitution reactions of cis-platinum (II) complexes containing bidentate N, N-donor pyridinecarboxamide ligands with different substituents. *Journal of Coordination Chemistry* **2022**, *75* (19-24), 2557-2573.
  30. Summa, N.; Schiessl, W.; Puchta, R.; van Eikema Hommes, N.; van Eldik, R., Thermodynamic and kinetic studies on reactions of Pt (II) complexes with biologically relevant nucleophiles. *Inorganic Chemistry* **2006**, *45* (7), 2948-2959.
  31. Kinunda, G.; Jaganyi, D., A kinetic study of aqua ligand substitution in dinuclear Pt (II) complexes containing four non-coplanar pyridine ligands. *Transition Metal Chemistry* **2014**, *39*, 939-949.
  32. Hochreuther, S.; Puchta, R.; van Eldik, R., Thermodynamic and kinetic studies on novel dinuclear platinum (II) complexes containing bidentate N, N-donor ligands. *Inorganic Chemistry* **2011**, *50* (18), 8984-8996.
  33. Shoeib, T.; Sharp, B. L., Interactions of oxaliplatin with the cytoplasmic thiol containing ligand glutathione. *Metallomics* **2012**, *4* (12), 1308-1320.
  34. Banjo, S., Density Functional Theory studies on electronic properties of thiophene S-oxides as aromatic dienophiles for reactivity prediction in Diels-Alder reactions. *Pakistan Journal of Scientific & Industrial Research Series A: Physical Sciences* **2013**, *56* (1), 14-18.
  35. Jaganyi, D.; Tiba, F.; Munro, O. Q.; Petrović, B.; Bugarčić, Ž. D., Kinetic and mechanistic study on the reactions of [Pt (bpma)(H<sub>2</sub>O)]<sup>2+</sup> and [Pd (bpma)(H<sub>2</sub>O)]<sup>2+</sup> with some nucleophiles. Crystal structure of [Pd (bpma)(py)](ClO<sub>4</sub>)<sub>2</sub>. *Dalton Transactions* **2006**, (24), 2943-2949.
  36. Tobe, M. L.; Burgess, J., *Inorganic Reaction Mechanisms*. Longman: 1999.
  37. Hochreuther, S.; Puchta, R.; van Eldik, R., Novel dinuclear platinum (II) complexes containing mixed nitrogen-sulfur donor ligands. *Inorganic Chemistry* **2011**, *50* (24), 12747-12761.

## CHAPTER 4

### Synthesis of Novel Palladium(II)-Pyridine Carboxamide Complexes

#### 4.1 Introduction

The success of *cis*-diamminedichloro-platinum(II) (*cisplatin*) as an anticancer drug led to an increase in the synthesis and biological application of Pt-based anticancer agents.<sup>1-6</sup> Due to several side effects associated with the administration of *cisplatin* and Pt based anticancer agents such as nephrotoxicity to drug resistance of the tumour cells, researchers are exploring alternatives. One such alternate is the use of transition metal-based anticancer drugs.<sup>7-11</sup> Palladium-based complexes have gained significant attention due to their structural and thermodynamic similarities, and significant overlap of coordination chemistry to Pt(II) complexes. Pd(II) complexes exhibit promising activity towards cisplatin-resistant cells.<sup>12-14</sup>

The coordination of biologically active molecules to metal centres shows promising activity due to the ability of the complexes to bind to different biological targets.<sup>15, 16</sup> The incorporation of carboxamide groups in the ligands and preparation of new complexes allows for the unique electronic and the steric effect control of the properties of the coordinated Pd(II) metal. The carboxamide ligand has a diverse chemistry due to its multifunction coordination modes.<sup>17-19</sup> The carboxamide group is an important biological molecule which forms part of the primary structure of proteins and forms metal complexes that are similar to metal peptides.<sup>10</sup> Pyridine carboxamides ligands are a class of mono/bidentate ligands that are formed from condensation reactions between pyridyl-bearing carboxylic acid and amine precursors, promoted by triphenylphosphite coupling agent.<sup>11-16</sup>

As such, the *N*-(4-bromophenyl)-pyridine-2-carboxamide ligand, which acts as a bidentate-chelating ligand, was reacted with a Pd(II) metal precursor to form two Pd(II) complexes, i.e. **Pd1** and **Pd2**.

#### 4.2 Chemicals and Reagents

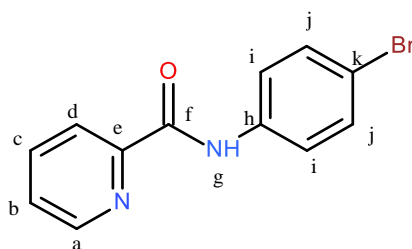
All synthesis was performed under nitrogen using the standard Schlenk line techniques. Potassium tetrachloropalladate, 2-picolinic acid, 4-bromoaniline and triphenylphosphite were purchased from Sigma-Aldrich and used without further purification. All solvents (pyridine, diethyl ether, dichloromethane) were procured from Sigma-Aldrich and were of analytical grade.

### 4.3 Physical Measurements

$^1\text{H}$  NMR spectra were acquired on Bruker Avance III 400 MHz NMR spectroscopy with a 5 mm TBIZ probe at 30 °C. Chemical shifts were reported in ppm in relation to the solvent residual peak. Coupling constants (J) were calculated in hertz (Hz). The infrared spectrum was recorded using a Bruker Alpha II FT-IR spectrometer and the data were reported as a percentage transmittance at the respective wavenumbers ( $\text{cm}^{-1}$ ). Exemplary  $^1\text{H}$  NMR and IR spectra of the ligand and **Pd1** and **Pd2** are shown in the appendix section (**Figure A49-A55**).

The X-ray crystallographic data of the complexes were collected and evaluated on a Bruker APEX Duo<sup>17</sup> CCD area detector diffractometer with an Incoatec micro source working at 30 W power. The crystal was kept at 99.97 K during data collection using an Oxford Instruments Cryojet accessory. The data were collected with  $\text{Cu}(\text{K}\alpha)$ ,  $\lambda = 1.54178$ , at a crystal-to-detector distance of 50 mm. The SAINT<sup>18</sup> program was used to reduce the structure using the outlier rejection, scan speed scaling and the standard Lorentz and polarization correction factors. The non-hydrogen atoms were initially refined isotropically and then by anisotropic refinement with a full-matrix least-squares method based on  $F^2$ . All hydrogen atoms were included and positioned geometrically on their parent atoms. The crystal structure was solved with Olex2<sup>19</sup>, while the SHELXS<sup>20</sup> and SHELX<sup>21</sup> programs were used for structural refinement. The crystallographic data were visualized using WinGX<sup>22</sup> and Mercury v.4.3.<sup>23</sup> The crystallographic data and structure refinement parameters of **Pd1** and **Pd2** are given in Table 1.

### 4.4 Synthesis of the Ligand



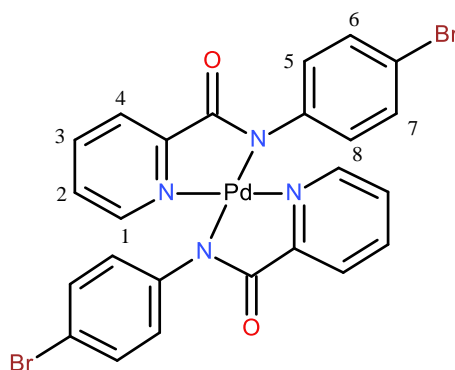
The *N*-(4-bromophenyl)pyridine-2-carboxamide was synthesized following a reported procedure with slight modifications.<sup>24</sup> Solutions of 2-picolinic acid (5 mmol) and 4-bromoaniline (5 mmol) in pyridine (5 mL) were mixed for 15 minutes under stirring. The temperature was raised to 100 °C followed by the dropwise addition of triphenylphosphite (5 mmol). The mixture was further stirred for 4 hours at 100 °C, then cooled to room

temperature. The cooled solution was concentrated, and an off-white precipitate was formed and washed with cold diethyl ether.

*N*-(4-bromophenyl)pyridine-2-carboxamide was obtained as an off-white solid (0.629 g, 45.39 %).  $^1\text{H}$  NMR (400 MHz,  $\text{CDCl}_3$ , ppm): 9.96 (s, 1H, - $\text{H}_g$ -), 8.53 (d, 1H,  $J = 8.46$  Hz, - $\text{H}_a$ -), 8.20 (d, 1H,  $J = 8.46$  Hz, - $\text{H}_d$ -), 7.83 (td, 1H,  $J_1 = 8.08$  Hz,  $J_2 = 1.72$  Hz, - $\text{H}_c$ -), 7.61 (d, 1H,  $J = 9.23$  Hz, - $\text{H}_b$ -), 7.41 (m, 4H, - $\text{H}_i$ -, - $\text{H}_j$ -). FT-IR (liquid neat;  $\text{cm}^{-1}$ ) 3001 (-NH), 1709 (C=C), 1357 (C-N aromatic), 1217, 902, 525. TOF-MS  $\text{ES}^+$ ,  $m/z = 279.01$  (calculated  $m/z$  278.11), [ $\text{M}^+ + \text{H}$ ].

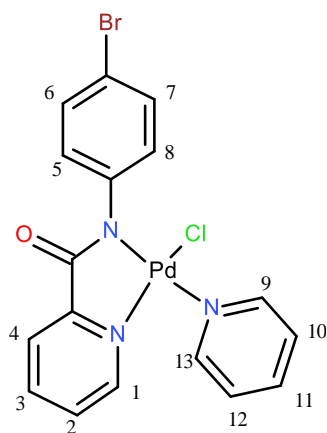
## 4.5 Synthesis of the Pd(II) Complexes

### 4.5.1 bis[*N*-(4-bromophenyl)pyridine-2-carboxamidato]Palladium, Pd1



*N*-(phenyl) pyridine-2-carboxamide ligand was coordinated to Pd(II) using a literature method.<sup>25</sup> An aqueous solution of potassium tetrachloropalladate (0.3063 mmol, 0.10 g) was added dropwise to a solution of the *N*-(phenyl) pyridine-2-carboxamide ligand (0.6127 mmol, 0.17 g) in DCM (10 mL) under inert nitrogen. The mixture was stirred under reflux for 6 hours and allowed to cool to room temperature. The precipitate formed was filtered and washed with cold ultra-pure water and methanol. The resulting product was crystallized from the 1:1 dichloromethane and hexane solution to obtain crystals suitable for X-ray crystallography. Yield: 0.085 g (42%),  $^1\text{H}$ -NMR (400 MHz,  $\text{CD}_3\text{COCD}_3$ , ppm): 8.67 (d,  $J = 4.9$  Hz, 2H,  $\text{H}_1$ -py), 8.23 (d,  $J = 7.2$  Hz, 2H,  $\text{H}_4$ -py), 8.06 (td,  $J = 7.7$  Hz, 2H,  $\text{H}_3$ -py), 7.93 (d,  $J = 8.8$  Hz, 4H,  $\text{H}_5$  and  $\text{H}_8$ ), 7.64 (t,  $J = 6.4$  Hz, 2H,  $\text{H}_2$ -py), 7.54 (d,  $J = 8.8$  Hz, 4H,  $\text{H}_6$  and  $\text{H}_7$ ). FT-IR ( $\text{cm}^{-1}$ ): 3001, 1709, 1357, 1217, 902, 525.

#### 4.5.2 Palladium(II) [*N*-(4-bromophenyl)-2-pyridinecarboxamide], pyridine chloride, **Pd2**

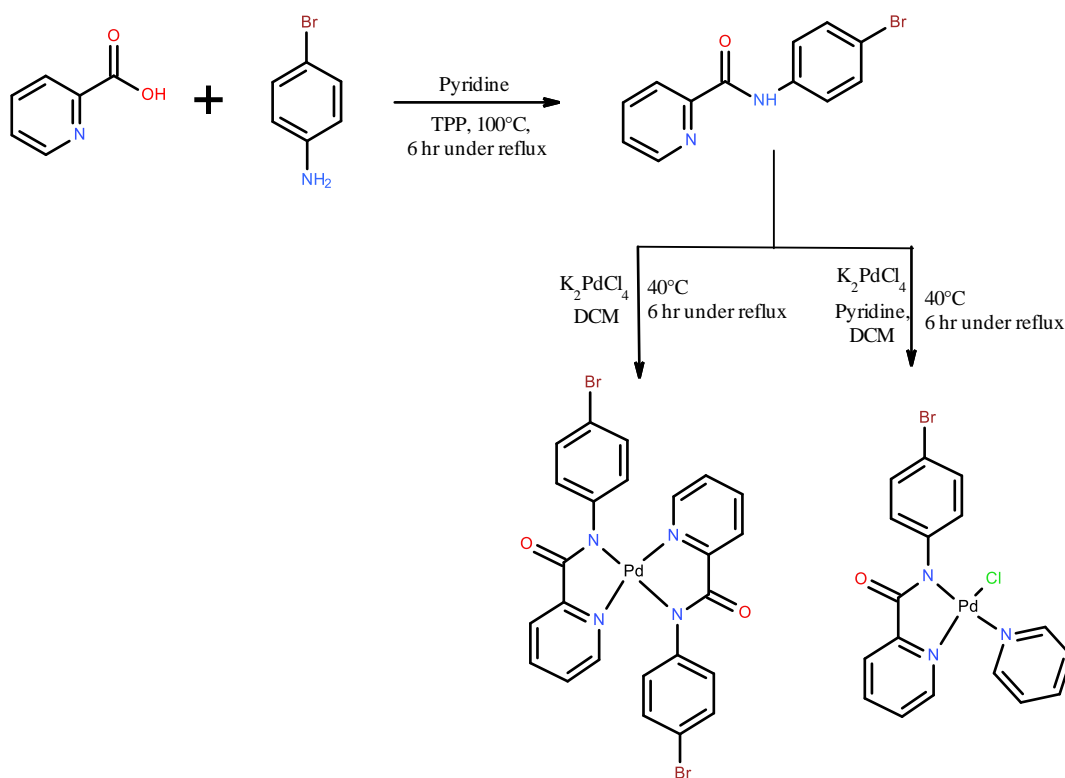


To an aqueous solution of potassium tetrachloropalladate (0.3063 mmol, 0.10 g) was added a solution of the *N*-(phenyl) pyridine-2-carboxamide ligand (0.3063 mmol, 0.085 g) in DCM (10 mL) and pyridine (0.3063 mmol, 24.2 mg) under inert nitrogen. The mixture was stirred under reflux for 6 hours and allowed to cool to room temperature. The precipitate formed was filtered and washed with cold ultra-pure water and methanol. The resulting product was crystallized from the 1:1 dichloromethane and hexane solution to obtain crystals suitable for X-ray crystallography. Yield: 0.054 g (35.29 %),  $^1\text{H-NMR}$  (400 MHz,  $\text{CD}_3\text{COCD}_3$ , ppm): 8.37 (d,  $J = 5.4$  Hz, 2H), 8.06 (d,  $J = 5.44$  Hz, 1H), 7.91 (d,  $J = 4.5$  Hz, 2H), 7.29 (td,  $J = 7.7$  Hz, 2H), 7.05 (t,  $J = 7.71$  Hz, 2H), 6.97 (t,  $J = 7.71$  Hz, 2H), 6.87 (t,  $J = 6.8$  Hz, 2H). FT-IR ( $\text{cm}^{-1}$ ): 3411, 3005, 1709, 1533, 1358, 1220, 895, 830, 604, 528. TOF-MS  $\text{ES}^+$ :  $m/z = 496.91$  (calculated  $m/z$  497.08).

## 4.6 Results and Discussion

### 4.6.1 Synthesis of Ligand and Complexes

*N*-(4-bromophenyl)-pyridine-2-carboxamide ligand was synthesised from the reaction of 2-picolinic acid and 4-bromoaniline in the presence of triphenylphosphite to produce the corresponding ligand in excellent yield. Treatment of *N*-(4-bromophenyl)-pyridine-2-carboxamide ligand with aqueous potassium tetrachloropalladate ( $\text{K}_2\text{PdCl}_4$ ) produced **Pd1** in moderate yield (**Scheme 4.1**). **Pd2** was synthesized using a similar procedure as **Pd1**, with the addition of pyridine. The ligand and the corresponding Pd(II) complexes were characterised using  $^1\text{H}$  NMR, FT-IR spectroscopy, mass spectrometry and X-ray crystallography.



**Scheme 4. 1:** Synthesis of N-(4-bromophenyl) pyridine-2-carboxamide and corresponding Pd(II) complexes, **Pd1** and **Pd2**.

In the subsequent Pd(II) complexes (**Pd1** and **Pd2**), the *N*-(4-bromophenyl)-pyridine-2-carboxamide ligand acted as bidentate and was coordinated via anionic N<sub>amide</sub> and neutral N<sub>pyridine</sub> sites *via* two five-membered chelate rings. <sup>1</sup>H NMR spectra of the ligand and the corresponding Pd(II) complexes show the expected peak multiplicities and integrations (Appendix, **Figure A49 & A52**). In the <sup>1</sup>H NMR spectrum of the Pd(II) complexes the expected chemical shifts of the protons were observed and deshielded compared to the free ligand. The formation of the **Pd1** complex was revealed by the disappearance of the NH peak at 9.803 ppm in the <sup>1</sup>H NMR spectrum, which was attributed to the coordination of the Pd to the N<sub>amido</sub>. A similar trend was observed for **Pd2**, where the pyridine peak that is coordinated to the Pd ion was also observed. The formation of **Pd1** and **Pd2** was further confirmed using FT-IR, where the N–H stretches of the ligand at 3321 cm<sup>-1</sup> (**Figure A50**) disappeared when compared to the FT-IR spectrum of **Pd1** and **Pd2** (**Figure A53 & A54**). The FTIR spectra of the **Pd1** and **Pd2** showed that the peaks for the C=O amide bands (1709 cm<sup>-1</sup>) shifted by a small margin when

compared to the corresponding ligand ( $1673\text{ cm}^{-1}$ ). This observation clearly indicates that the C = O group is uncoordinated to the Pd(II) metal the of two complexes.

#### 4.6.2 X-ray Crystallography

The molecular structure of **Pd1** and **Pd2** were further confirmed by X-ray crystallography. Both complexes were crystallized from the 1:1 dichloromethane and hexane solution to obtain crystals suitable for X-ray crystallography. The crystallographic data and structure refinement parameters of the complexes are given in **Table 4.1**.

**Table 4.1.** Crystal structure and structure refinement for **Pd1** and **Pd2**.

Identification Code	cu_SS_PM_Br_Pd_Comp_0m (Pd1)	cu_SS_PM_P_Anι_Comp_0ma (Pd2)
Empirical formula	C <sub>12</sub> H <sub>8</sub> BrN <sub>2</sub> OPd <sub>0.5</sub>	C <sub>17</sub> H <sub>15</sub> BrClN <sub>3</sub> O <sub>2</sub> Pd
Formula weight	329.31	515.08
Temperature (K)	99.97	100.00
Crystal system	monoclinic	Orthorhombic
Space group	P2 <sub>1</sub> /c	Pbca
a (Å)	6.22590(10)	16.5311(3)
b (Å)	12.9253(3)	8.6466(2)
c (Å)	13.6735(3)	25.0634(5)
α (°)	90	90
β (°)	94.8170(10)	90
γ (°)	90	90
Volume (Å <sup>3</sup> )	1096.44(4)	3582.51(13)
Z	4	8
ρ <sub>calc</sub> (g cm <sup>-3</sup> )	1.995	1.910
μ (mm <sup>-1</sup> )	11.358	12.484
F (000)	640.0	2016.0
Crystal size (mm <sup>3</sup> )	0.205 × 0.075 × 0.065	0.25 x 0.18 x 0.15
Radiation source, λ (Å)	Cu(K <sub>α</sub> ), λ = 1.54178	Cu(K <sub>α</sub> ), λ = 1.54178
2θ range for data collection (°)	9.432 to 144.36	7.054 to 144.266
Index ranges	-7 ≤ h ≤ 6, -15 ≤ k ≤ 15, -16 ≤ l ≤ 16	-20 ≤ h ≤ 20, -10 ≤ k ≤ 10, -30 ≤ l ≤ 30
Reflections collected	14012	31164
Independent reflections	2097 [R <sub>int</sub> = 0.0247, R <sub>σ</sub> = 0.0160]	3526 [R <sub>int</sub> = 0.0292, R <sub>σ</sub> = 0.0160]
Data/restraints/parameters	2097/0/151	3526/0/229
Goodness-of-fit on F <sup>2</sup>	1.125	1.135
Final R indexes [I ≥ 2σ (I)]	R <sub>1</sub> = 0.0213, wR <sub>2</sub> = 0.0513	R <sub>1</sub> = 0.0210, wR <sub>2</sub> = 0.0519
Final R indexes (all data)	R <sub>1</sub> = 0.0216, wR <sub>2</sub> = 0.0515	R <sub>1</sub> = 0.0214, wR <sub>2</sub> = 0.0523
Largest diff. peak/hole (e Å <sup>-3</sup> )	0.49/-0.79	0.45/-0.63

The crystal structure of **Pd1** (**Figure 4.1**) assumes the distorted square-planar coordination geometry around the metal centre and belongs to the monoclinic system, with the space group  $P21/c$ . The selected bond lengths and bond angles of **Pd1** are represented in **Table 4.2**. **Pd1** adopts a distorted square-planar coordination geometry around the metal centre, with the angles  $N2-Pd1-N1$ ,  $N2^1-Pd1-N1^1$ ,  $N2-Pd1-N1^1$  and  $N2^1-Pd1-N1$  deviating by approximately  $10^\circ$  from the expected square-planar angle of  $90^\circ$ . The bond lengths reported in **Table 4.2** indicate that the values relative to the pyridine N donors ( $Pd1-N1$ ,  $Pd1-N1^1$ ) are slightly longer by ca.  $0.038 \text{ \AA}$  than those of the amide nitrogen atoms.

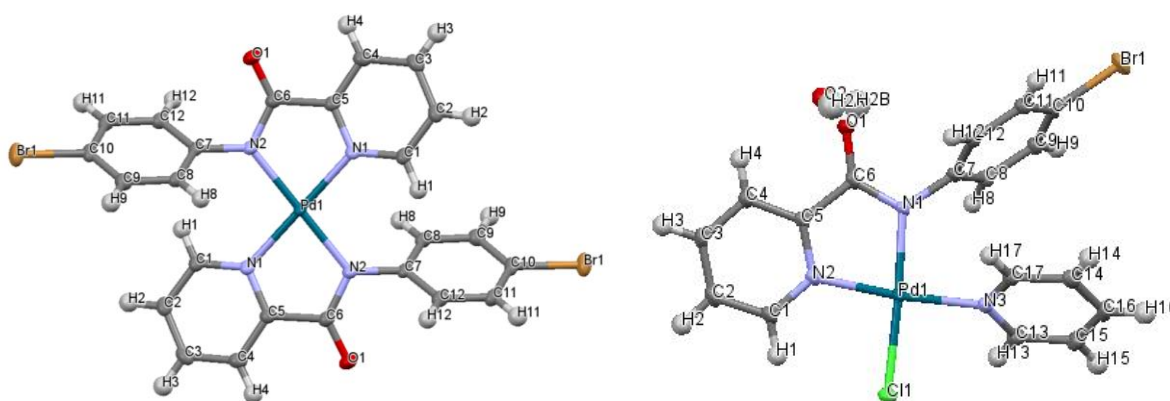


**Figure 4. 1:** The ORTEP diagram of **Pd1** and **Pd2** with the thermal ellipsoids drawn at the 50% probability level.

**Table 4.2.** Selected geometrical parameters for **Pd1**.

Atom	Length/ $\text{\AA}$	Atom	Angle/ $^\circ$
$Pd1-N2^1$	2.0361(19)	$N2^1-Pd1-N2$	180.0
$Pd1-N2$	2.0361(19)	$N2-Pd1-N1$	80.35(8)
$Pd1-N1^1$	2.0399(19)	$N2^1-Pd1-N1^1$	80.35(8)
$Pd1-N1$	2.0400(19)	$N2-Pd1-N1^1$	99.65(8)
		$N2^1-Pd1-N1$	99.65(8)
$^11-X, ^11-Y, ^11-Z$		$N1^1-Pd1-N1$	180.0

The crystal structure of **Pd2** (**Figure 4.1**) belongs to the orthorhombic system, with the space group  $Pbca$ . The selected bond lengths and bond angles of **Pd1** are represented in **Table 4.3**. **Pd2** also adopts a distorted square-planar coordination geometry around the metal centre, with the bidentate ligand angle deviating ( $N1-Pd1-N3$ ) from  $90^\circ$  by approximately  $10^\circ$ . The bond lengths for  $Pd1-N1$  ( $N_{amide}$ ) and  $Pd1-N2$  ( $N_{pyridine}$ ) of the *N*-(4-bromophenyl)-pyridine-2-carboxamide ligand are similar, while the bond length of the coordinated pyridine ligand ( $Pd1-$

N3) is slightly elongated. The Pd1-Cl1 bond length is the longest when compared to the N-donor ligands coordinated to the metal centre.

**Table 4.3.** Selected geometrical parameters for **Pd2**.

Atom	Length/Å	Atom	Angle/°
Pd1-N3	2.0224(18)	N3-Pd1-Cl1	89.94(5)
Pd1-N1	2.0191(17)	N1-Pd1-Cl1	175.22(5)
Pd1-N2	2.0190(18)	N1-Pd1-N3	93.98(7)
Pd1-Cl1	2.3157(5)	N2-Pd1-Cl1	95.78(5)
		N2-Pd1-N3	171.31(7)
<sup>1</sup> 1-X, 1-Y, 1-Z		N2-Pd1-N1	80.65(7)

#### 4.7 Conclusion

We have successfully synthesized two palladium(II) (**Pd1** and **Pd2**) complexes with *N*-(4-bromophenyl)-pyridine-2-carboxamide ligand. The ligand binds to the palladium in a bidentate fashion, forming a five-membered chelate ring through N-bonding of the N<sub>pyridine</sub> and N<sub>amide</sub>. In **Pd1** coordination of the Pd metal to the ligand was through the formation of two five membered chelate rings. Whilst in **Pd2**, the metal is coordinated to the bidentate *N*-(4-bromophenyl)-pyridine-2-carboxamide, a pyridine and a chloride ligand. The two complexes were characterised with <sup>1</sup>H NMR, FT-IR, LC-MS spectroscopic techniques and single X-ray crystallography. **Pd1** crystallizes in the monoclinic crystal system and in the P21/c space group, and **Pd2** crystallizes in the orthorhombic system, with the space group Pbca.

## 4.8 References

1. Rosenberg, B.; Vancamp, L.; Trosko, J. E.; Mansour, V. H., Platinum compounds: a new class of potent antitumour agents. *nature* **1969**, 222 (5191), 385-386.
2. Reedijk, J., Improved understanding in platinum antitumour chemistry. *Chemical Communications* **1996**, (7), 801-806.
3. Kostova, I., Platinum complexes as anticancer agents. *Recent patents on anti-cancer drug discovery* **2006**, 1 (1), 1-22.
4. Reedijk, J., New clues for platinum antitumor chemistry: kinetically controlled metal binding to DNA. *Proceedings of the National Academy of Sciences* **2003**, 100 (7), 3611-3616.
5. Guo, Z.; Sadler, P. J., Medicinal inorganic chemistry. In *Advances in inorganic chemistry*, Elsevier: 1999; Vol. 49, pp 183-306.
6. Wang, D.; Lippard, S. J., Cellular processing of platinum anticancer drugs. *Nature reviews Drug discovery* **2005**, 4 (4), 307-320.
7. Casini, A.; Messori, L., Molecular mechanisms and proposed targets for selected anticancer gold compounds. *Current topics in medicinal chemistry* **2011**, 11 (21), 2647-2660.
8. Bindoli, A.; Rigobello, M. P.; Scutari, G.; Gabbiani, C.; Casini, A.; Messori, L., Thioredoxin reductase: A target for gold compounds acting as potential anticancer drugs. *Coordination Chemistry Reviews* **2009**, 253 (11-12), 1692-1707.
9. Jakupec, M. A.; Galanski, M. S.; Arion, V. B.; Hartinger, C. G.; Keppler, B. K., Antitumour metal compounds: more than theme and variations. *Dalton transactions* **2008**, (2), 183-194.
10. Ott, I., On the medicinal chemistry of gold complexes as anticancer drugs. *Coordination Chemistry Reviews* **2009**, 253 (11-12), 1670-1681.
11. Mukherjee, R., Coordination chemistry with pyrazole-based chelating ligands: molecular structural aspects. *Coordination Chemistry Reviews* **2000**, 203 (1), 151-218.
12. Barnes, D.; Chapman, R.; Vagg, R.; Watton, E., Synthesis of novel bis (amides) by means of triphenyl phosphite intermediates. *Journal of Chemical and Engineering Data* **1978**, 23 (4), 349-350.
13. Munro, O. Q.; Wilson, C., Amide hydrogen bonding: control of the molecular and extended structures of two symmetrical pyridine-2-carboxamide derivatives. *Acta*

- Crystallographica Section C: Crystal Structure Communications* **2010**, *66* (11), o535-o539.
14. Khavasi, H. R.; Ghanbarpour, A.; Tehrani, A. A., The role of intermolecular interactions involving halogens in the supramolecular architecture of a series of Mn (II) coordination compounds. *RSC advances* **2016**, *6* (3), 2422-2430.
  15. Lumb, I.; Hundal, M. S.; Corbella, M.; Gómez, V.; Hundal, G., Copper (II) Complexes of N, N-Diisopropylpicolinamide–Solvatochromic and Thermo-chromic Phase Change of a Monomeric Complex to a Ferromagnetically Coupled Dimeric Complex. *European Journal of Inorganic Chemistry* **2013**, *2013* (27), 4799-4811.
  16. Biswas, M. K.; Patra, S. C.; Maity, A. N.; Ke, S.-C.; Weyhermüller, T.; Ghosh, P., Asymmetric cleavage of 2, 2'-pyridil to a picolinic acid anion radical coordinated to ruthenium (ii): splitting of water to hydrogen. *Chemical Communications* **2013**, *49* (40), 4522-4524.
  17. CrysAlis, C., CrysAlis Red. *Rigaku Oxford Diffraction* **2008**.
  18. SAINT, B., Data Reduction Software, Bruker AXS. Inc., Madison, WI **2009**.
  19. Dolomanov, O. V.; Bourhis, L. J.; Gildea, R. J.; Howard, J. A.; Puschmann, H., OLEX2: a complete structure solution, refinement and analysis program. *Journal of applied crystallography* **2009**, *42* (2), 339-341.
  20. Sheldrick, G. M., SHELXT–Integrated space-group and crystal-structure determination. *Acta Crystallographica Section A: Foundations and Advances* **2015**, *71* (1), 3-8.
  21. Sheldrick, G. M., A short history of SHELX. *Acta Crystallographica Section A: Foundations of Crystallography* **2008**, *64* (1), 112-122.
  22. Farrugia, L. J., WinGX and ORTEP for Windows: an update. *Journal of Applied Crystallography* **2012**, *45* (4), 849-854.
  23. Macrae, C. F.; Bruno, I. J.; Chisholm, J. A.; Edgington, P. R.; McCabe, P.; Pidcock, E.; Rodriguez-Monge, L.; Taylor, R.; Streek, J.; Wood, P. A., Mercury CSD 2.0–new features for the visualization and investigation of crystal structures. *Journal of Applied Crystallography* **2008**, *41* (2), 466-470.
  24. Ray, M.; Ghosh, D.; Shirin, Z.; Mukherjee, R., Highly stabilized low-spin iron (III) and cobalt (III) complexes of a tridentate bis-amide ligand 2, 6-bis (N-phenylcarbamoyl) pyridine. Novel nonmacrocyclic tetraamido-N coordination and two unusually short metal–pyridine bonds. *Inorganic chemistry* **1997**, *36* (16), 3568-3572.

25. Shi, C.-Y.; Gao, E.-J.; Ma, S.; Wang, M.-L.; Liu, Q.-T., Synthesis, crystal structure, DNA-binding and cytotoxicity in vitro of novel cis-Pt (II) and trans-Pd (II) pyridine carboxamide complexes. *Bioorganic & medicinal chemistry letters* **2010**, *20* (24), 7250-7254.

## CHAPTER 5

### 5.1 Overall Conclusions and Future Work

#### 5.1.1 Conclusion

Five bidentate Pd(II) complexes containing different *para* substituted N-((pyridin-2-yl)methyl)aniline chelating spectator ligands of different electronic properties (**PdL1**, **PdL2**, **PdL3**, **PdL4** and **PdL5**) and two Pd(II) complexes with *N*-(4-bromophenyl)-pyridine-2-carboxamide (**Pd1** and **Pd2**) were synthesized. The purity of the complexes was confirmed using <sup>1</sup>H NMR, <sup>13</sup>C NMR, FTIR, LC-MS, elemental analysis and X-ray crystallography. **Pd1** crystallizes in the monoclinic crystal system and in the P21/c space group, and **Pd2** crystallizes in the orthorhombic system, with the space group Pbca. The kinetics and mechanism of substitution reactions of the *para* substituted N-((pyridin-2-yl)methyl)aniline Pd(II) complexes with sulfur-donor nucleophiles were studied under *pseudo* first-order conditions with **TU**, **DMTU** and **TMTU** nucleophiles. The reactivity of the complexes is influenced by electronic effects, while that of the nucleophiles is influenced by steric effects.

#### 5.1.2 Recommendations for Future Work

This study revealed that the synthesized *N,N'*-pyridyl Pd(II) complexes have a relatively high kinetic reactivity towards less sterically hindered nucleophiles, viz. thiourea (**TU**), *N,N'*-dimethylthiourea (**DMTU**), compared to the bulky *N,N,N',N'*-tetramethylthiourea (**TMTU**). Therefore, it would be interesting to study the kinetics of these complexes against bulkier nucleophiles such as Glutathione (GSH) or <sub>L</sub>-Methionine (<sub>L</sub>-Met), **Figure 5.1**. Studies involving models of amino acids (<sub>L</sub>-Met) and peptides (GSH), would also assist in understanding the interactions of the Pd(II) complexes with DNA.

Further studies should also involve DNA binding analysis of these complexes against human cancer cell lines, as well as cytotoxicity studies. Such information would broaden the knowledge on the design of alternative Pd-based anticancer agents.

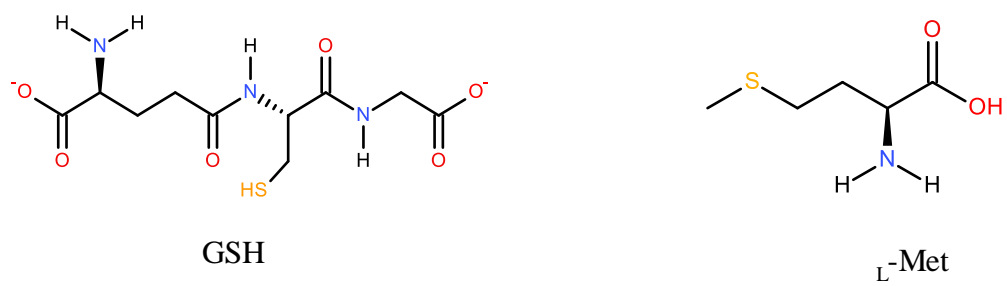


**Figure 5. 1:** Alternative biomolecules for further studies.

## Appendix

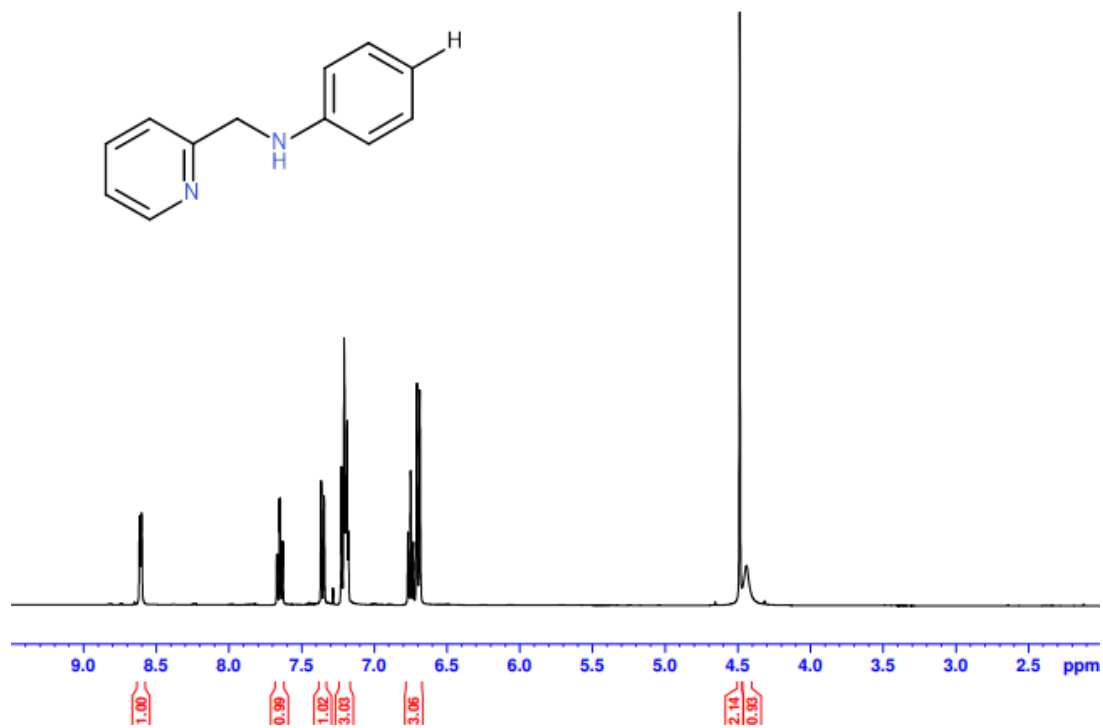
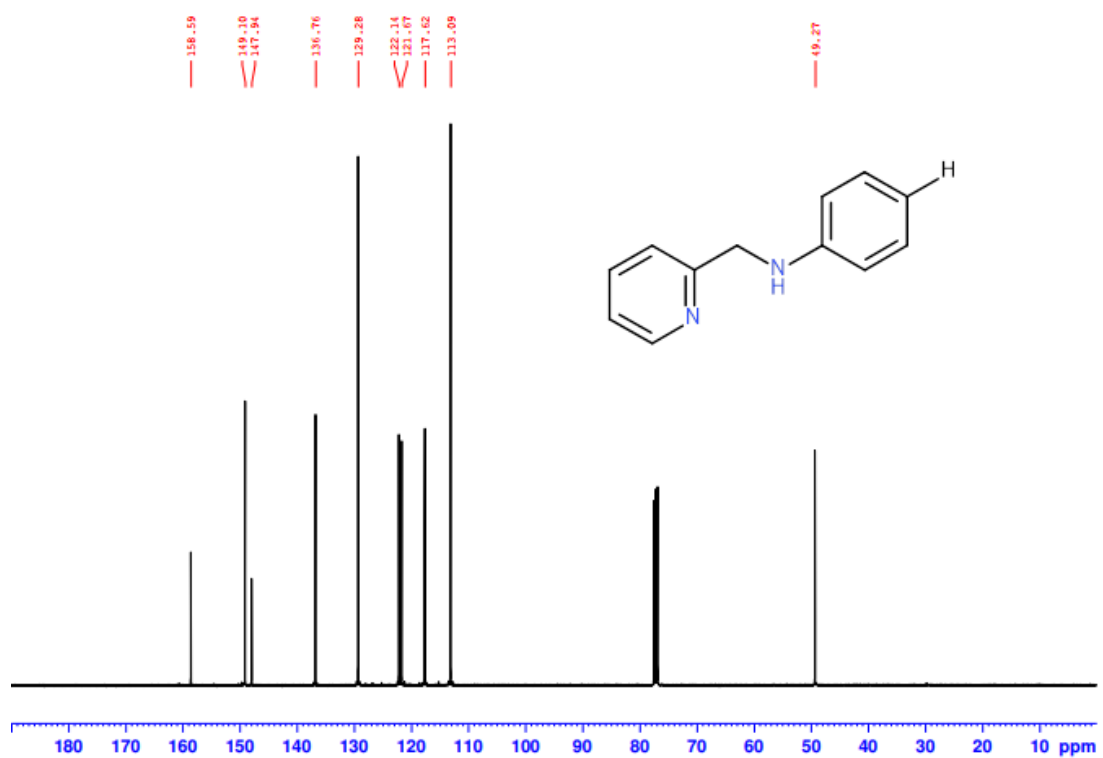
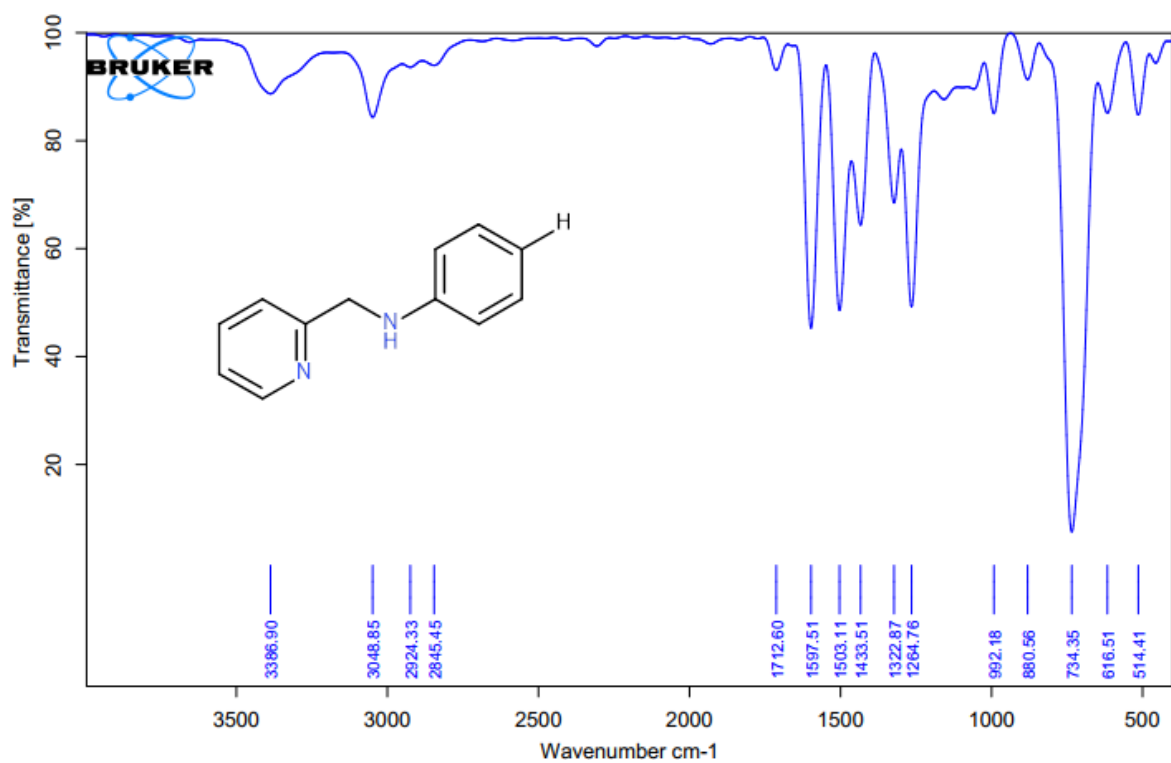


Figure A1  $^1\text{H}$  NMR spectrum for L1 ligand.



**Figure A2**  $^{13}\text{C}$  NMR spectrum for **L1** ligand.



**Figure A3** IR spectrum for **L1** ligand.

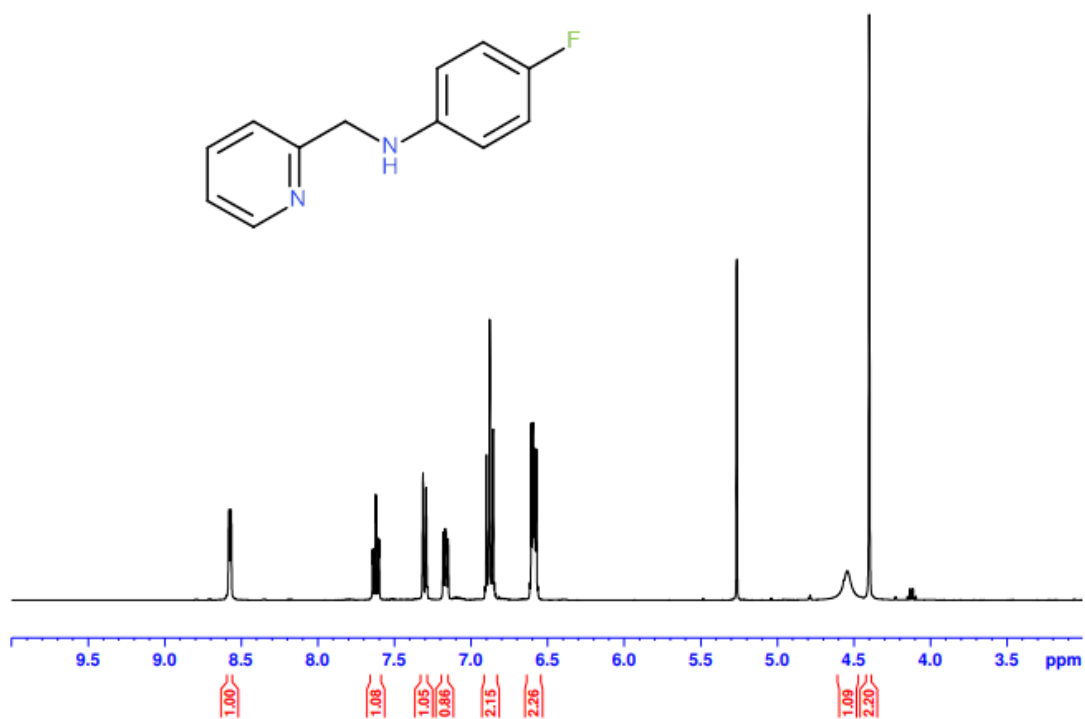


**Figure A4**  $^1\text{H}$  NMR spectrum for **L2** ligand.

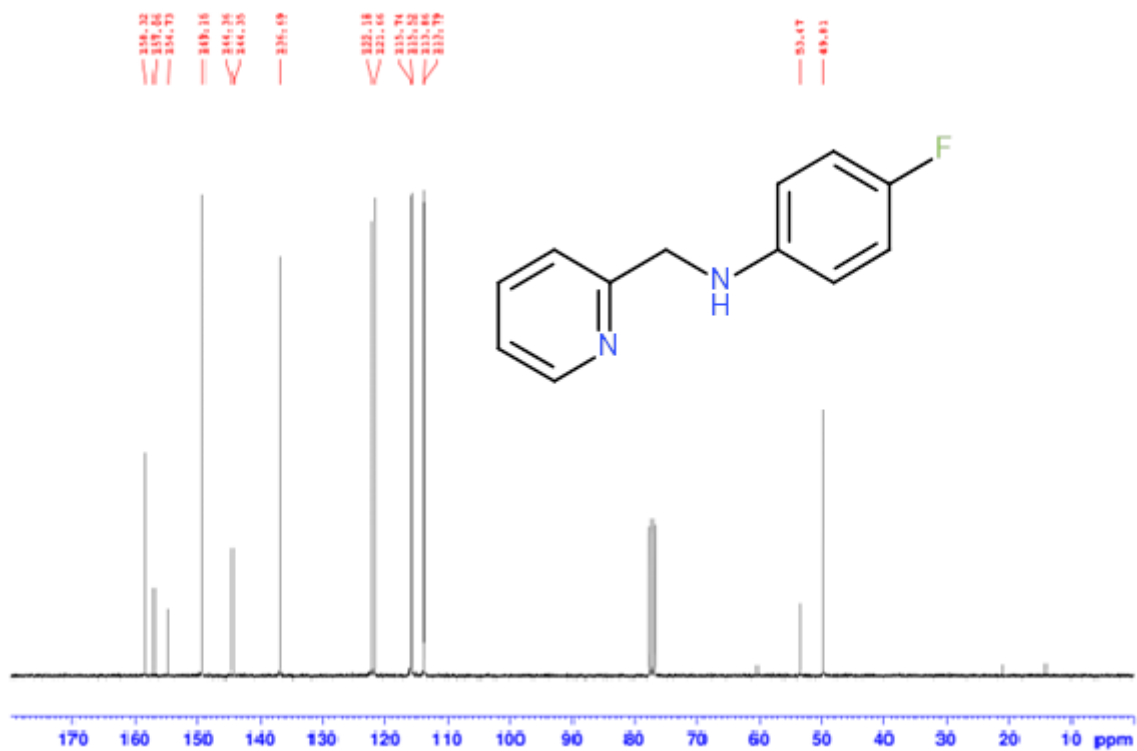


Figure A5 <sup>13</sup>C NMR spectrum for L2 ligand.

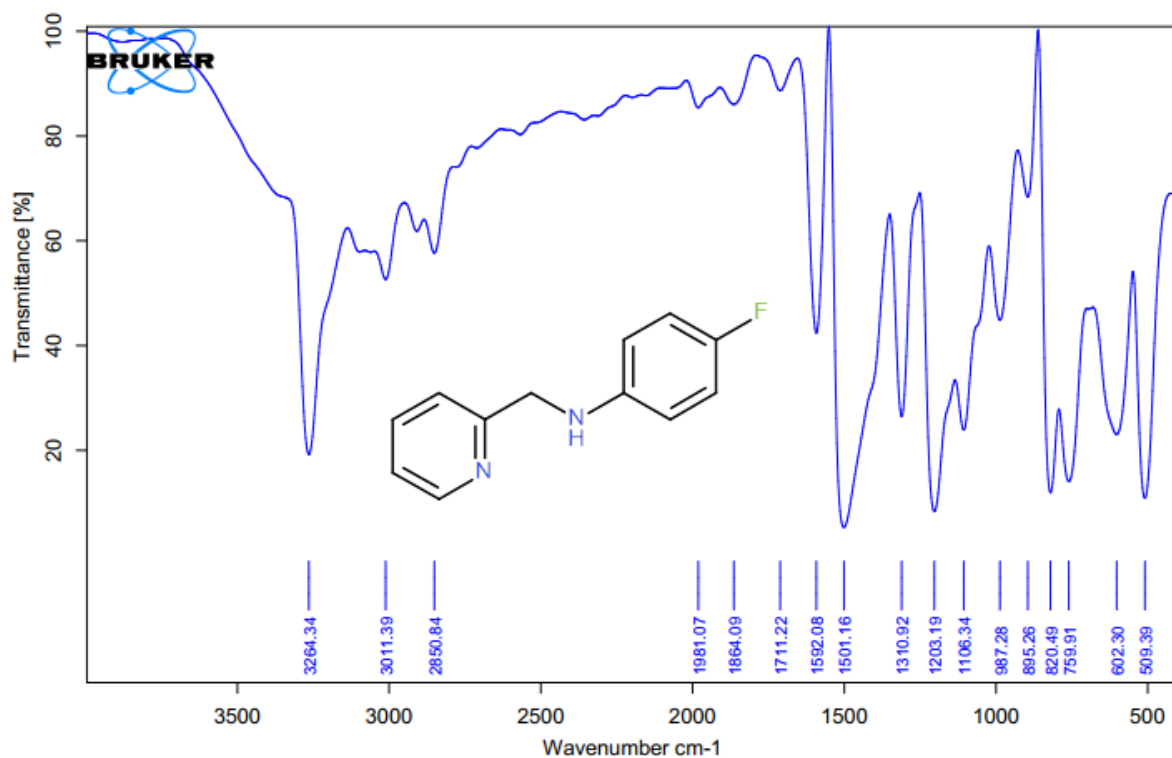


Figure A6 IR spectrum for L2 ligand.

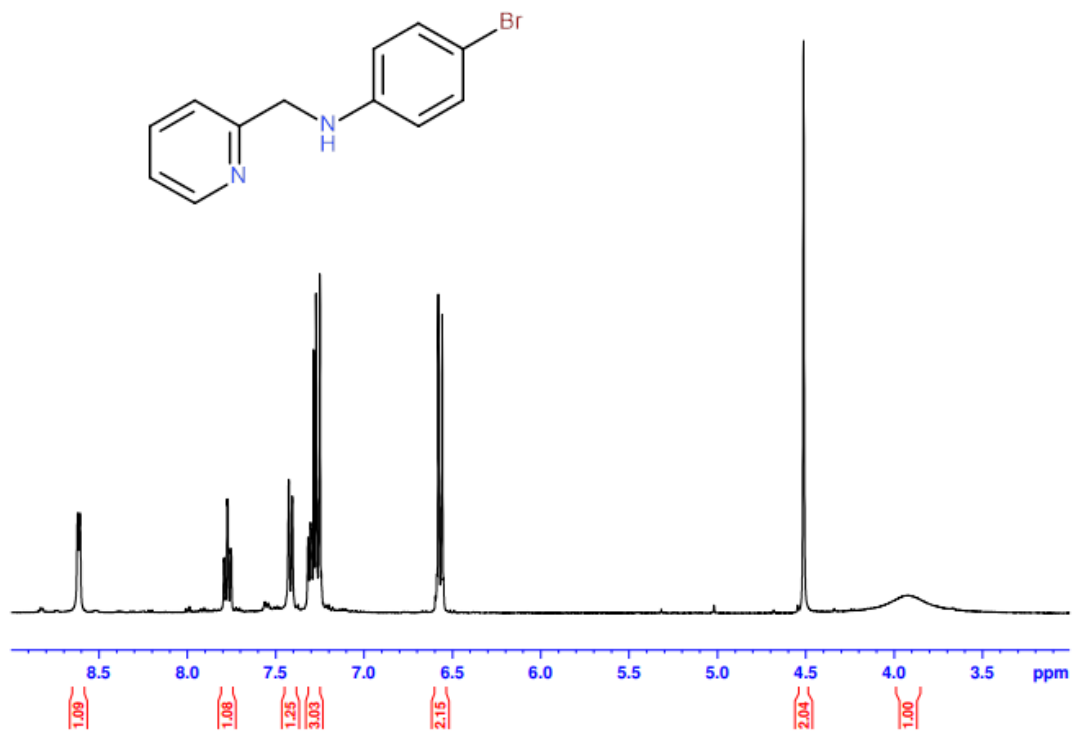


Figure A7  $^1\text{H}$  NMR spectrum for L3 ligand.

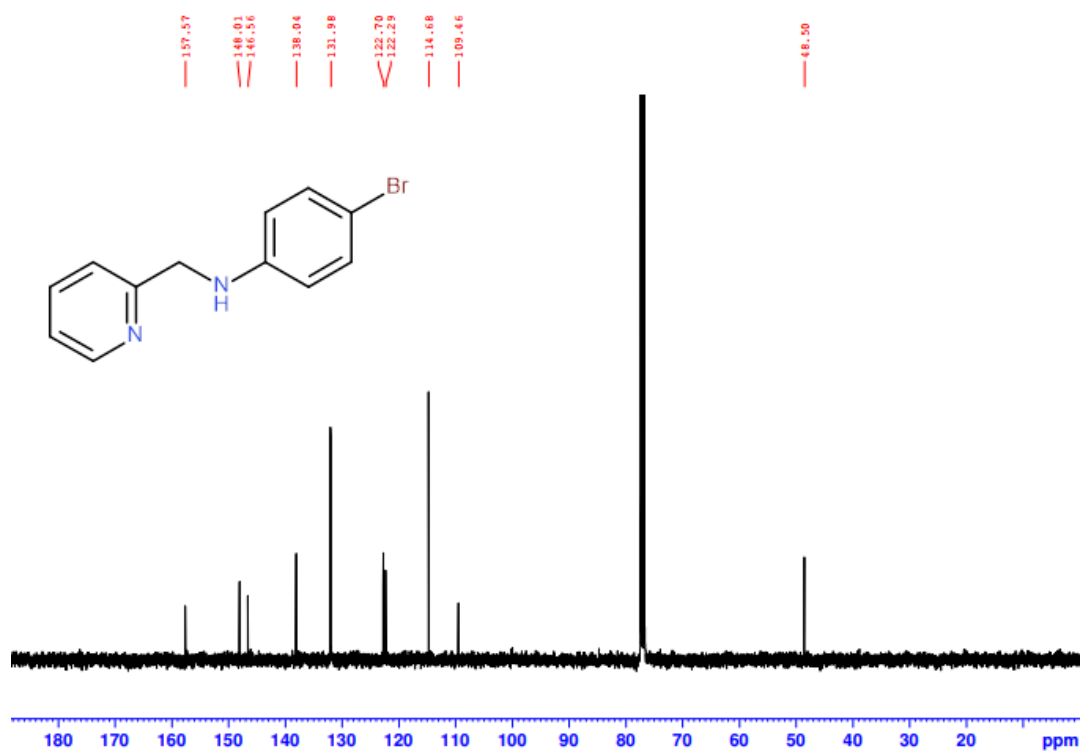


Figure A8  $^{13}\text{C}$  NMR spectrum for L3 ligand.

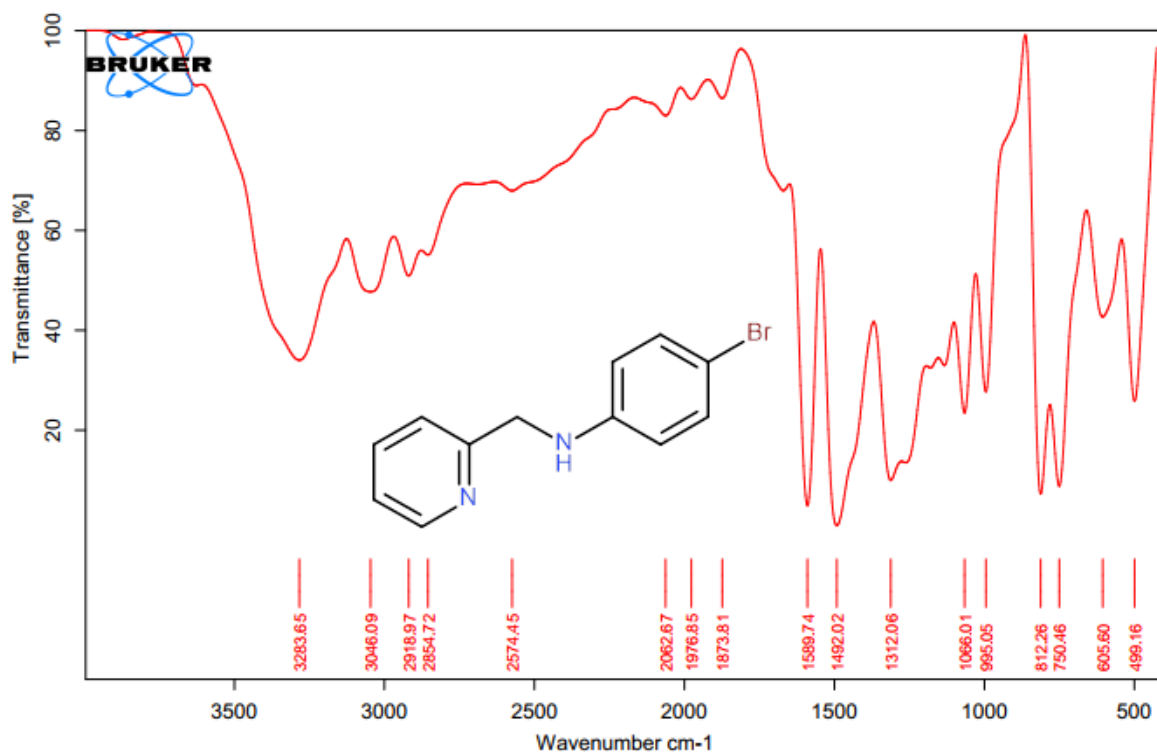


Figure A9 IR spectrum for L3 ligand.

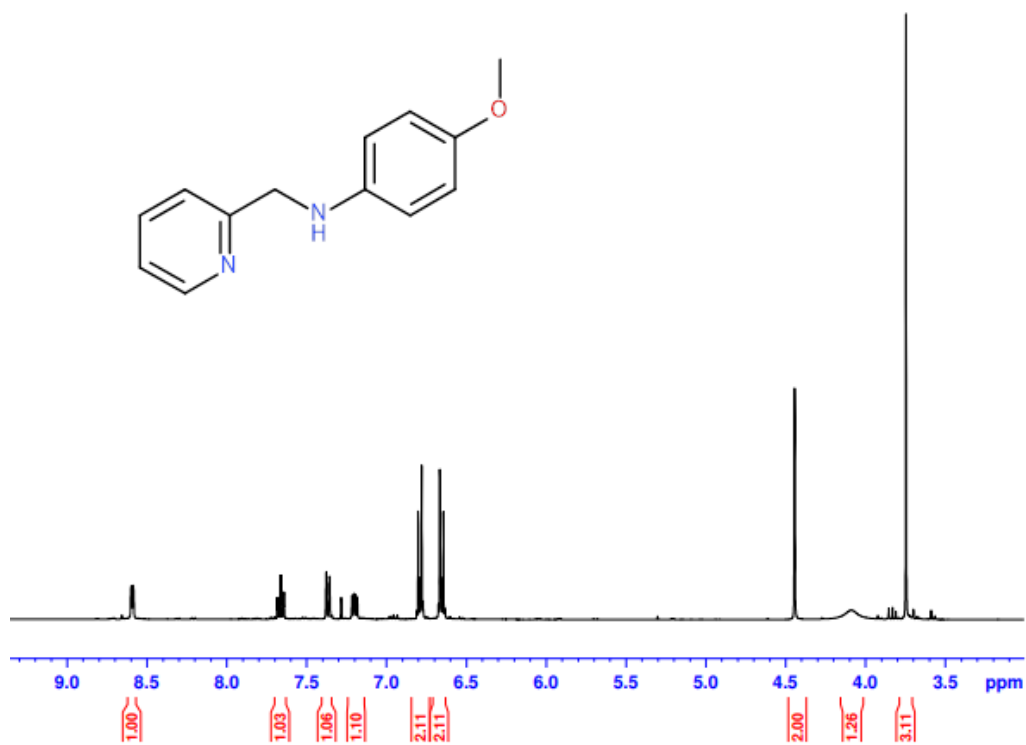


Figure A10 <sup>1</sup>H NMR spectrum for L4 ligand.

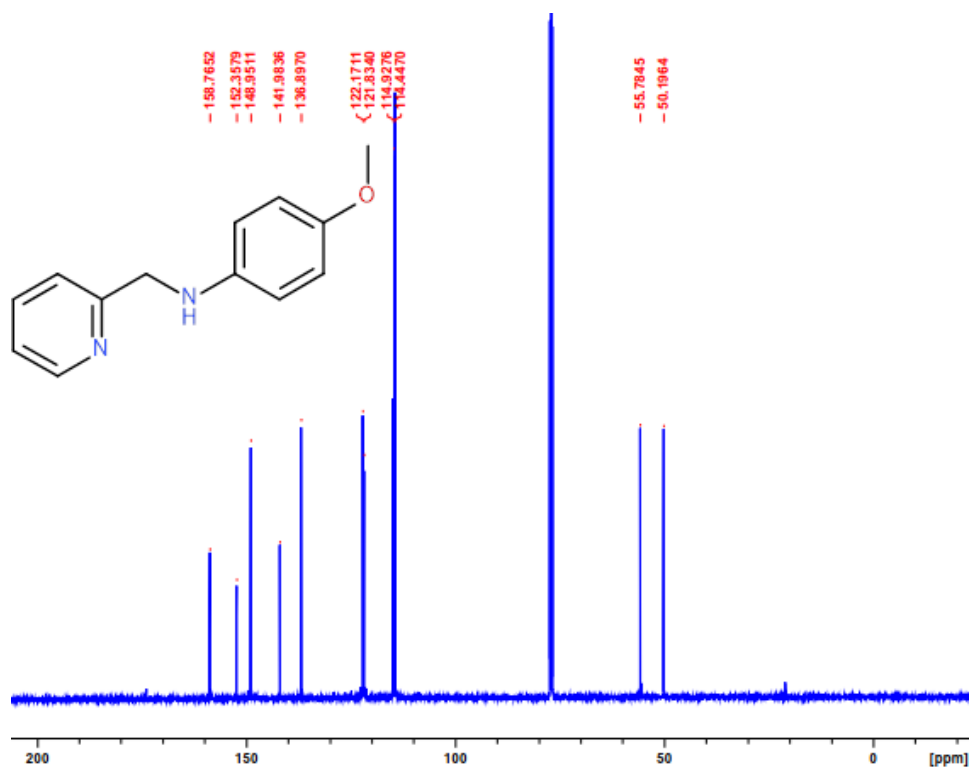


Figure A11 <sup>13</sup>C NMR spectrum for L4 ligand.

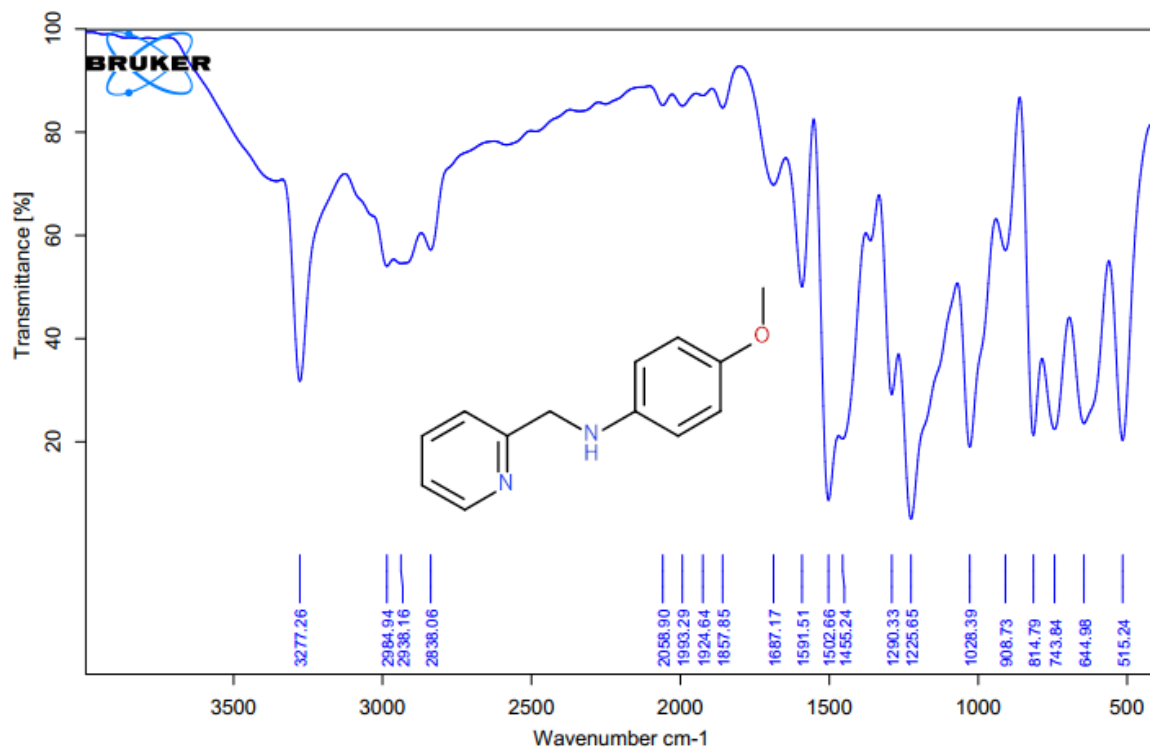


Figure A12 IR spectrum for L4 ligand.

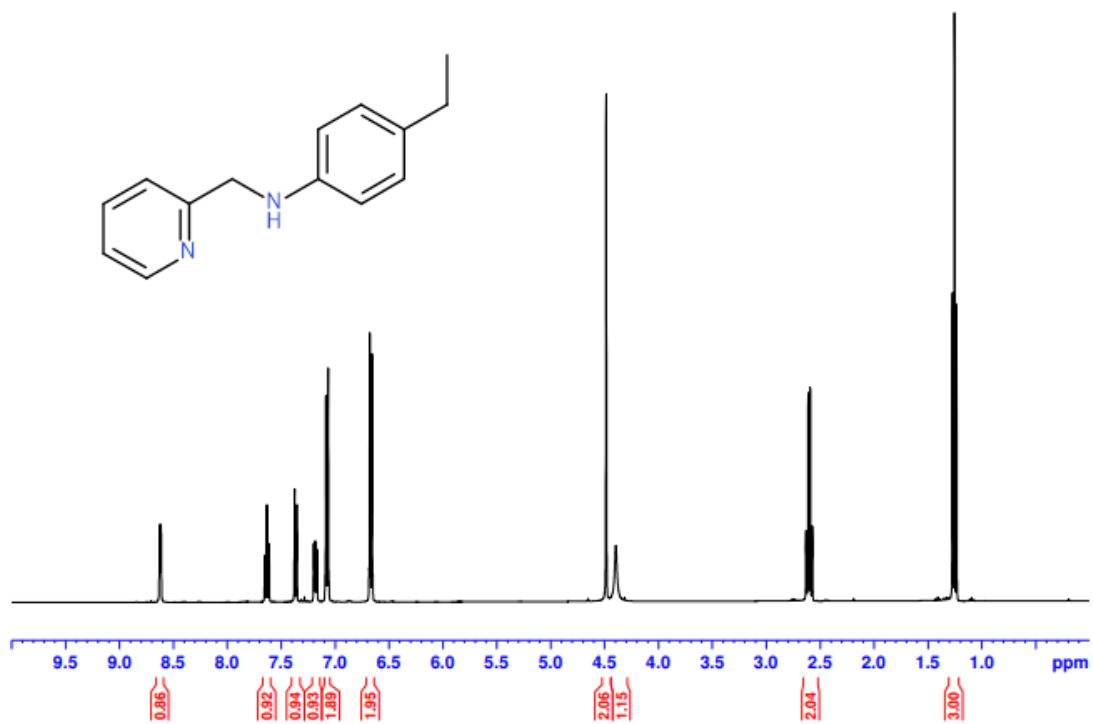


Figure A13 <sup>1</sup>H NMR spectrum for L5 ligand.

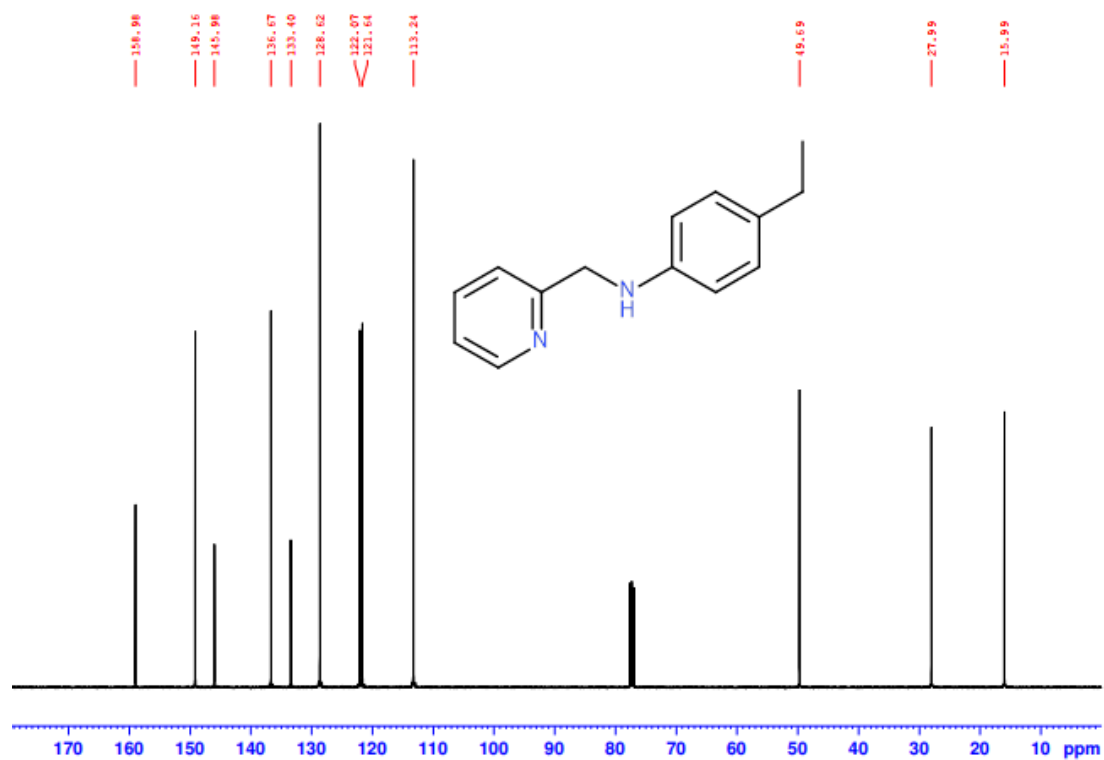


Figure A14 <sup>13</sup>C NMR spectrum for L5 ligand.

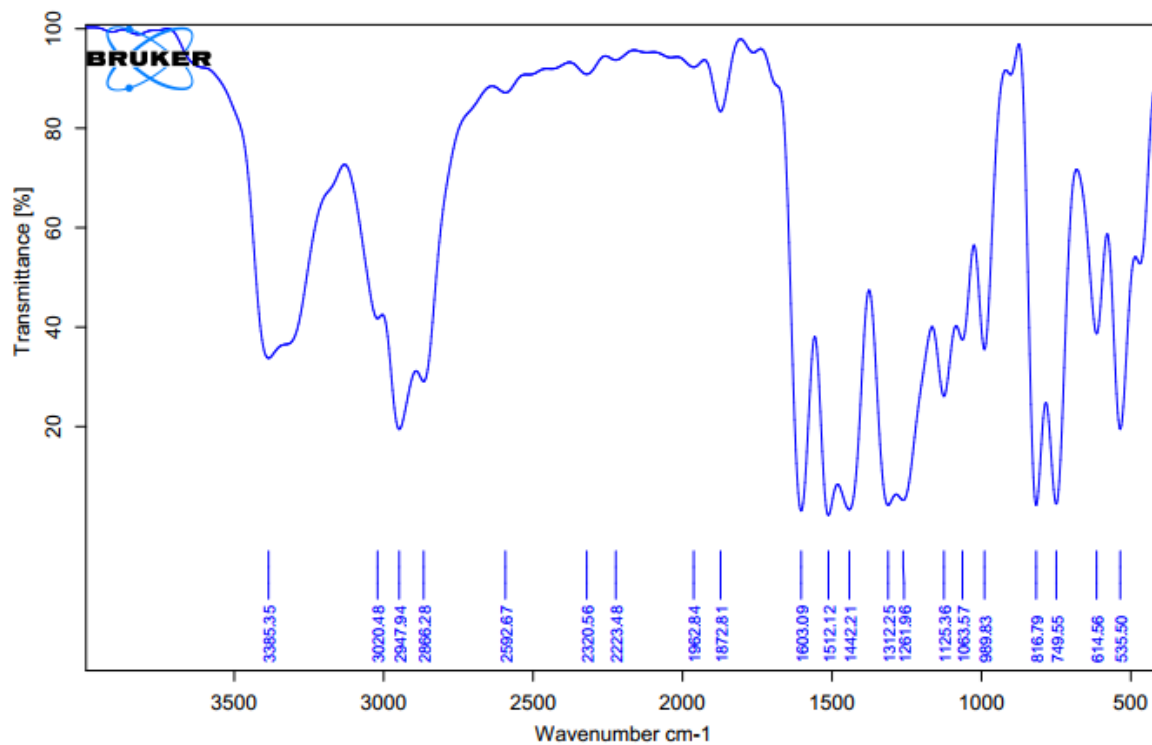


Figure A15 IR spectrum for **L5** ligand.

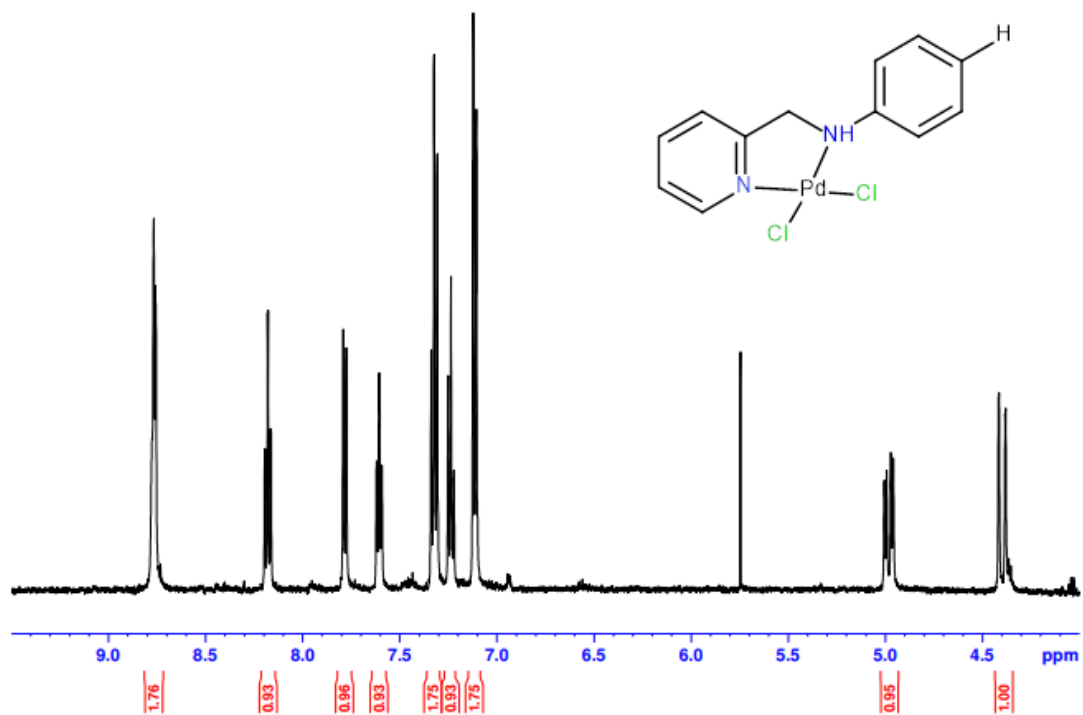


Figure A16 <sup>1</sup>H NMR spectrum for **PdL1** complex.

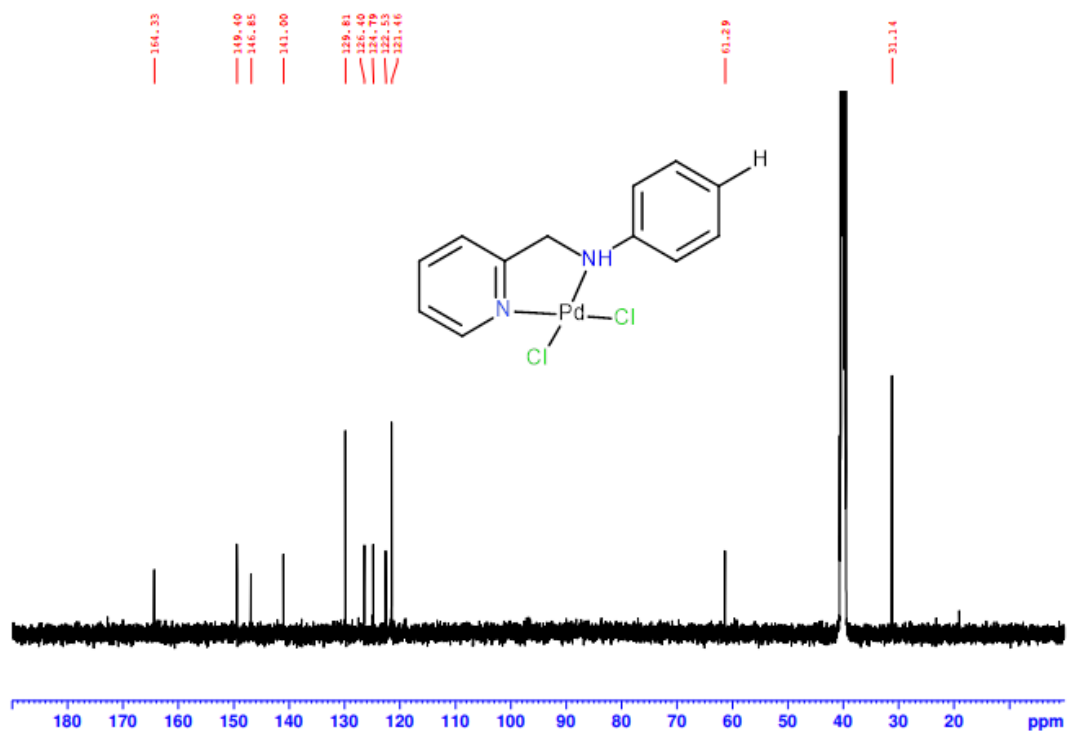


Figure A17  $^{13}\text{C}$  NMR spectrum for PdL1 complex.

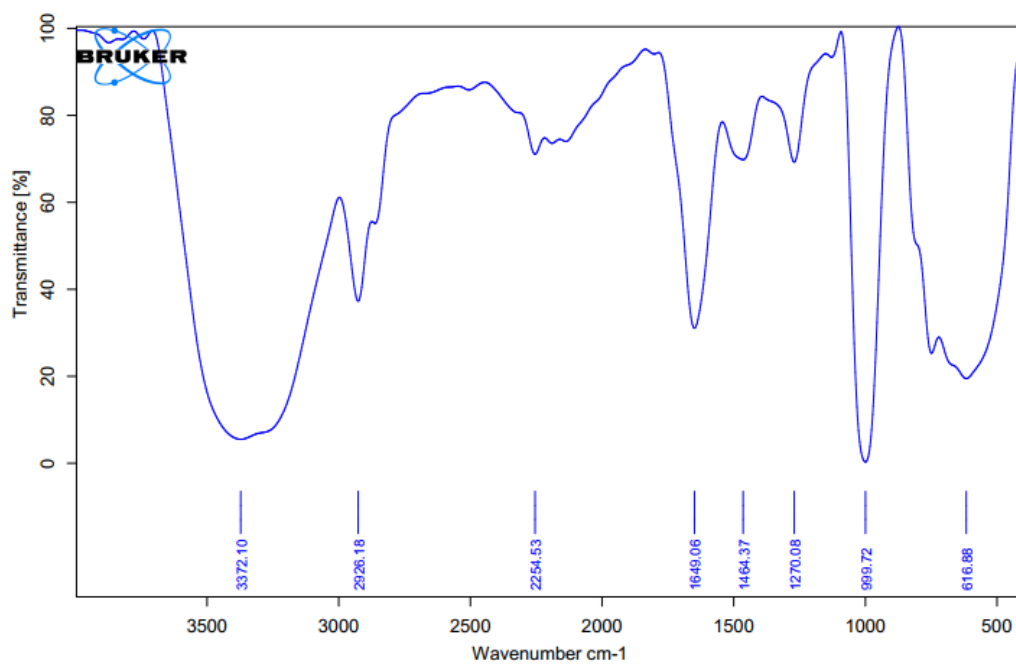
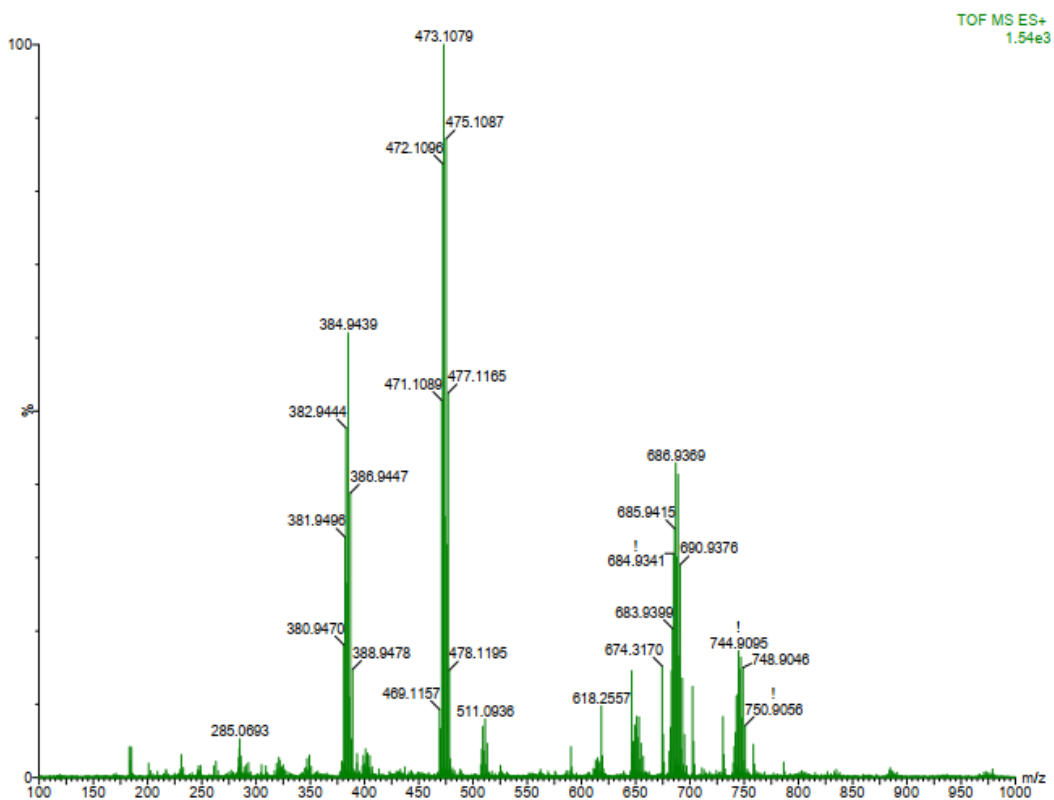
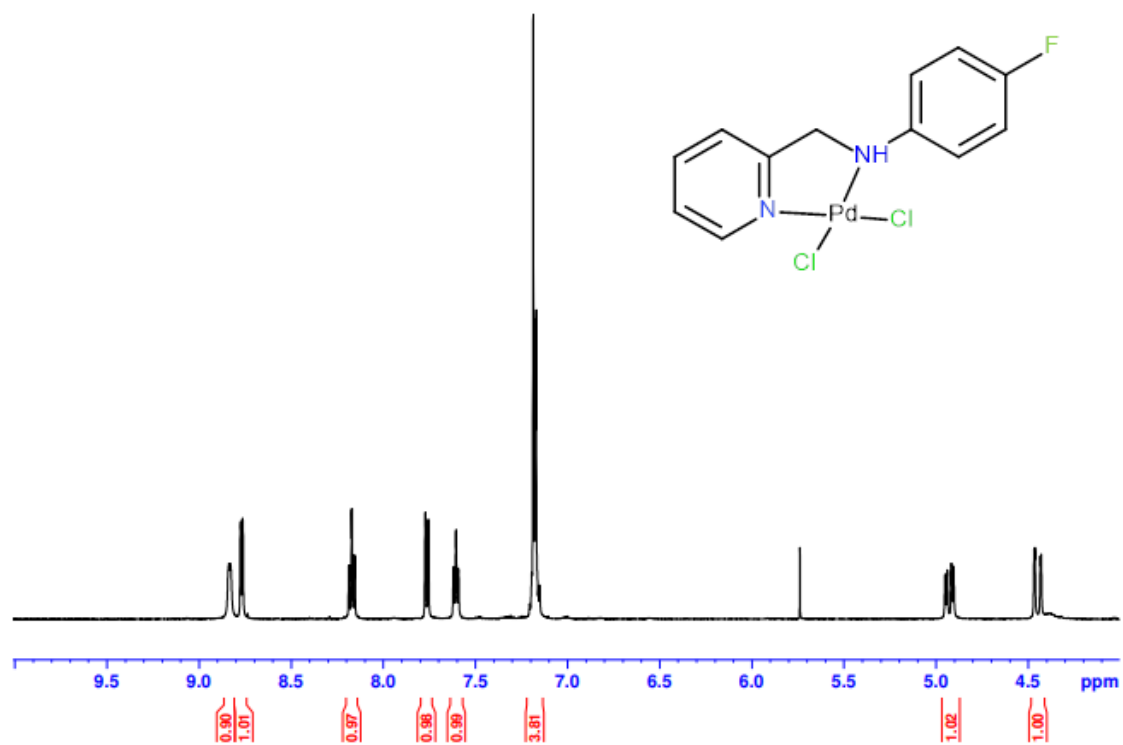


Figure A18 IR spectrum for PdL1 complex.



**Figure A19** lrms spectrum for **PdL1** complex.



**Figure A20**  $^1\text{H}$  NMR spectrum for **PdL2** complex.

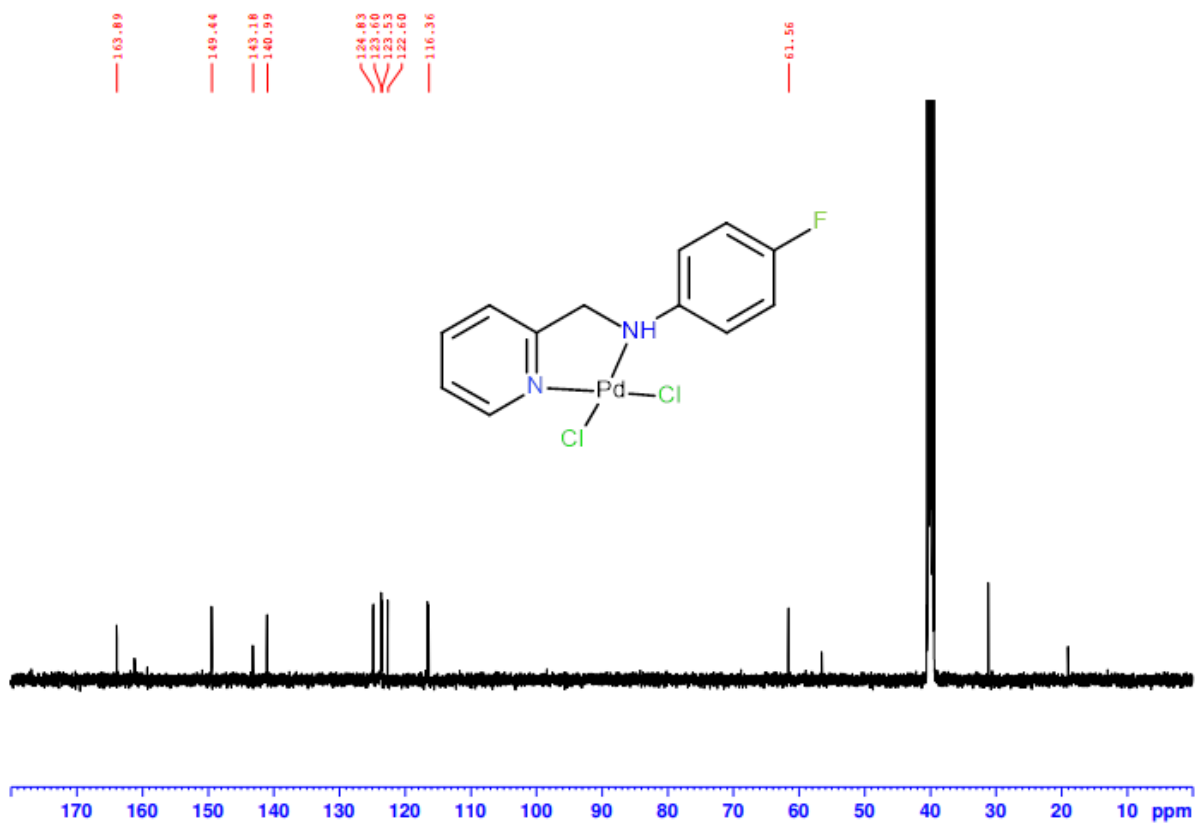


Figure A21 <sup>13</sup>C NMR spectrum for PdL2 complex.

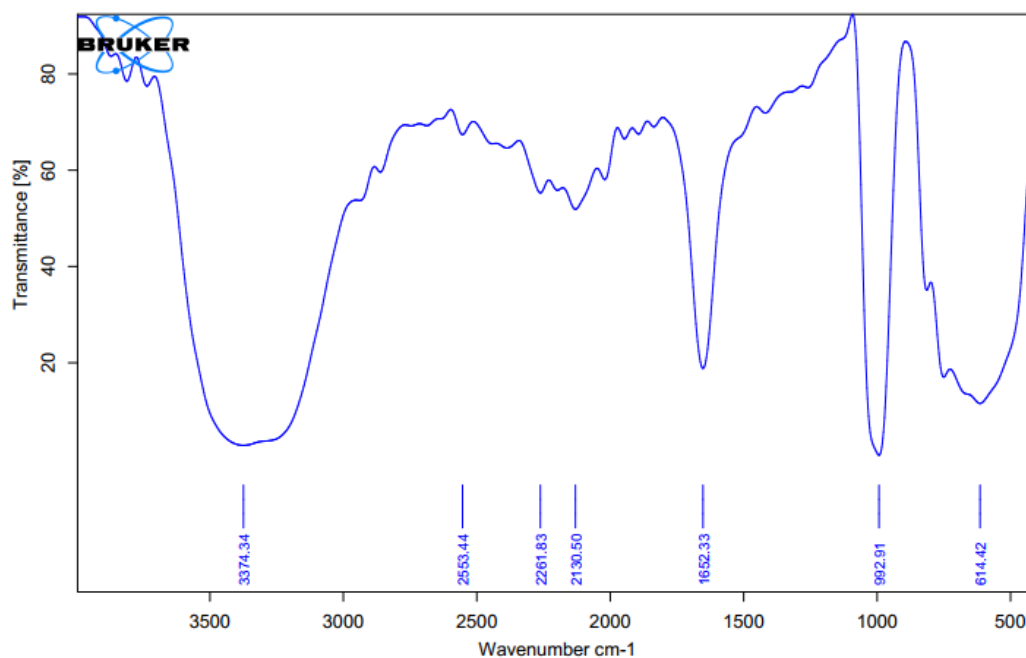


Figure A22 IR spectrum for PdL2 complex.

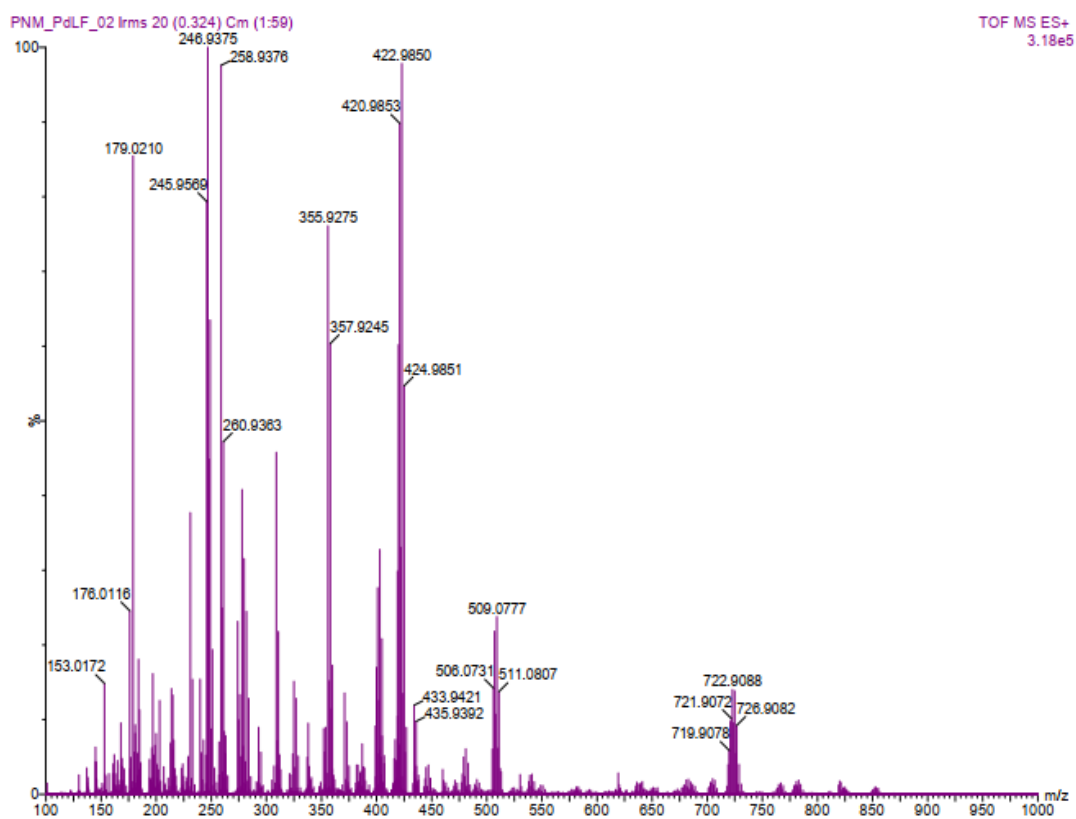


Figure A23 lrms spectrum for PdL2 complex.

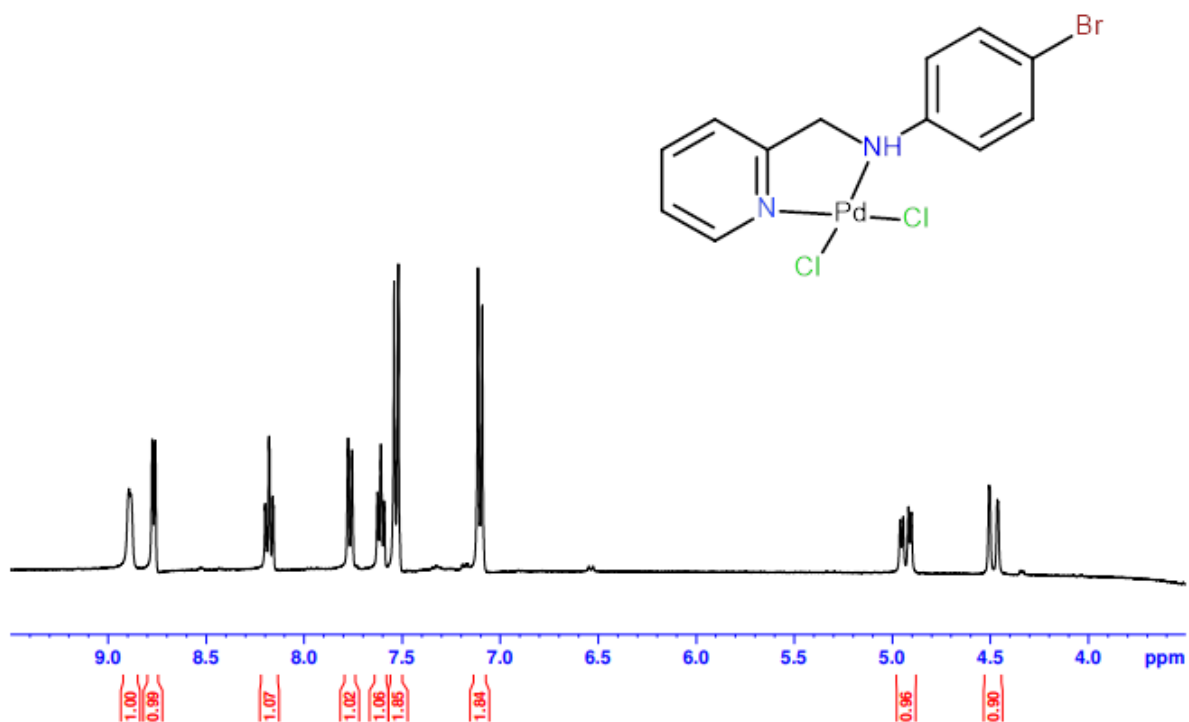


Figure A24  $^1\text{H}$  NMR spectrum for PdL3 complex.

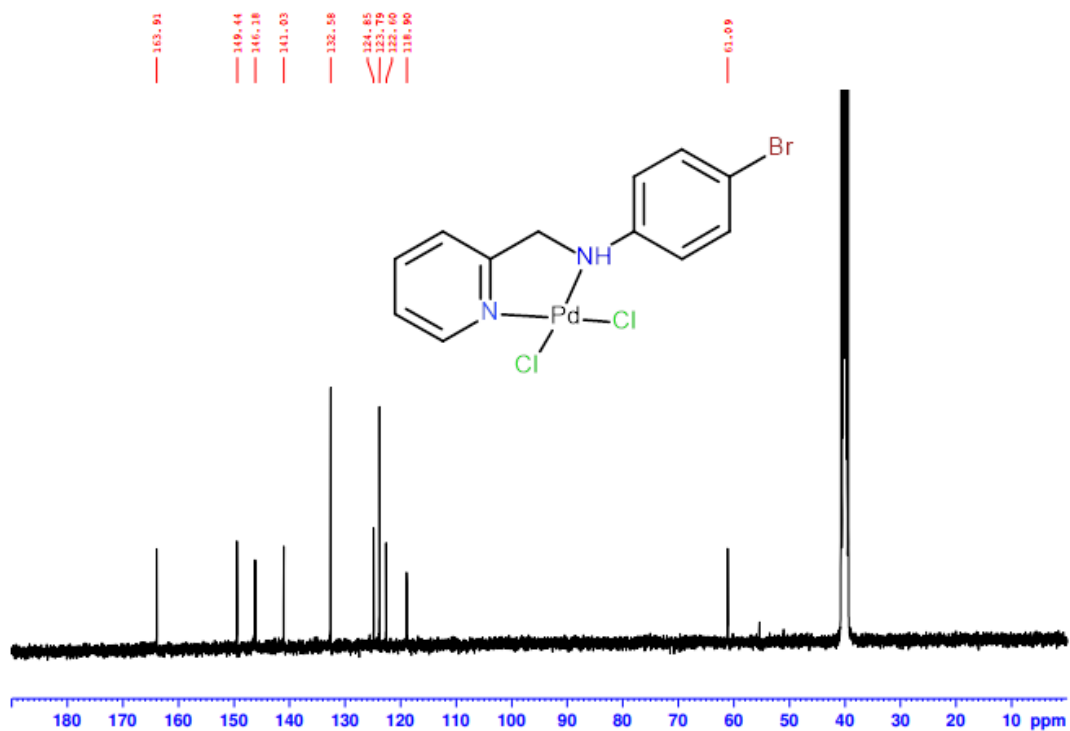


Figure A25  $^{13}\text{C}$  NMR spectrum for PdL3 complex.

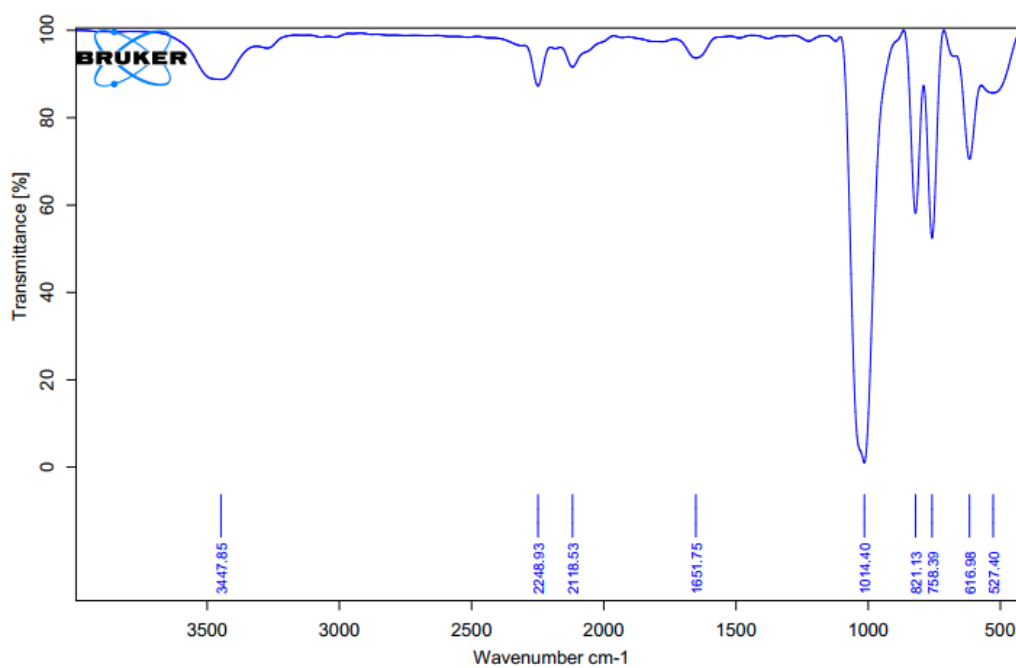


Figure A26 IR spectrum for PdL3 complex.

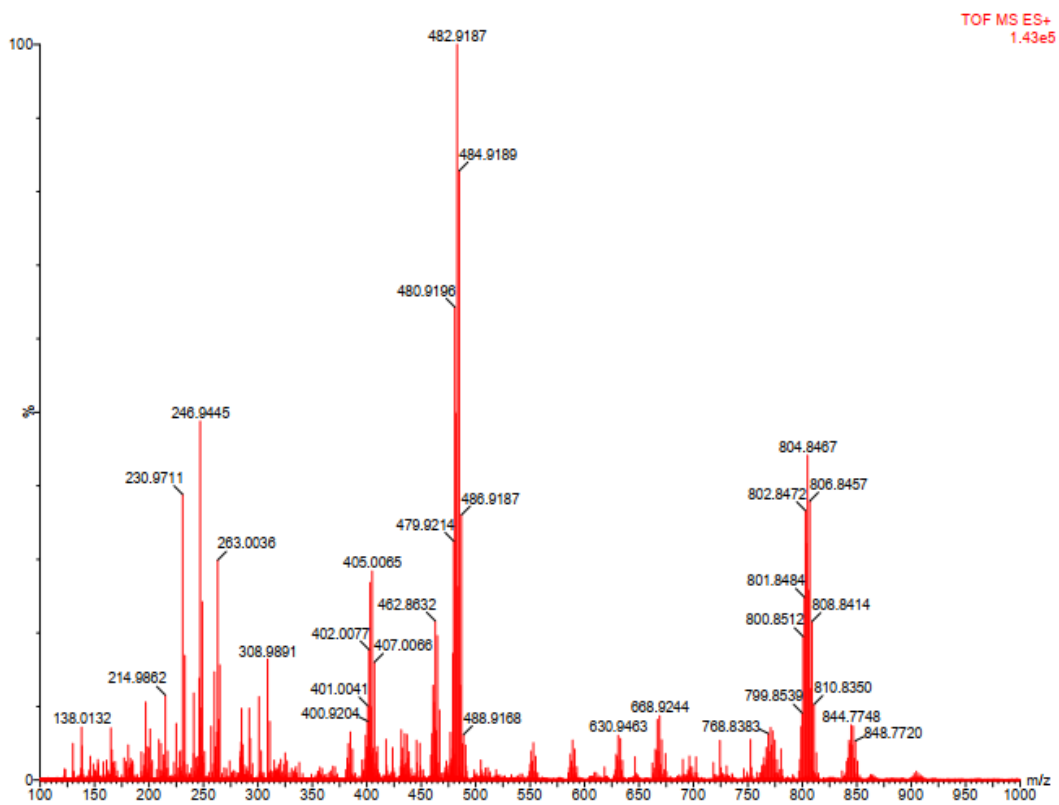


Figure A27 lrms spectrum for PdL3 complex.

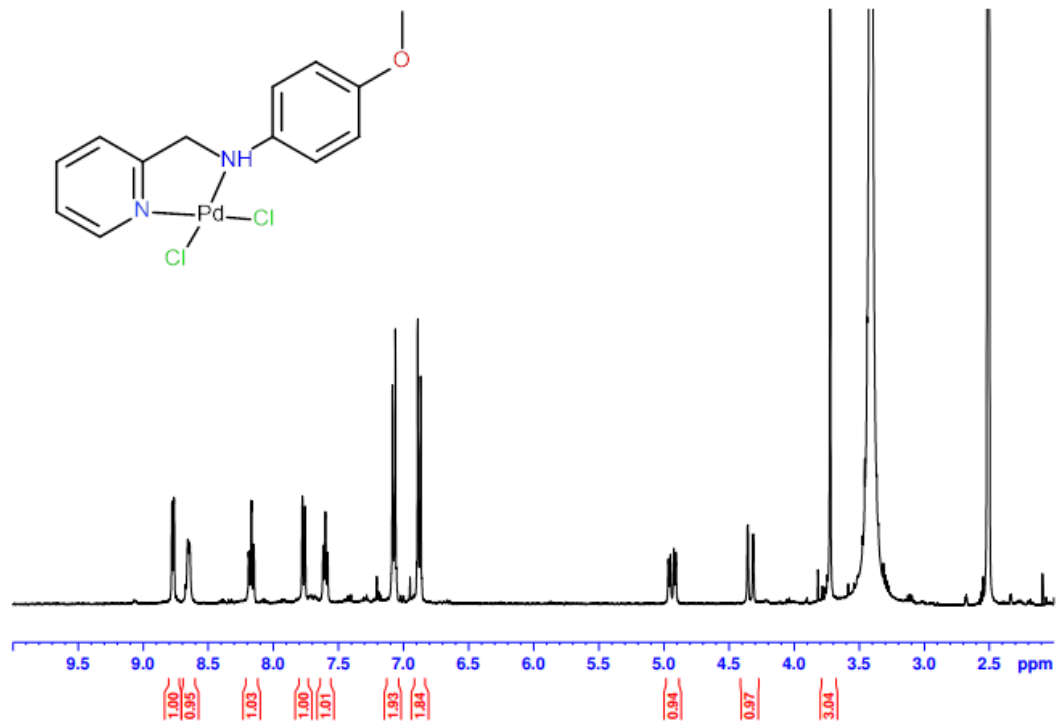


Figure A28  $^1\text{H}$  NMR spectrum for PdL4 complex.

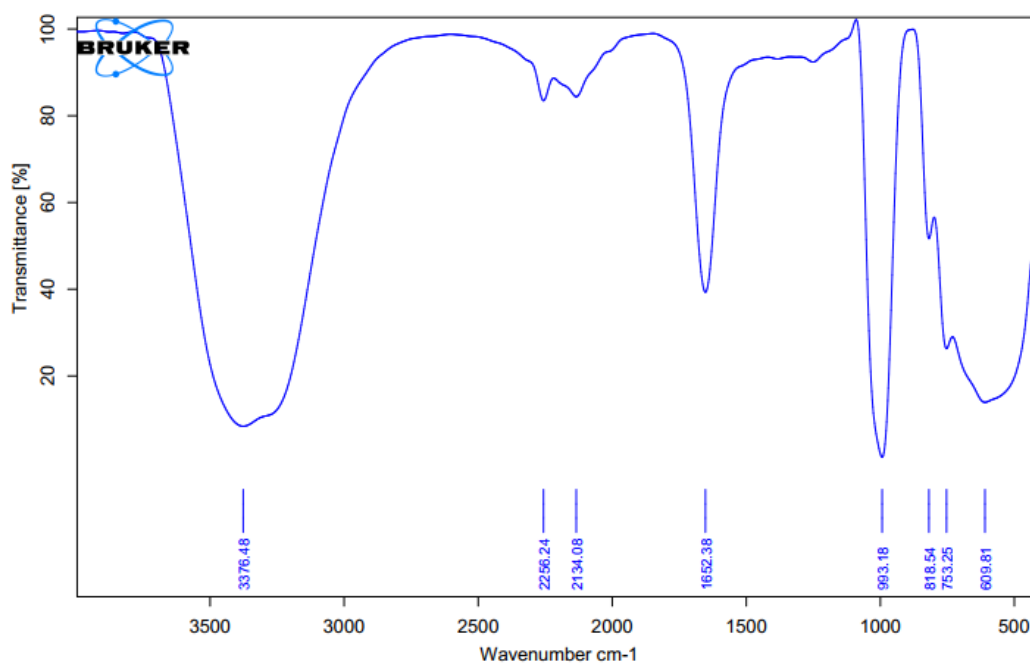


Figure A29 IR spectrum for **PdL4** complex.

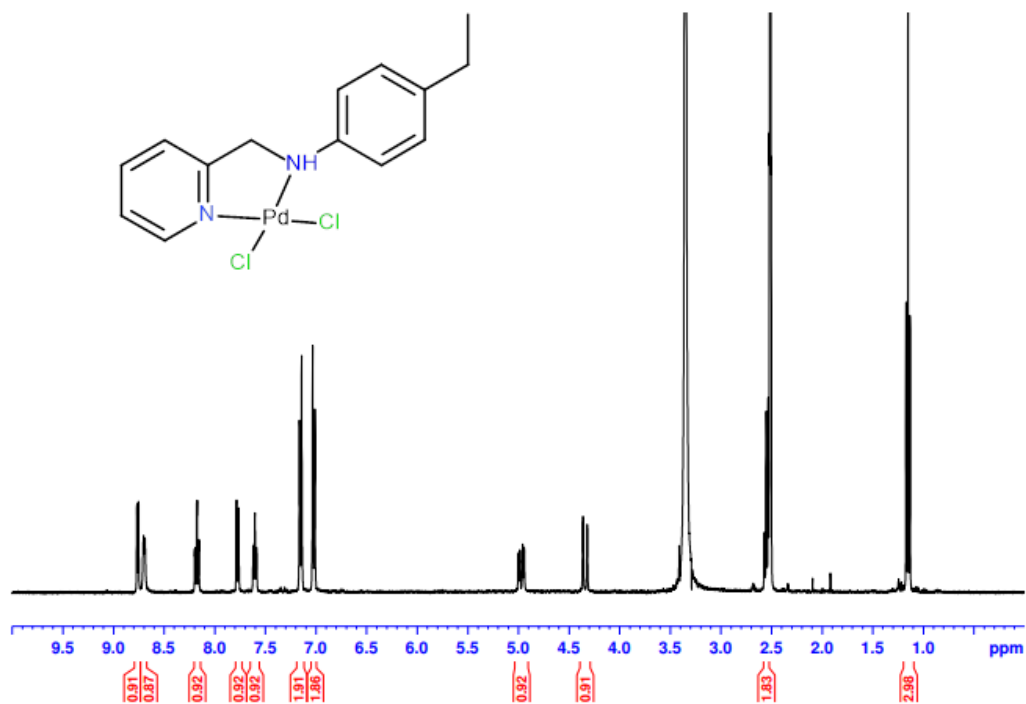


Figure A30 <sup>1</sup>H NMR spectrum for **PdL5** complex.

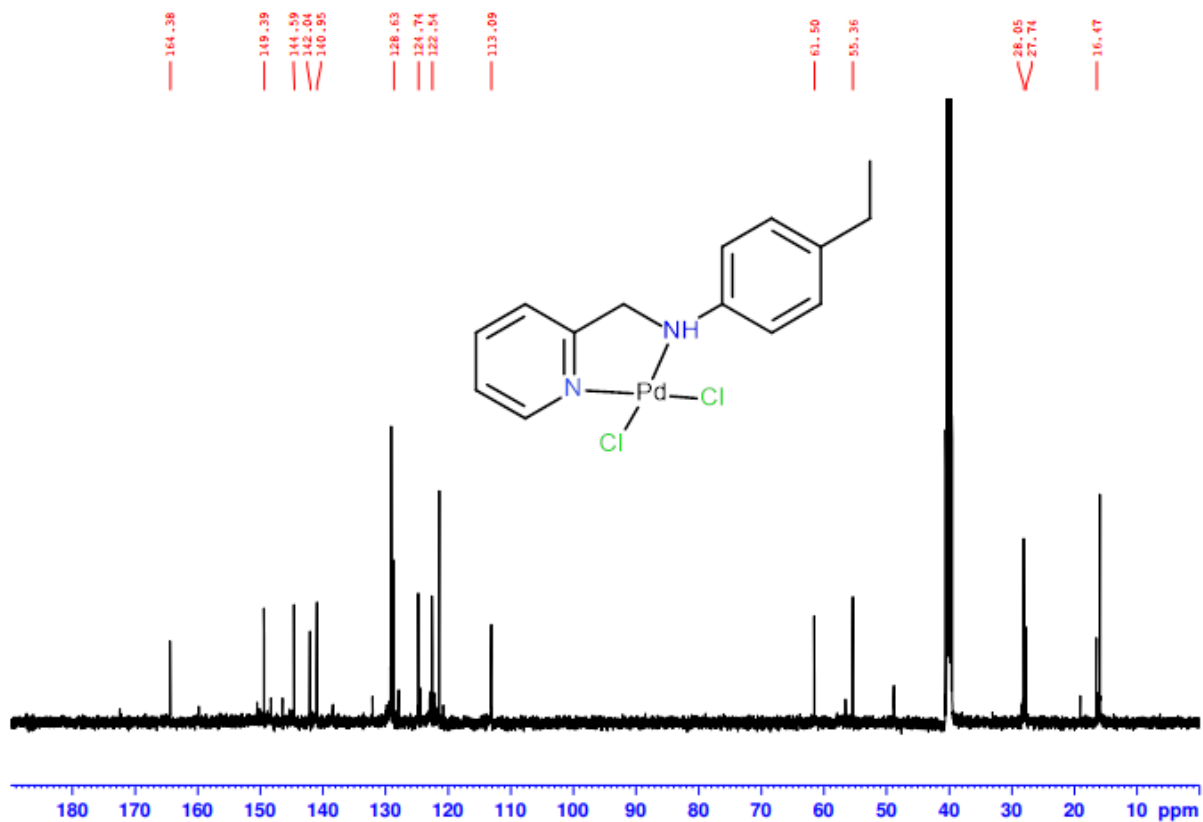


Figure A31  $^{13}\text{C}$  NMR spectrum for PdL5 complex.

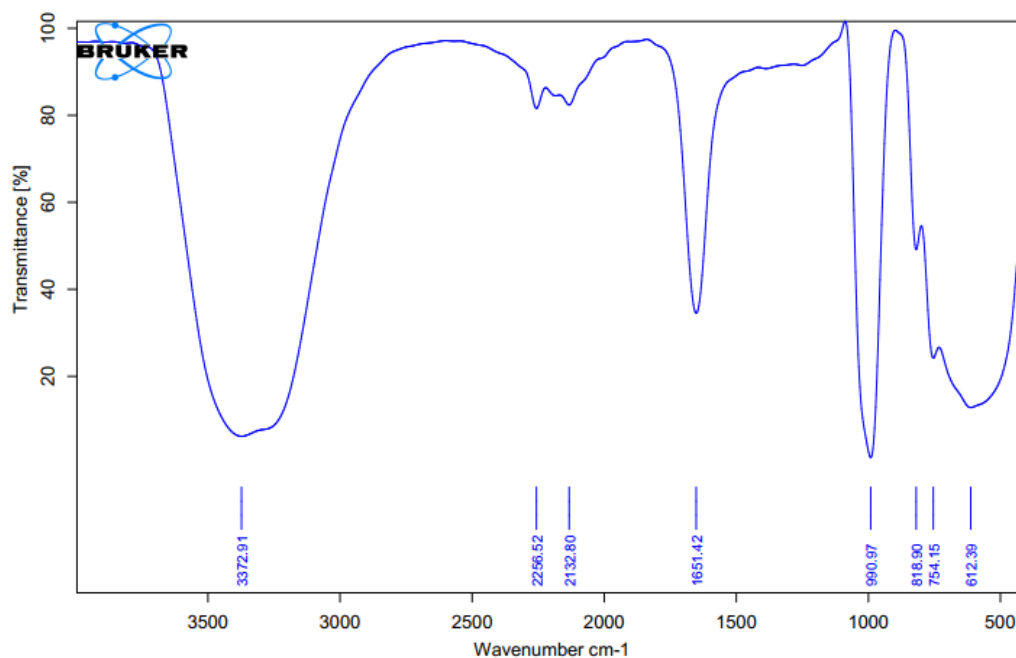
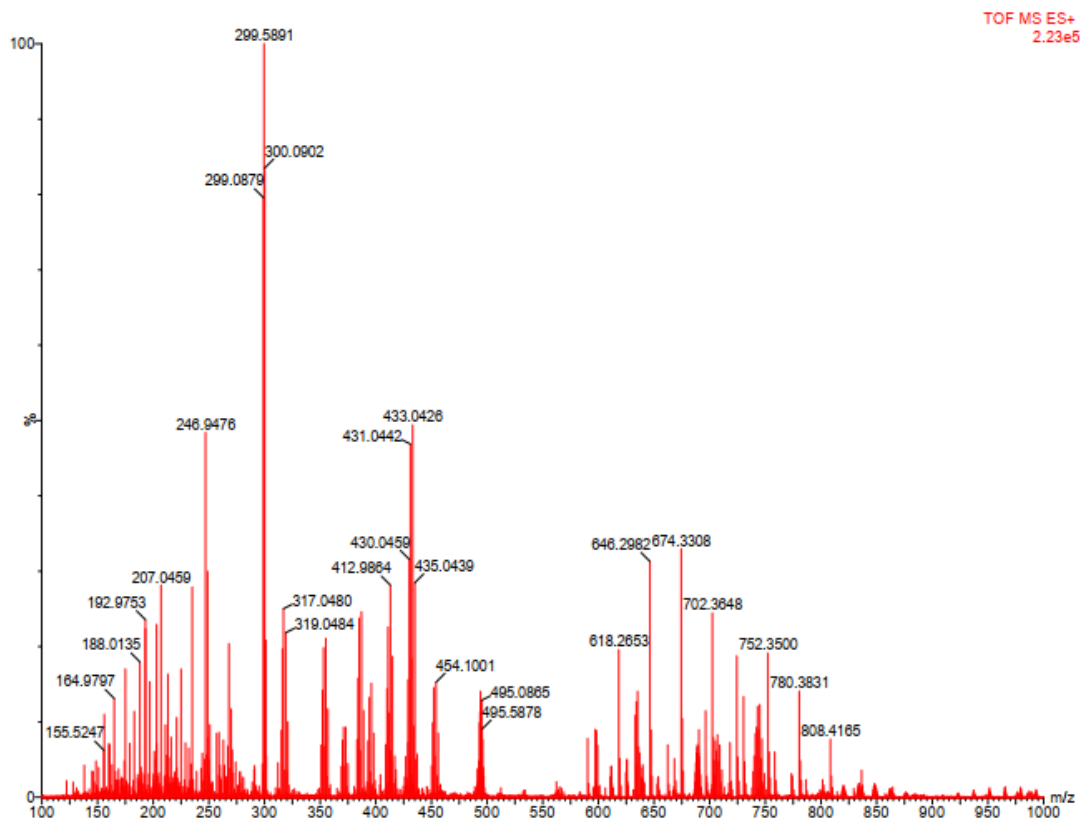


Figure A32 IR spectrum for PdL5 complex.



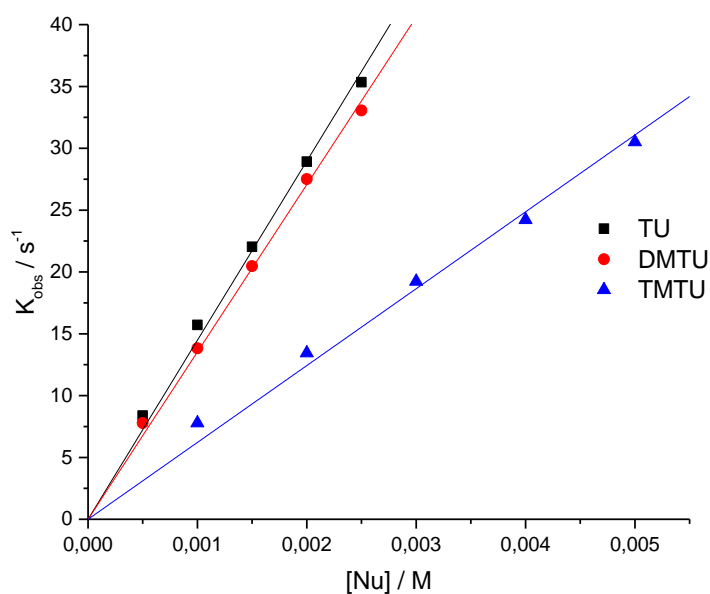
**Figure A33** lrms spectrum for **PdL5** complex.

**Table A1** Selected wavelengths (nm) used for studying the kinetic reactions of Pd(II) complexes with the thiourea nucleophiles.

Complex	Nucleophile	Wavelength, nm
<b>PdL1</b>	TU	295
	DMTU	300
	TMTU	305
<b>PdL2</b>	TU	295
	DMTU	300
	TMTU	305
<b>PdL3</b>	TU	295
	DMTU	300
	TMTU	305
<b>PdL4</b>	TU	305
	DMTU	310
	TMTU	315
<b>PdL5</b>	TU	305
	DMTU	310
	TMTU	315

**Table A2** Average  $k_{obs}$  ( $s^{-1}$ ) for the reaction of **PdL1** with thiourea nucleophiles at 298 K.

[Nu]/M	$k_{obs}$ ( $s^{-1}$ )		
	TU	DMTU	TMTU
5E-4	8,38659	7,78387	
1E-3	15,71827	13,82924	7,78222
0,0015	22,02881	20,46773	
0,002	28,91626	27,5083	13,44462
0,0025	35,34436	33,05594	
0,003			19,23206
0,004			24,2184
0,005			30,51809

**Figure A34** Dependence of  $k_{obs}$  on the entering nucleophile concentration for the displacement of chloride<sub>1</sub> on **PdL1** complex in water, I = 0.1 M (LiCl), T = 298 K.**Table A3** Average  $k_{obs}$  ( $s^{-1}$ ) for the reaction of **PdL2** with thiourea nucleophiles at 298 K.

[Nu]/ M	$k_{obs}$ ( $s^{-1}$ )		
	TU	DMTU	TMTU
5E-4		8,59634	
1E-3	17,69165	15,04729	3,31477
0,0015	25,0257	22,05998	

0,002	32,70792	29,19449	6,59285
0,0025	39,40044	35,4036	
0,003	45,75664		9,75402
0,004			13,20481
0,005			16,00193

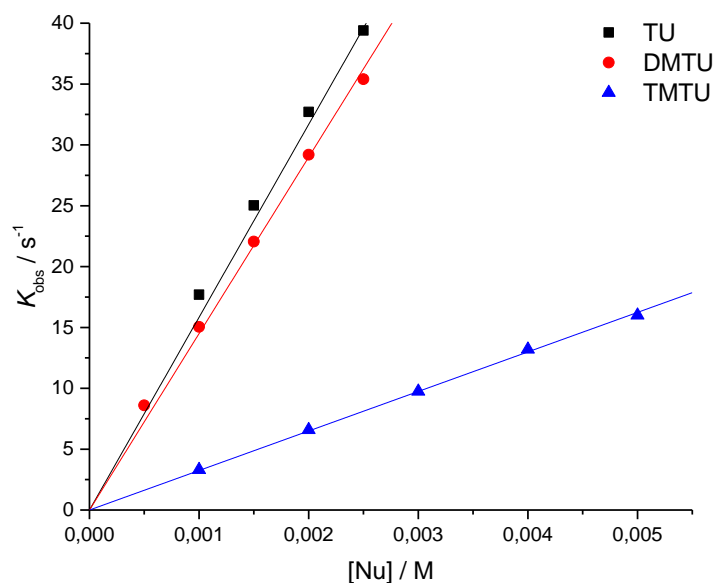


**Figure A35** Dependence of  $k_{obs}$  on the entering nucleophile concentration for the displacement of chloride<sub>1</sub> on **PdL2** complex in water,  $I = 0.1$  M (LiCl),  $T = 298$  K.

**Table A4** Average  $k_{obs}$  ( $s^{-1}$ ) for the reaction of **PdL3** with thiourea nucleophiles at 298 K.

[Nu]/ M	$k_{obs}$ ( $s^{-1}$ )		
	TU	DMTU	TMTU
5E-4	11,10406	10,99755	
1E-3	19,27723	20,44256	8,4122
0,0015	25,55497	28,90848	
0,002	35,40424	37,12629	15,24913
0,0025	43,57588	45,4378	
0,003			21,62503
0,004			28,45985
0,005			34,55511

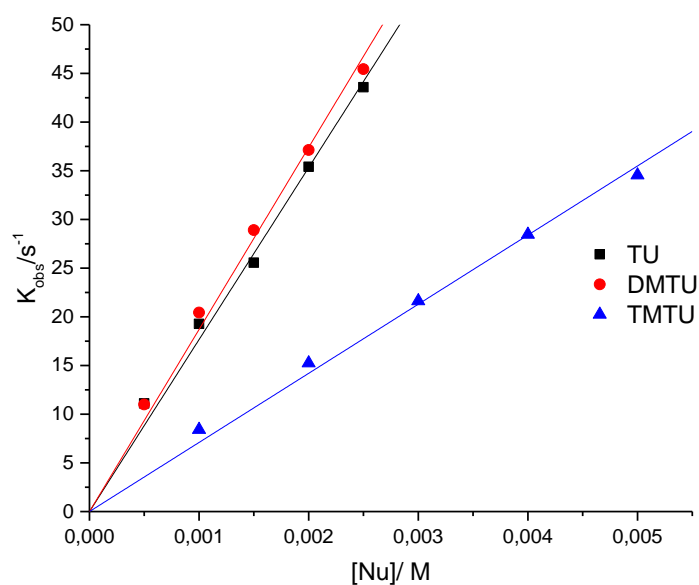


**Figure A36** Dependence of  $k_{obs}$  on the entering nucleophile concentration for the displacement of chloride<sub>1</sub> on **PdL3** complex in water,  $I = 0.1$  M (LiCl),  $T = 298$  K.

**Table A5** Average  $k_{obs}$  ( $s^{-1}$ ) for the reaction of **PdL4** with thiourea nucleophiles at 298 K.

[Nu]/ M	$k_{obs}$ ( $s^{-1}$ )		
	<b>TU</b>	<b>DMTU</b>	<b>TMTU</b>
1E-3	10,63101	8,22445	5,08328
0,0015	17,36058	12,54762	
0,002	21,77975	17,0761	7,65118
0,0025	26,90649	21,13419	
0,003	33,38247	25,08066	11,04213
0,004			14,25341
0,005			17,984

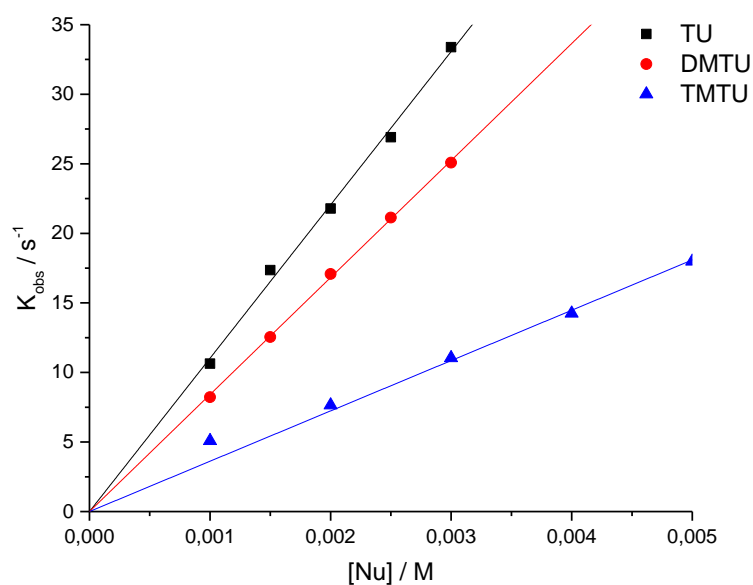


**Figure A37** Dependence of  $k_{obs}$  on the entering nucleophile concentration for the displacement of chloride<sub>1</sub> on **PdL4** complex in water, I = 0.1 M (LiCl), T = 298 K.

**Table A6** Average  $k_{obs}$  ( $s^{-1}$ ) for the reaction of **PdL5** with thiourea nucleophiles at 298 K.

[Nu]/ M	$k_{obs}$ ( $s^{-1}$ )		
	<b>TU</b>	<b>DMTU</b>	<b>TMTU</b>
5E-4	7,18999	6,29023	
1E-3	11,496	11,4255	9,28011
0,0015	16,6402	16,47458	
0,002	22,05958	22,35079	17,68069
0,0025	28,46814	26,97597	
0,003			24,95068
0,004			31,96058
0,005			40,7972

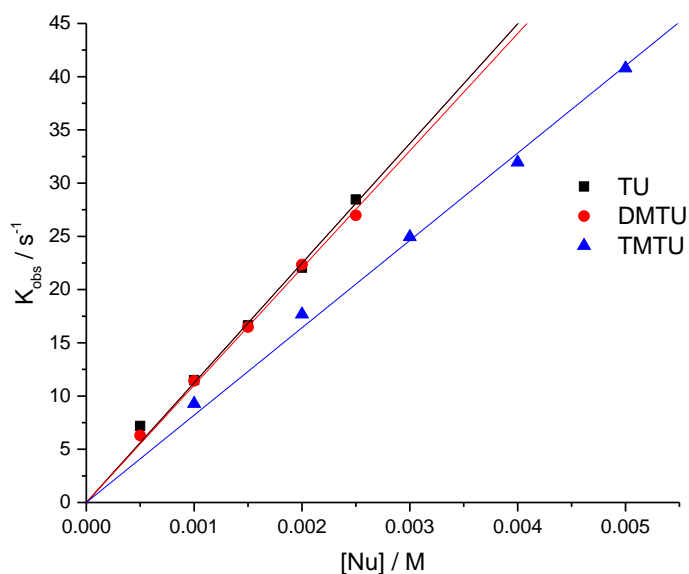


**Figure A38** Dependence of  $k_{obs}$  on the entering nucleophile concentration for the displacement of chloride<sub>1</sub> on **PdL5** complex in water, I = 0.1 M (LiCl), T = 298 K.

**Table A7** Temperature dependence of  $k_2$  for the reaction of **PdL5** with thiourea nucleophiles at 288-308 K.

(1/T)/K <sup>-1</sup>	$\ln(k_2/T)$		
	TU	DMTU	TMTU
0,00347	-2,9753	-3,02343	-3,1872
0,00341	-2,7702	-2,84346	-2,9171
0,00335	-2,62138	-2,67824	-2,7003
0,0033	-2,47292	-2,5407	-2,4487
0,00325	-2,18985	-2,31107	-2,2636

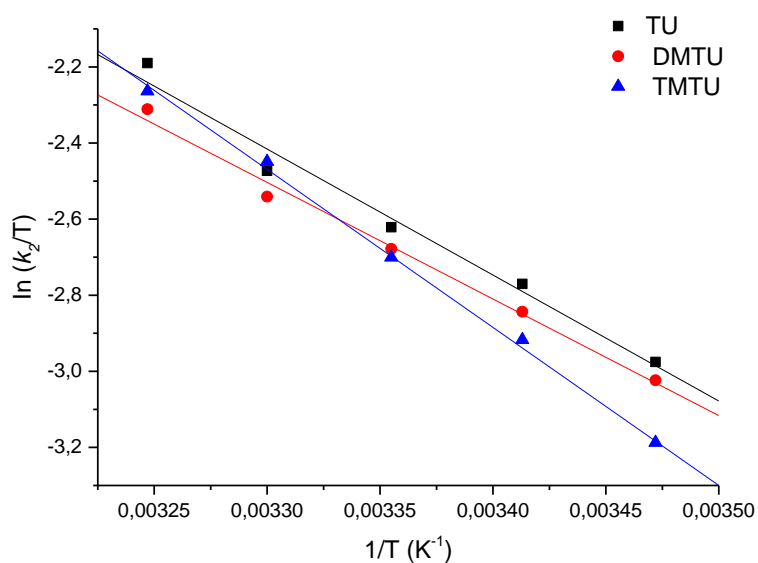


**Figure A39** Eyring plot for the reaction of **PdL1** with the three nucleophiles at various temperatures in the temperature range 288–308 K.

**Table A8** Temperature dependence of  $k_2$  for the reaction of **PdL2** with thiourea nucleophiles at 288–308 K.

(1/T)/K <sup>-1</sup>	ln(k <sub>2</sub> /T)		
	TU	DMTU	TMTU
0,00347	-2,5586	-3,01201	-3,9659
0,00341	-2,4936	-2,77659	-3,7207
0,00335	-2,4022	-2,58236	-3,46098
0,0033	-2,333	-2,42102	-3,2983
0,00325	-2,2512	-2,28834	-3,15067

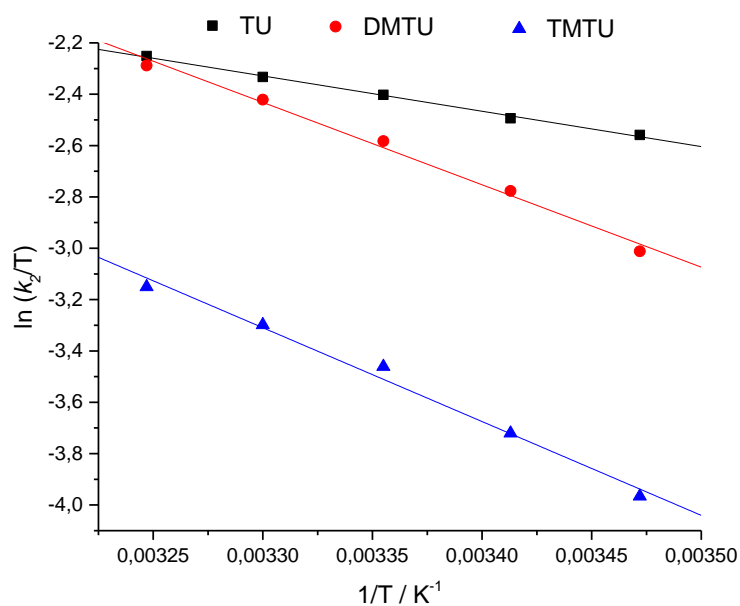


**Figure A40** Eyring plot for the reaction of **PdL2** with the three nucleophiles at various temperatures in the temperature range 288–308 K.

**Table A9** Temperature dependence of  $k_2$  for the reaction of **PdL3** with thiourea nucleophiles at 288–308 K.

(1/T)/K <sup>-1</sup>	$\ln(k_2/T)$		
	TU	DMTU	TMTU
0,00347	-2,7571	-2,64	-3,62532
0,00341	-2,6037	-2,45556	-3,33943
0,00335	-2,4617	-2,33296	-3,11045
0,0033	-2,3142	-2,23365	-2,86539
0,00325	-2,1858	-2,11862	-2,75606

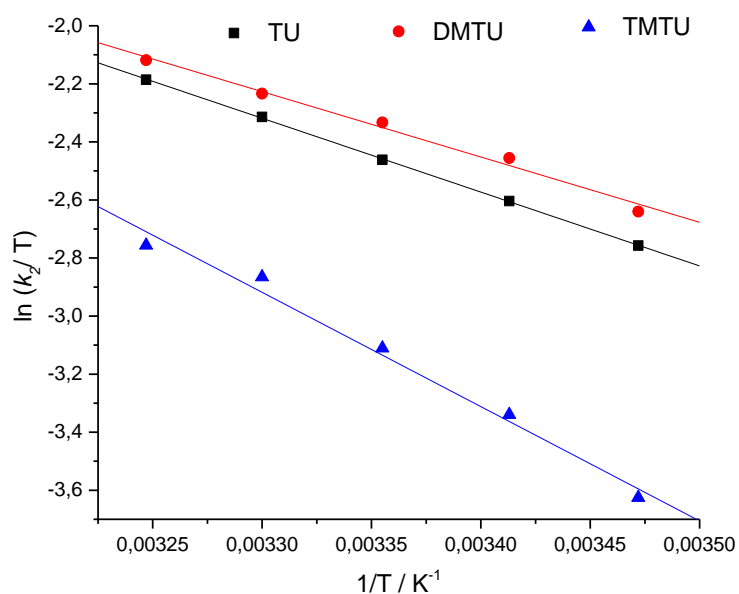


**Figure A41** Eyring plot for the reaction of **PdL3** with the three nucleophiles at various temperatures in the temperature range 288–308 K.

**Table A10** Temperature dependence of  $k_2$  for the reaction of **PdL4** with thiourea nucleophiles at 288–308 K.

$(1/T)/K^{-1}$	$\ln(k_2/T)$		
	<b>TU</b>	<b>DMTU</b>	<b>TMTU</b>
0,00347	-2,78959	-3,22837	-4,41441
0,00341	-2,58436	-3,07807	-3,80041
0,00335	-2,39947	-2,89801	-3,3903
0,0033	-2,19591	-2,74361	-3,09295
0,00325	-2,04393	-2,6355	-2,78671

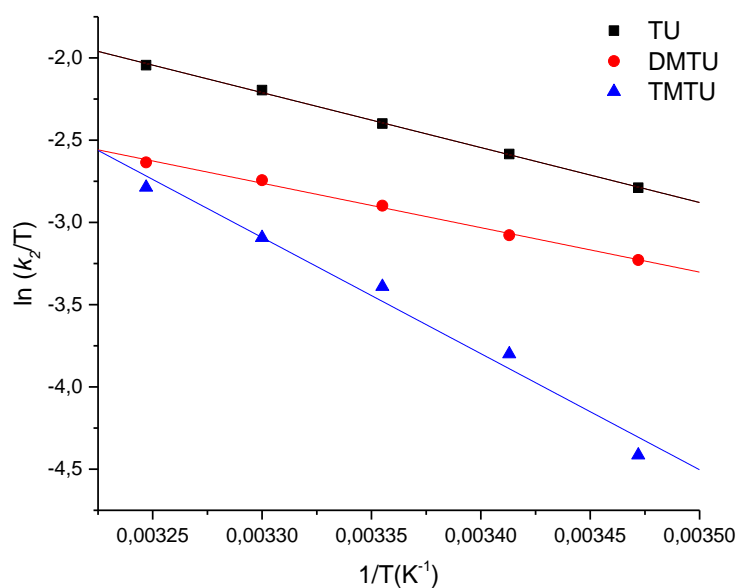


**Figure A42** Eyring plot for the reaction of **PdL4** with the three nucleophiles at various temperatures in the temperature range 288–308 K.

**Table A11** Temperature dependence of  $k_2$  for the reaction of **PdL5** with thiourea nucleophiles at 288–308 K.

(1/T)/K <sup>-1</sup>	$\ln(k_2/T)$		
	TU	DMTU	TMTU
0,00347	-3,53657	-3,30904	-2,86688
0,00341	-3,13294	-2,99307	-2,64378
0,00335	-2,83419	-2,7708	-2,45092
0,0033	-2,59693	-2,59131	-2,3024
0,00325	-2,36788	-2,42649	-2,11717

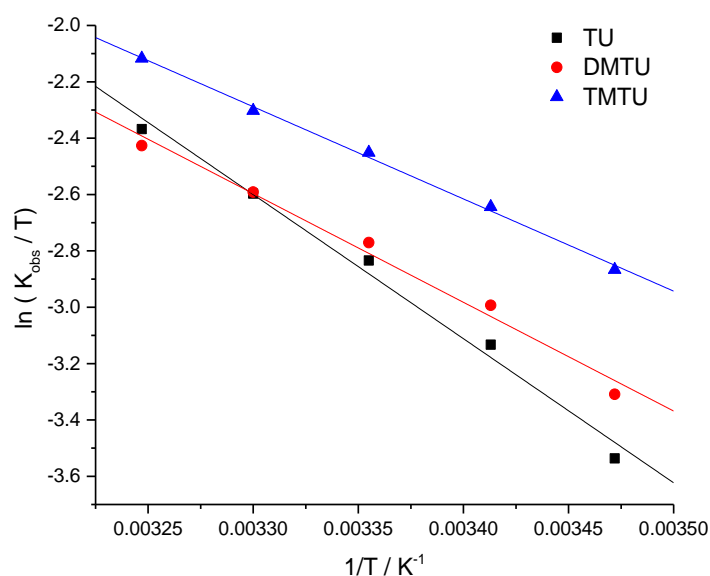


**Figure A43** Eyring plot for the reaction of **PdL5** with the three nucleophiles at various temperatures in the temperature range 288–308 K.

**Table A12** Average  $k_{obs}$  ( $\text{min}^{-1}$ ) for the reaction of **PdL1** with thiourea nucleophiles at 298 K.

[Nu]/ M	$k_{obs}$ ( $\text{min}^{-1}$ )		
	TU	DMTU	TMTU
5E-4	0.161	0.101	
0.001	0.162	0.103	0.045
0.0015	0.164	0.104	
0.002	0.162	0.105	0.055
0.0025	0.162	0.105	
0.003			0.058
0.004			0.061
0.005			0.062

**Table A13** Average  $k_{obs}$  ( $\text{min}^{-1}$ ) for the reaction of **PdL2** with thiourea nucleophiles at 298 K.

[Nu]/ M	$k_{obs}$ ( $\text{min}^{-1}$ )		
	TU	DMTU	TMTU
5E-4	0,266	0,129	
0.001	0,266	0,129	0.058

0.0015	0,267	0,129	
0.002	0,267	0,129	0.058
0.0025	0,267	0,128	
0.003			0,058
0.004			0,0589
0.005			0,0609

**Table A14** Average  $k_{\text{obs}}$  ( $\text{min}^{-1}$ ) for the reaction of **PdL3** with thiourea nucleophiles at 298 K.

[Nu]/ M	$k_{\text{obs}}$ ( $\text{min}^{-1}$ )		
	TU	DMTU	TMTU
5E-4	0,595	0,277	
0.001	0,597	0,277	0.06
0.0015	0,597	0,277	
0.002	0,597	0,276	0.06
0.0025	0,297	0,276	
0.003			0,06
0.004			0,06
0.005			0,06

**Table A15** Average  $k_{\text{obs}}$  ( $\text{min}^{-1}$ ) for the reaction of **PdL4** with thiourea nucleophiles at 298 K.

[Nu]/ M	$k_{\text{obs}}$ ( $\text{min}^{-1}$ )		
	TU	DMTU	TMTU
5E-4	0,133	0,053	
0.001	0,133	0,053	0.017
0.0015	0,133	0,053	
0.002	0,133	0,053	0,015
0.0025	0,135	0,053	
0.003			0,013
0.004			0,012
0.005			0,011

**Table A16** Average  $k_{\text{obs}}$  ( $\text{min}^{-1}$ ) for the reaction of **PdL5** with thiourea nucleophiles at 298 K.

[Nu]/ M	$k_{\text{obs}}$ ( $\text{min}^{-1}$ )		
	TU	DMTU	TMTU
5E-4	0,142	0,071	
0.001	0,142	0,069	0.029
0.0015	0,142	0,065	
0.002	0,142	0,062	0,0029
0.0025	0,142	0,062	
0.003			0,029
0.004			0,029
0.005			0,029

**Table A17** Temperature dependence of  $k_2$  for the reaction of **PdL1** with thiourea nucleophiles between the temperature range 288 – 308 K.

(1/T)/K <sup>-1</sup>	$\ln(k_2/T)$		
	TU	DMTU	TMTU
0,00347	-11,6638	-12,8854	-13,5625
0,00341	-11,6311	-12,4776	-13,2501
0,00335	-11,6104	-12,0587	-12,6703
0,00330	-11,5596	-11,7432	-12,2227
0,00325	-11,5205	-11,5674	-11,9233

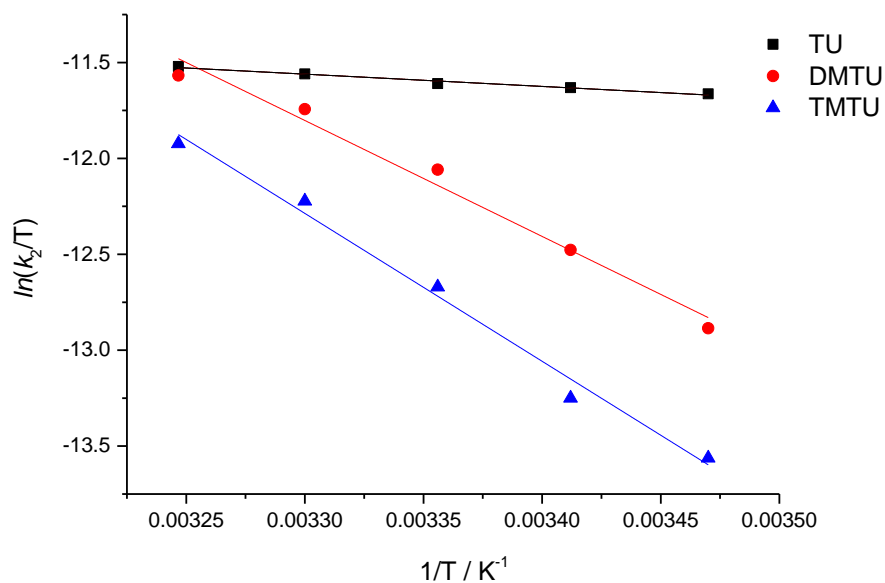


**Figure A44** Eyring plot for the reaction of **PdL1** with the three nucleophiles at various temperatures in the temperature range 288 – 308 K.

**Table A18** Temperature dependence of  $k_2$  for the reaction of **PdL2** with thiourea nucleophiles between the temperature range 288 – 308 K.

(1/T)/K <sup>-1</sup>	ln(k <sub>2</sub> /T)		
	TU	DMTU	TMTU
0,00347	-11,3769	-12,753	-13,7972
0,00341	-11,227	-12,4252	-13,1737
0,00335	-11,1134	-11,99409	-12,7449
0,00330	-11,0016	-11,6724	-12,0497
0,00325	-10,8805	-11,50841	-11,685

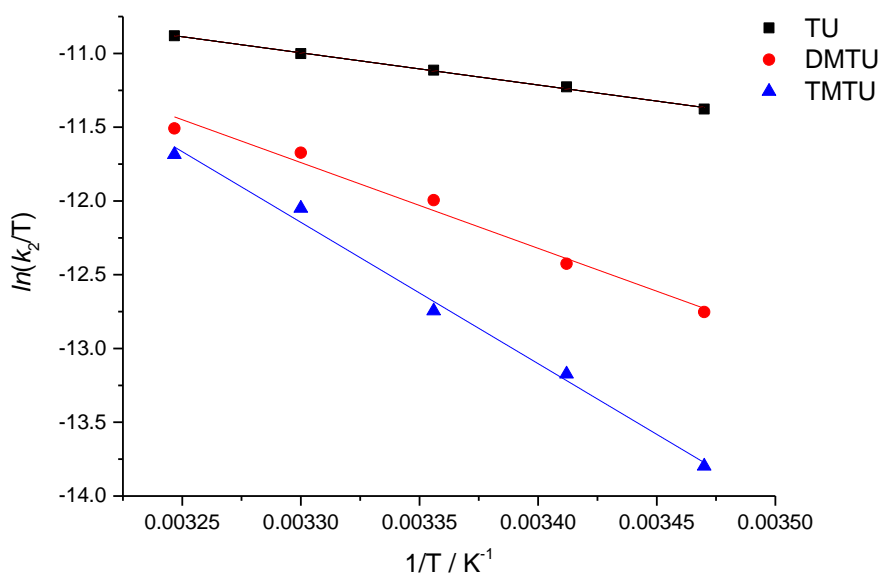


**Figure A45** Eyring plot for the reaction of **PdL2** with the three nucleophiles at various temperatures in the temperature range 288 – 308 K.

**Table A19** Temperature dependence of  $k_2$  for the reaction of **PdL3** with thiourea nucleophiles between the temperature range 288 – 308 K.

(1/T)/K <sup>-1</sup>	ln(k <sub>2</sub> /T)		
	TU	DMTU	TMTU
0,00347	-10,7657	-11,7277	-13,2639
0,00341	-10,5524	-11,4663	-12,9934
0,00335	-10,37139	-11,0766	-12,7048
0,00330	-10,0778	-10,8432	-12,5092
0,00325	-9,85904	-10,5945	-12,3502

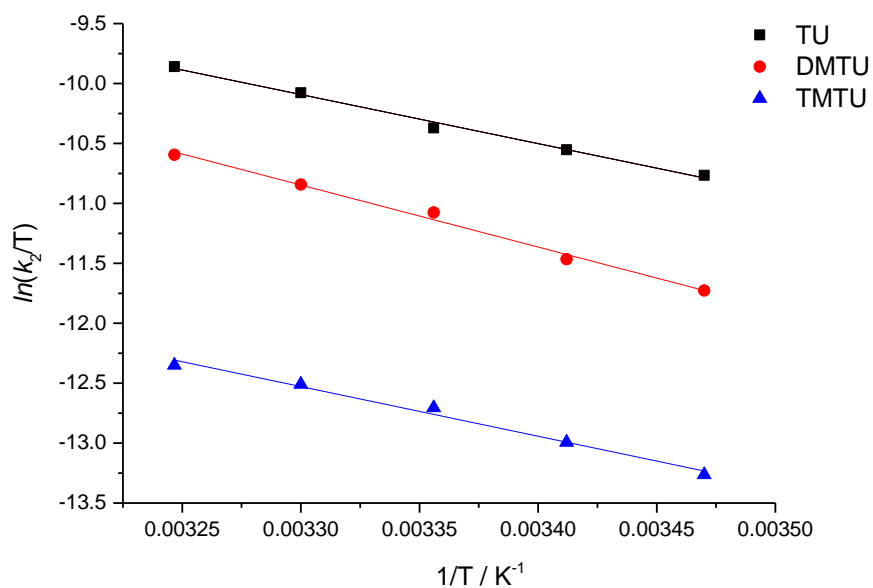


**Figure A46** Eyring plot for the reaction of **PdL3** with the three nucleophiles at various temperatures in the temperature range 288 – 308 K.

**Table A20** Temperature dependence of  $k_2$  for the reaction of **PdL4** with thiourea nucleophiles between the temperature range 288 – 308 K.

(1/T)/K <sup>-1</sup>	ln(k <sub>2</sub> /T)		
	TU	DMTU	TMTU
0,00347	-12,4907	-13,4147	-15,2788
0,00341	-12,1284	-13,0500	-14,4631
0,00335	-11,8058	-12,6289	-13,7509
0,00330	-11,6147	-12,2281	-12,8905
0,00325	-11,4643	-11,8269	-12,3910

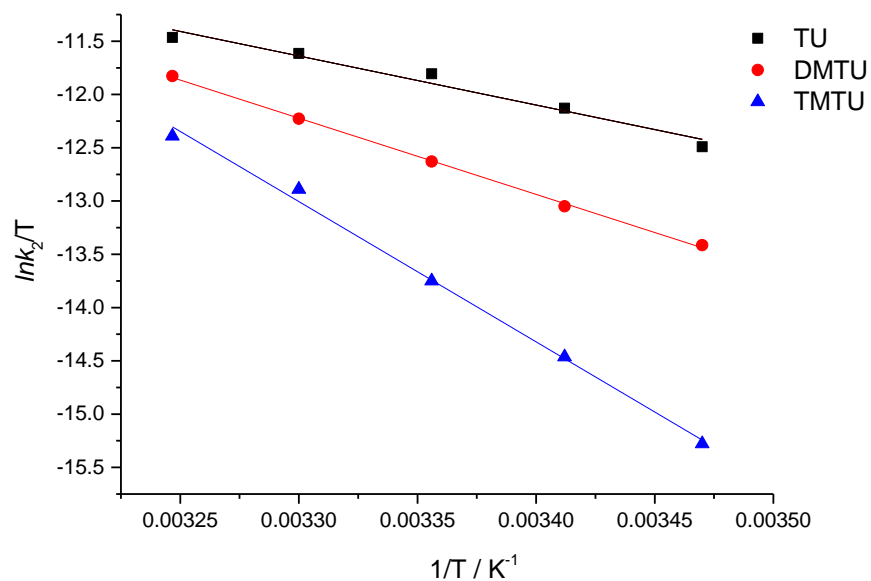


**Figure A47** Eyring plot for the reaction of **PdL4** with the three nucleophiles at various temperatures in the temperature range 288 – 308 K.

**Table A21** Temperature dependence of  $k_2$  for the reaction of **PdL5** with thiourea nucleophiles between the temperature range 288 – 308 K.

(1/T)/K <sup>-1</sup>	ln(k <sub>2</sub> /T)		
	TU	DMTU	TMTU
0,00347	-12,7152	-13,3187	-14,7896
0,00341	-12,2027	-12,9884	-14,3864
0,00335	-11,8434	-12,5126	-13,93319
0,00330	-11,5943	-11,9833	
0,00325	-11,3271	-11,6202	

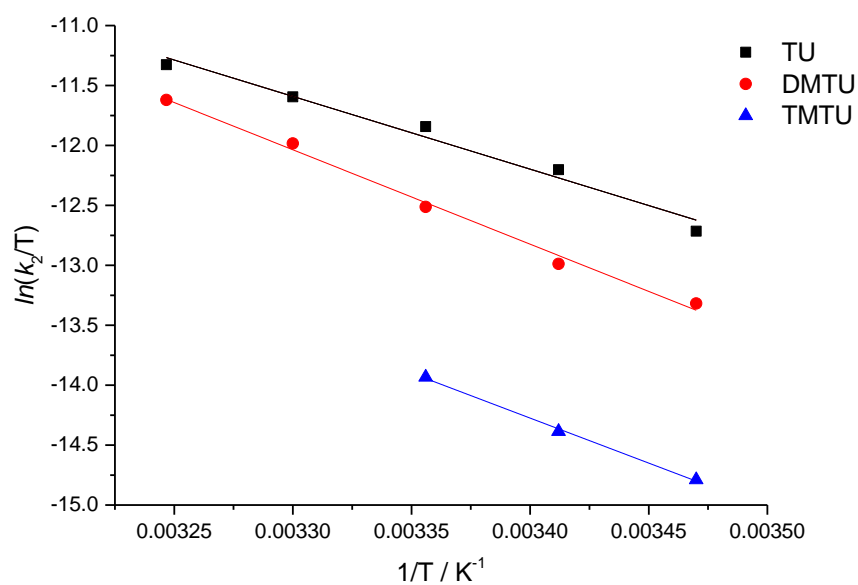


**Figure A48** Eyring plot for the reaction of **PdL5** with the three nucleophiles at various temperatures in the temperature range 288 – 308 K.

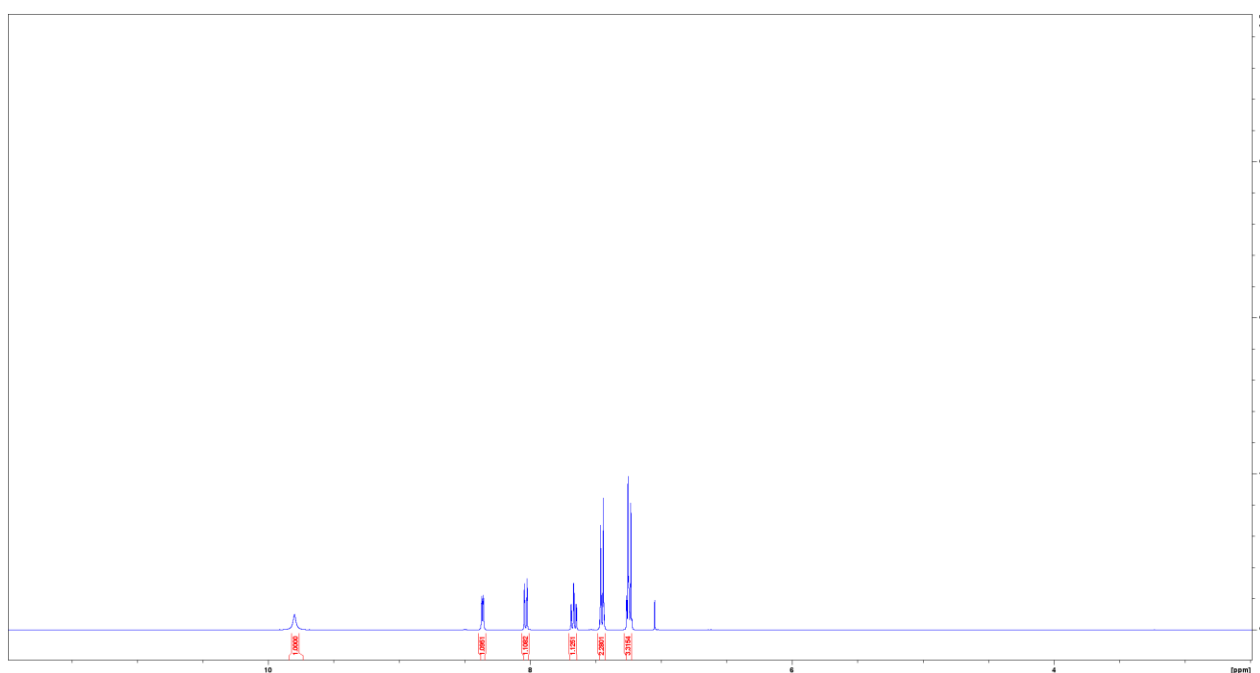


**Figure A49** <sup>1</sup>H NMR spectrum of *N*-(4-bromophenyl)pyridine-2-carboxamide.

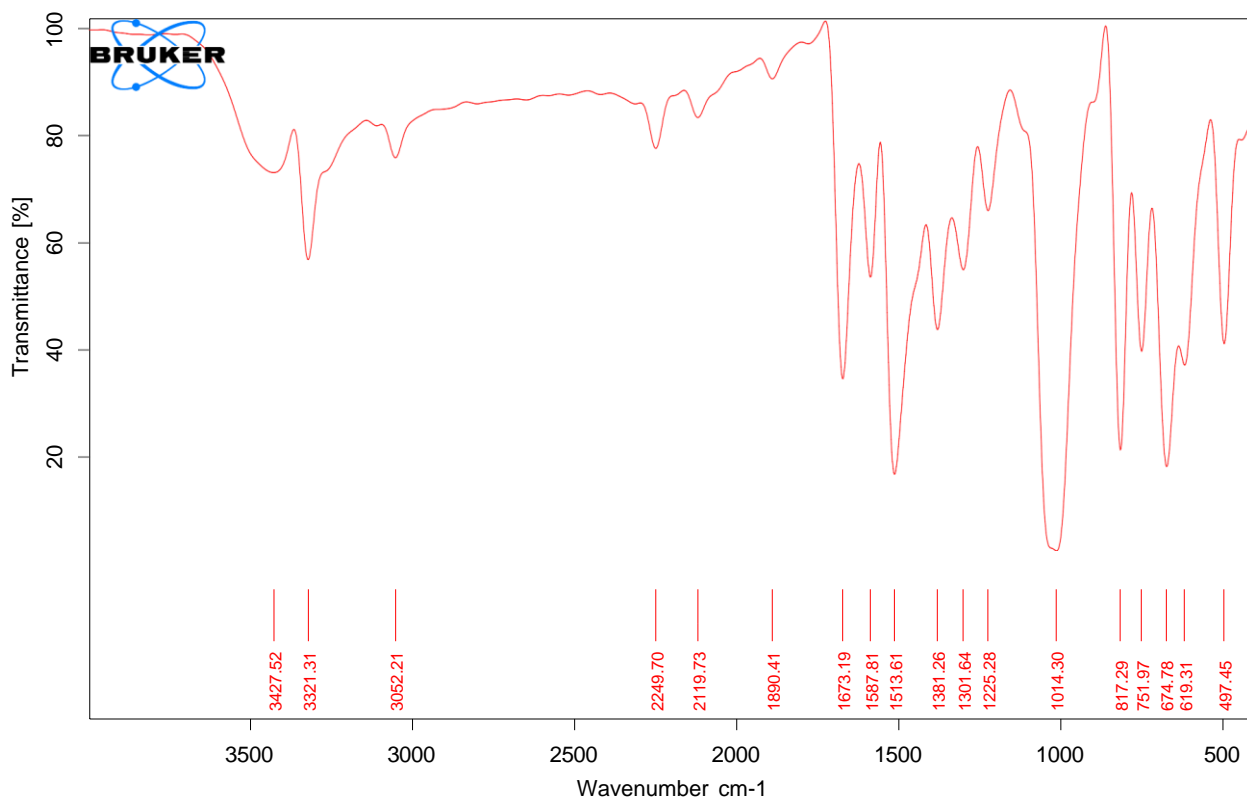


**Figure A50** IR spectrum of *N*-(4-bromophenyl)pyridine-2-carboxamide.

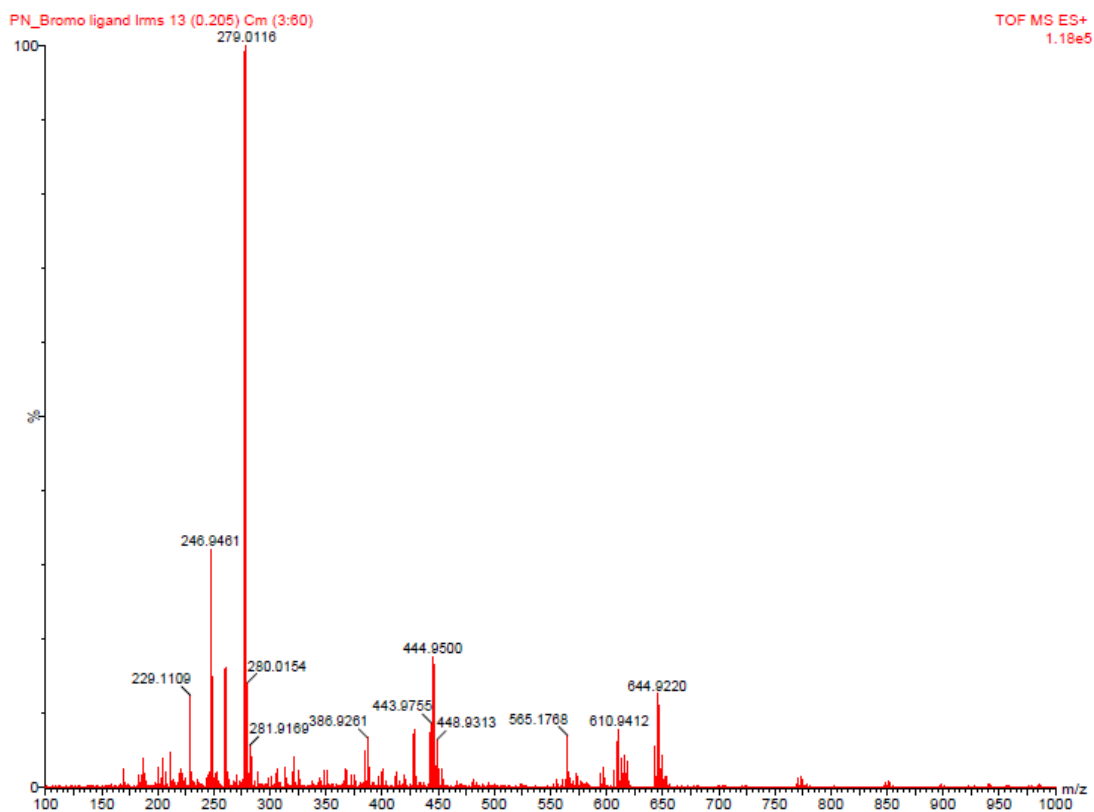


**Figure A51** LRMS for *N*-(4-bromophenyl)pyridine-2-carboxamide.

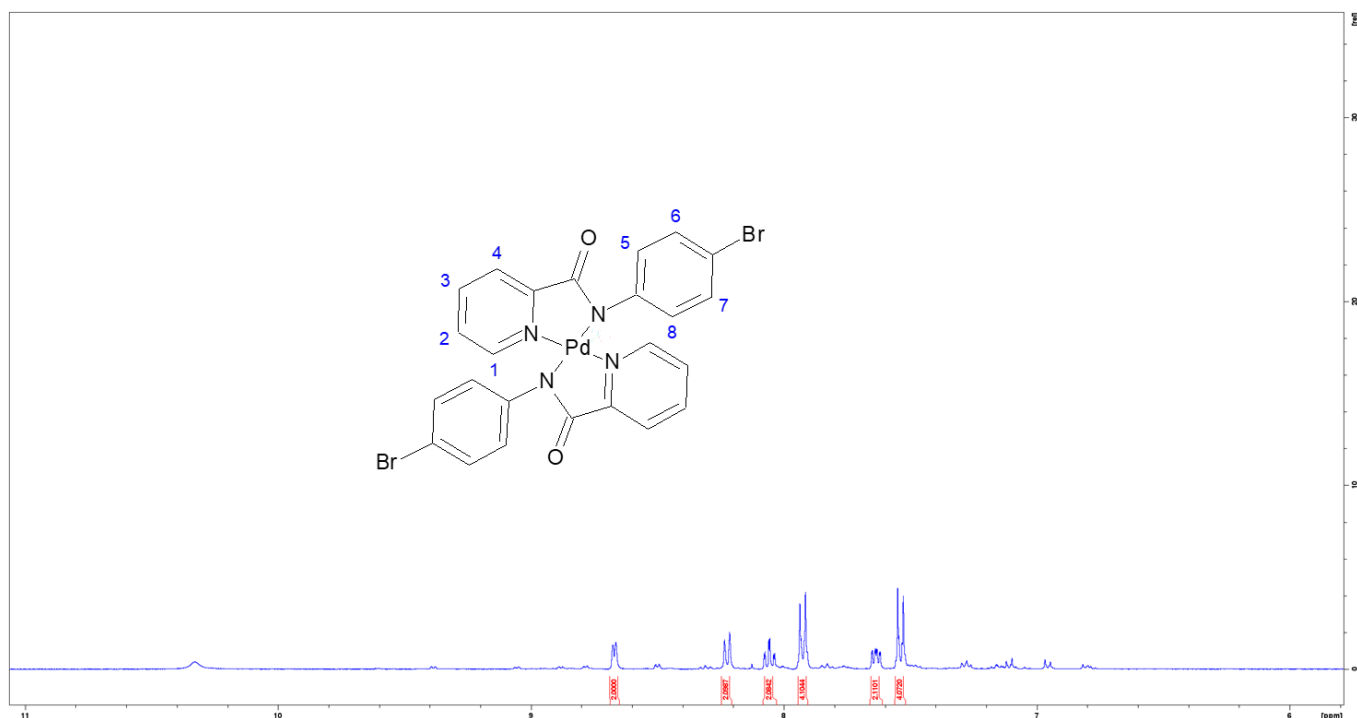


**Figure A52** <sup>1</sup>H NMR spectrum of *bis*[*N*-(4-bromophenyl)-2-pyridinecarboxamide]Palladium (Pd1).

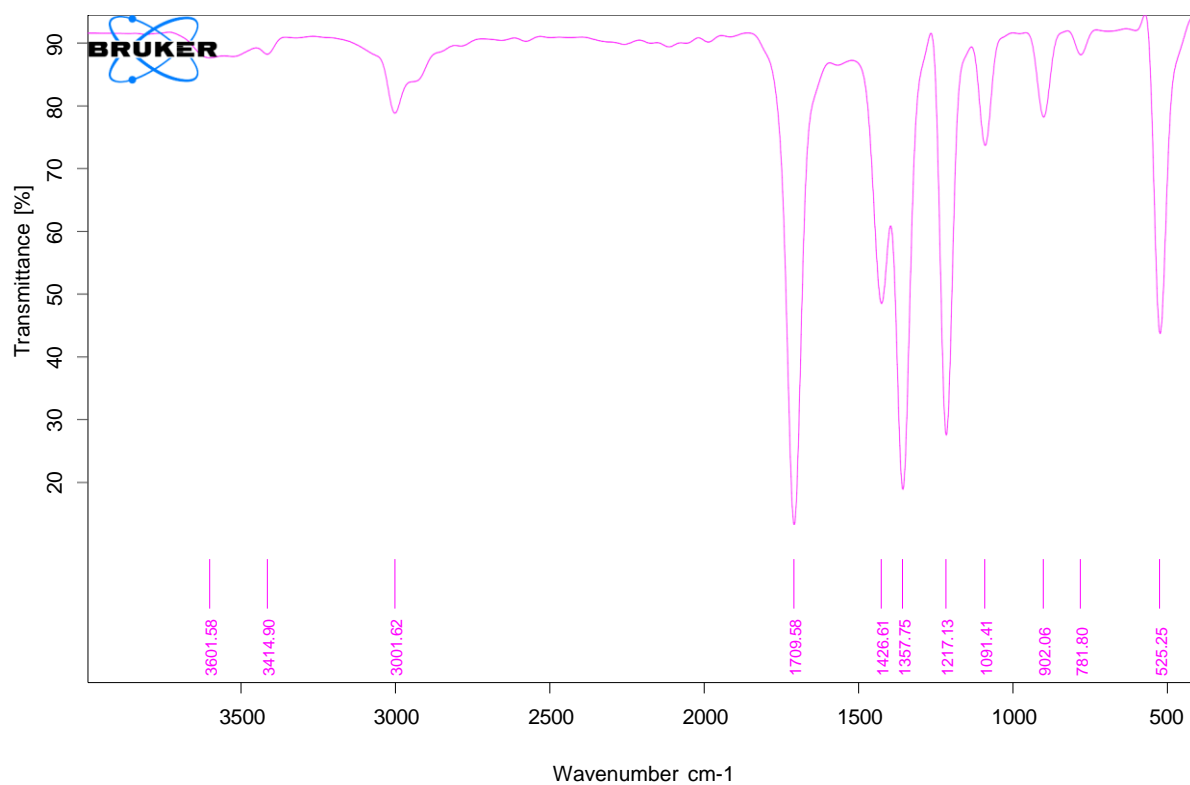


**Figure A53** IR spectrum of *bis*[*N*-(4-bromophenyl)-2-pyridinecarboxamide]Palladium (Pd1).

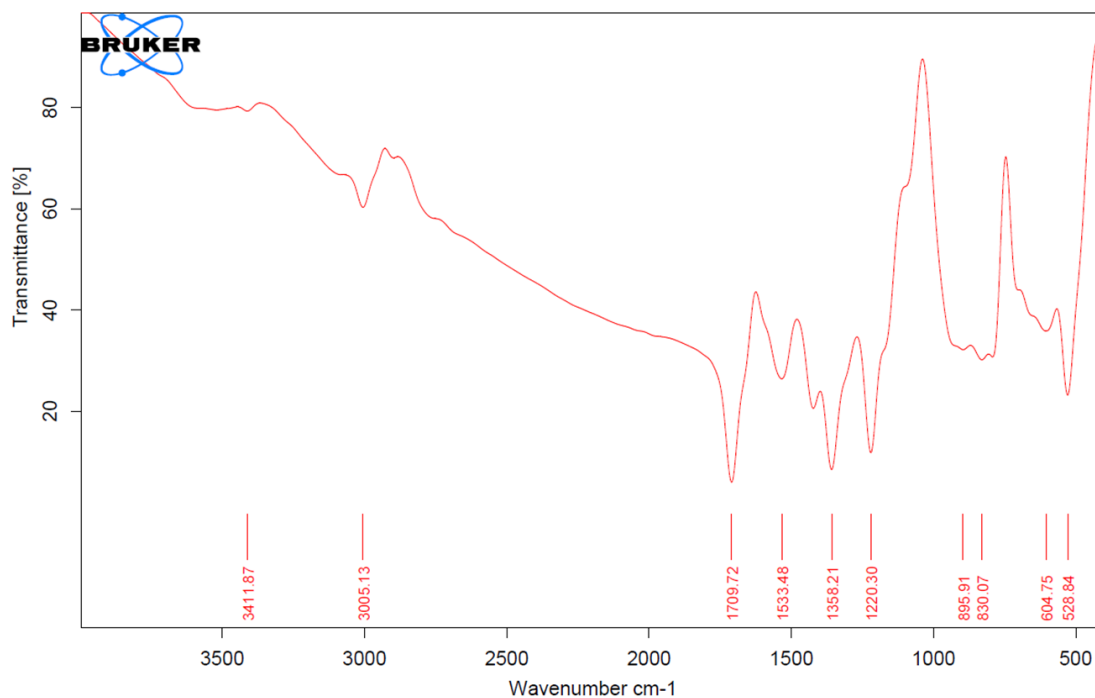


**Figure A54** IR spectrum of Palladium(II) [N-(4-bromophenyl)-2-pyridinecarboxamide], pyridine chloride (**Pd2**).

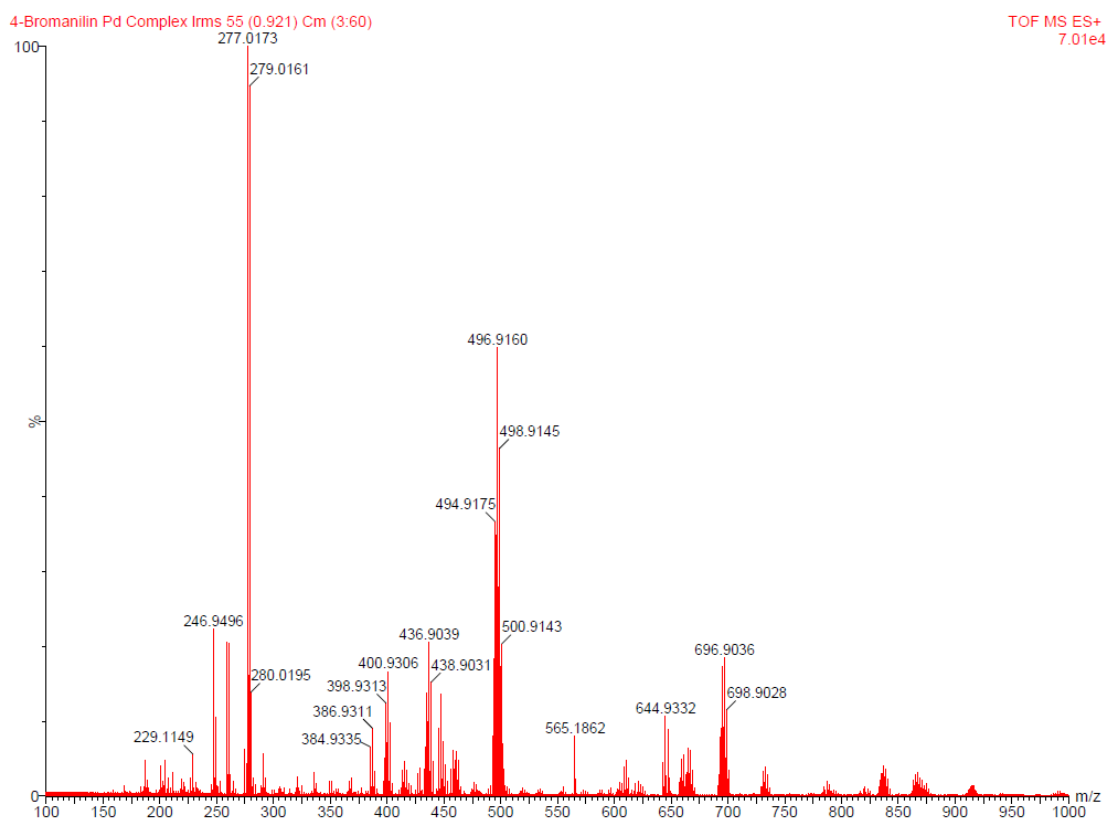


**Figure A55** LRMS of [N-(4-bromophenyl)-2-pyridinecarboxamide], pyridine chloride (**Pd2**)